Prion Protein In Health and Disease

by

Andrew D. Steele

A.B. Biology
University of Chicago, 2001

Submitted to the Department of Biology in partial fulfillment of the requirements for the degree of

DOCTOR OF PHILOSOPHY IN BIOLOGY

at the

MASSACHUSETTS INSTITUTE OF TECHNOLOGY

FEBRUARY 2008

Signature of Author: _____
Department of Biology
December 18th, 2007

Certified by: _____
Susan L. Lindquist
Professor of Biology
Thesis Supervisor

Accepted by: _____
Stephen P. Bell
Professor of Biology
Co-Chair, Biology Graduate Committee

Prion protein in health and disease

by

Andrew D. Steele

Submitted to the Department of Biology on January 14, 2008 in Partial Fulfillment of the Requirements for the Degree of Doctor of Philosophy in Biology

ABSTRACT

The prion protein (PrP) is a conserved glycoprotein tethered to cell membranes by a glycosylphosphatidylinositol anchor. In mammals, PrP is expressed in many tissues, most abundantly in brain, heart, and muscle. Importantly, PrP is required for prion diseases, which are neurodegenerative diseases associated with misfolding and aggregation of PrP. PrP can adopt a self-perpetuating conformation that templates the misfolding of normal PrP molecules into its pathogenic conformation, termed PrP^{Sc}. The role of PrP^{Sc} in the pathogenesis of prion diseases, or transmissible spongiform encephalopathies, has been studied intensively yet the mechanism by which PrP misfolding in neurons leads to injury and death remains enigmatic. Much less attention has been focused on the role of PrP in normal physiology despite the possibility that deciphering PrP's normal function could help to understand prion diseases. My thesis work has spanned both the study of the normal function of PrP and the neurotoxic pathways that are involved in prion pathogenesis.

Because prion disease and other neurodegenerative diseases share protein misfolding as the primary etiology, I aimed to determine whether PrP contributed to other neurodegenerative diseases apart from prion diseases. We deleted PrP from several well established transgenic mouse models of neurodegenerative disease, including Tauopathy, Parkinson's and Huntington's diseases. Deleting PrP did not substantially alter the disease phenotypes of the models that we tested, suggesting that PrP is not a major contributor to or protector against these disorders.

In addition, in collaborative efforts we determined that PrP knockout mice have defects in hematopoiesis and neurogenesis. Hematopoietic stem cells from PrP knockout mice have defects in self-renewal, as manifested during serial bone marrow transplantation or during the aging process. PrP knockout mice also display a slight reduction in cellular proliferation and/or neurogenesis in the adult brain.

I also participated in the development of a video based behavior recognition system. We used this system to quantify the home cage behavioral changes in two mouse models of neurodegeneration, Huntington's disease and prion disease.

Because studies of prion disease have been focused primary on the pathological level, I have attempted to elucidate the molecular pathways responsible for mediating neurotoxicity in a mouse model of infectious prion disease. In the first series of studies we tested whether apoptotoic cell death pathways are activated in prion disease. We inoculated mice deficient for Caspase-12 and Bax, both of which have been implicated in mediating prion toxicity, but did not observe any protection against disease in these mice. Also, neuronal overexpression of Bcl-2 did not protect against prion toxicity and instead, inhibition of apoptosis may have enhanced several aspects of disease (as did deletion of Bax). In a second attempt at determining pathways involved in prion toxicity, I determined that deletion of heat shock factor 1 (Hsf1), a stress responsive transcription factor, protects against prion toxicity. Mice that are deficient for Hsf1 succumb to prion disease faster than controls, despite similar pathological and behavioral onset.

Thesis supervisor: Susan Lindquist
Title: Professor of Biology

ACKNOWLDEGEMENTS

First and foremost, I thank my advisor, Susan Lindquist for giving me the support and the courage to pursue these projects. For reasons that are still not clear to me, Susan always had a strong belief in my abilities even when I did not believe in myself. As a student I was given incredible opportunities for which I am forever grateful.

I am also very grateful to my thesis committee for being so generous with their time and for tolerating a constantly changing and long list of projects and priorities. My committee chair, David Housman, was with me since my first committee meeting. David was not only insightful and had a good vision for timelines and pitfalls, but also kind, supportive, and fun to talk to. Harvey Lodish was great to have as a collaborator and a mentor. He also has an uncanny ability to always make me excited to go back to the bench and do experiments. I thank Hidde Ploegh for several flashes of insight, healthy skepticism, and occasional conversation while walking our dogs in the park. Finally, I thank Mel Feany for serving as my outside committee member for my thesis defense.

I am deeply indebt to the Lindquist lab as a whole for my PhD training. There is an expression that "it takes a village to raise a child" and I think that expression holds true for PhD students as well. I also apologize for occasional volatility and undiplomatic remarks. It would be impossible for me to overstate the commitment, precision, dedication, diligence, and good-humor of Artur Topolszki—without whom this thesis would not exist. Another very talented technician, Melissa Topolszki, has contributed in many ways to the work presented in the following pages. Walker Jackson's hands have contributed to several of the projects presented in this thesis and I thank him for his guidance and patience—I have learned a lot about the mouse as a model system and how to do science from Walker "Scrapie" Jackson. A talented technician, Andrew Borkowski, has been a pleasure to work with in the past year and has helped a great deal with the behavioral analyses presented in Chapters 4 and 5. I am very grateful to James Shorter for his constant companionship, support, sympathy, and advice for five years as my baymate. Another member of WIBR room 655, Rajaraman Krishnan has been a pleasure to work across from for the past five plus years. Finally, I thank Martin Duennwald and Brooke Bevis for being so supportive to Brooke for doing a superb job managing our laboratory. Karen Allendoerfer has been invaluable as an editor and to bounce ideas off when putting papers together.

I had numerous collaborators both within and outside of MIT. Some of these collaborators such as Harvey Lodish (MIT), Jeffrey Macklis (Harvard Medical School), Adriano Aguzzi (University Hospital Zurich), and Junying Yuan (Harvard Medical School) were kind enough to let me physically work in their laboratories. From my numerous collaborators I have learned a great deal and had an unusually diverse training in biology. I have included appendices at the end of each chapter detailing co-author contributions. I hope that I did not forget anyone in the hurry of putting this thesis together.

Finally, I am grateful to my grandfather, Alfred Sarofeen, my girlfriend, Caroline Yi, and our dog, Duke, for occasionally reminding me what is truly important in life.

TABLE OF CONTENTS

Chapter 1

Mammalian Prion Protein (PrP): From Normal Function to Pathological Dysfunction in Prion Diseases

Much of this chapter was published in Prion *Vol. 1(2): 83-93 by Andrew Steele, Susan Lindquist, and Adriano Aguzzi.*

Introduction: prion diseases are prototypic neurodegenerative diseases of protein misfolding

Neurodegenerative diseases are among the most common affliction of the aged population; millions suffer worldwide from Alzheimer's disease (AD), Parkinson's disease (PD), Taupathies (TP), and Huntington's disease (HD) (Prusiner, 2001; Shastry, 2003). Neurodegenerative diseases usually manifest as clinically separable disorders where certain regions of the brain deteriorate, but one commonality is the presence of specific misfolded protein(s) (Aguzzi and Haass, 2003). The underlying mechanism(s) of neuronal dysfunction and death in neurodegenerative diseases are debated intensely, and presumably, delineating the molecular pathways responsible for neuronal dysfunction and death will lead to therapeutic interventions for these devastating diseases. There is a growing consensus that neuronal dysfunction, which is of critical importance for the phenotypes observed in neurodegenerative disease, long precedes neuronal death (Jeffrey and Gonzalez, 2004). These is a critical need to understand what makes neurons selectively vulnerable to diseases of protein misfolding associated with aging and to unravel which (if any) of the misfolded isoforms of protein are mediating the toxic sequelae of neurodegeneation.

My thesis work focused on a prototypic protein misfolding disease of the central nervous system—tranmissible spongiform encephalopathies, or prion diseases. Prion diseases are a special class of protein misfolding disorders, in that they can be transmitted within and between species as well as sporadic and inherited (Prusiner, 1998). To date, prion diseases are the only neurodegenerative disease that can be transmissible. Yet the other main features of prion disease, such deposition of aggregated protein, proliferation and activation of glial cells, loss of neuronal

processes, loss of neurons, and ultimately, death are shared among all neurodegenerative diseases of aging.

Prion Diseases are caused by the misfolding of the host encoded prion protein

The prion protein (PrP^C) is a conserved glycoprotein tethered to cell membranes by a glycosylphosphatidylinositol anchor (Prusiner, 1998). PrP^C is expressed in many tissues, most abundantly in brain, heart, muscle, and also in select lymphoid and myeloid cells (Aguzzi and Heikenwalder, 2006). By a poorly defined mechanism, PrP^C can adopt a beta-sheet rich, self-perpetuating, and aggregation prone protein conformation (termed PrP^{Sc}) either spontaneously or by interaction with PrP^{Sc} (Prusiner, 1998). The crux of the prion hypothesis as formulated by Stanley Prusiner is that a "prion" can adopt a self-perpetuating protein conformation (Prusiner, 1982). Later work in yeast has shown prion phenomenon is not always associated with disease (Wickner, 1994; Lindquist, 1996) and may provide an additional layer of biological regulation (Shorter and Lindquist, 2005).

The key finding that PrP knockout mice are resistant to prion infection and cannot replicate prions strongly supports the prion hypothesis (Bueler et al., 1993; Sailer et al., 1994). This experiment—originally designed to disprove the prion hypothesis (Weissmann and Bueler, 2004)—solidified its central tenet: the requirement of a host protein for prion replication. Further variations of this experiment have taught us that PrP^C expression is important for determining prion-induced toxicity (Bueler et al., 1994). Neurografting brain tissue from wild-type mice into PrP KO brains revealed that *Prnp*$^{+/+}$ tissue grafts replicated prions with accompanying damage to neurons while nearby PrP-deficient tissue was unharmed (Brandner et al., 1996). Thus, PrP^C on neuronal cells is required for prion propagation associated toxicity. This evidence supports our

conjecture that deciphering the normal function or signaling pathway through which PrP^C operates will help illuminate the devastating sequence of events in prion disease.

How and why prion replication in mammals causes injury and death of neurons remains unknown. The vulnerability cells to prion toxicity appears to be highly specific for neuronal cells, as extra neural pathology is conspicuously absent, despite ample replication of prions in immune tissue (Aguzzi, 2006). The ongoing conversion of PrP^C to PrP^{Sc} is an absolute requirement for neurotoxicity in prion disease (Aguzzi, 2007 #171;Mallucci, 2003 #188), yet beyond this basic observation we know little about the pathways mediating neurodegeneration, which is one reason that I chose to pursue this avenue of research in my thesis work.

The cell biology and expression of prion protein

In the mid 1980's Bruce Chesebro, Stanley Prusiner, and Charles Weissmann's laboratories discovered that the so called "scrapie prion protein" was actually encoded as an mRNA both in scrapie infected and uninfected brain of mammals (Chesebro et al., 1985; Oesch et al., 1985). Previously, it had been assumed that the scrapie associated PrP fibrils were products of neurotropic viruses. Soon after the discovery of the PrP mRNA, the cDNA was transfected into mammalian cell lines. Initial observations suggested that overexpression of this protein did not lead to *de novo* generation of infectious material (Caughey et al., 1988). It was quickly determined that PrP was glycosylated and attached to the cell membrane by a phospholipid anchor, as the enzyme phospholipase released PrP into the culture media (Caughey et al., 1989). Mass spectrometry studies confirmed this finding (Baldwin et al., 1990). Interestingly, PrP contains a hydrophobic transmembrane-like region beginning at amino acid 112 and ending at 134. Lingappa and Prusiner laboratories have observed a transmembrane

topology of PrP (Hay et al., 1987), and its incidence increases during prion disease (Hegde et al., 1998; Hegde et al., 1999), yet there has been little follow up on this area of research in the last decade.

Several investigators have measured the half-lives of normal PrP^{C} and disease associated PrP^{Sc}. Byron Caughey was among the first to study the maturation of PrP^{C} in pulse-chase experiments in neuroblastoma cells ("N2a") (Caughey et al., 1989). PrP had a half-life of 3-6 hours in transfected cell lines. Prion infection of cultured cells does not appear to alter the rate of biosynthesis of normal PrP^{C} (Caughey et al., 1989). Pfeifer *et al.* measured the half-life of PrP mRNA, which was found to be 7 hours in N2a cells—whether or not they are infected with prions (Pfeifer et al., 1993). The half-life of PrP^{Sc} is considerably longer than that of PrP. In prion infected N2a cells proteinase K-resistant PrP has a half-life of approximately 30 hours (Peretz et al., 2001). *In vivo* experiments, where PrP expression is turned off using doxycycline showed that the half-life of PrP^{Sc} was approximately 1.5 days (Safar et al., 2005). Surprisingly, the enzymes responsible for degradation of PrP^{Sc} have not been determined.

Once PrP matures, transits though the secretory pathway, and reaches the cell surface it rapidly cycles between endocytic compartments and the cell surface. David Harris and colleagues used surface iodination and immunofluorescence microscopy to make these findings (Shyng et al., 1993). They observed that PrP is endocytosed and brought back to the cell surface in 60 minute periods; with each cycle about 5% of PrP is degraded (Shyng et al., 1994). Harris contends that PrP is endocytosed via clatharin coated pits (Shyng et al., 1994). However, others contend that PrP enters cells through caveolin mediated endocytosis (Peters et al., 2003), and interestingly, caveolin 1 is one of many PrP interaction partners (Mouillet-Richard et al., 2000).

Several groups have quantified the mRNA expression level of PrP in varios tissues using RT-PCR methods (Ning et al., 2005; Han et al., 2006). Consistently, investigators have found the highest message levels of PrP throughout the brain. PrP message is also detectable in peripheral organs, such as lymph node, spleen, heart, liver, lung, and kidney (Ning et al., 2005). Also, select blood cell lineages express PrP (Kubosaki et al., 2001). The most detailed and impressive study of PrP expression was conducted in the laboratory of Roger Morris, who used *in situ* hybridization and immunohistochemistry to study the expression of PrP in the brain and in many other organs (Ford et al., 2002b; Ford et al., 2002a). Interestingly, they discovered some discrepancy between PrP message and protein levels (Ford et al., 2002b), but overall their study was consistent with the findings described above.

The study of the normal function of PrP may help to understand prion disease

In contrast to the study of PrP misfolding in disease, much less attention has been focused on the role of PrP^{C} in normal physiology (Sakudo et al., 2006). Of note, normal function studies of proteins associated with other neurodegenerative diseases, such as amyloid precursor protein and the secretases for Alzheimer's disease (Aguzzi and Haass, 2003), α-synuclein for Parkinson's disease (Abeliovich et al., 2000), and huntingtin for Huntington's disease (Zuccato et al., 2001) are helping to provide deeper insights into the pathophysiology of these diseases. Analogously, a clearer understanding of the function of PrP^{C} in homeostasis may provide valuable insights into the molecular pathways of prion pathogenesis. However, the extent of overlap between understanding the pathogenic dysfunction of PrP^{Sc} in prion diseases and the normal function of PrP^{C} in cell physiology remains to be determined (depicted in Figure 1).

The PrP knockout mouse

Many approaches have been utilized to understand the physiological function of PrP^C, including but not limited to the identification of multiple interaction partners, human genetic studies of the *Prnp* (prion protein gene) locus, ectopic and over-expression of PrP^C in a variety of cell types and organisms, and finally deletion or 'knockout' (KO) studies in the mouse(Bueler et al., 1992), cow (Richt et al., 2006), and even goat (Yu et al., 2006), providing additional exciting tools for understanding aspects of PrP^C physiology that may not be addressable in mice (Fig. 2). The search for protein interaction partners of PrP^C, by a variety of methods, has led to interesting candidates but functional demonstration of the importance of these interactions is still missing.(Aguzzi and Heikenwalder, 2006; Marc et al., 2007) Furthermore, over-expression and ectopic expression studies of PrP^C, or expression of mammalian PrP^C in lower organisms is yet to reveal an irrefutable function for PrP^C. Another approach includes large scale genetic association studies to look for *PRNP* mutations or polymorphisms associated with human genetic disorders. Some interesting genetic associations with Alzheimer's disease susceptibility have been found but lack consensus in the field.(Riemenschneider et al., 2004; Ahn et al., 2006; Del Bo et al., 2006) Polymorphisms in PrP^C have been associated with rare forms of cortical malformation (Walz et al., 2004), differences in surgical outcome for a form of epilepsy (Walz et al., 2003), and even learning and memory (Papassotiropoulos et al., 2005).

Because PrP^C is so conserved among mammals, there was great expectation that ablation of *Prnp* in the mouse would reveal a normal function for this enigmatic gene (Weissmann and Bueler, 2004). Since the PrP KO mice have no overt phenotype (Bueler et al., 1992; Manson et al., 1994), it was clear that PrP^C is not essential for the survival of the laboratory mouse. However, genetic compensation and developmental plasticity may mask the phenotype of PrP^C

deficient mice and thus, it may take an appropriate challenge to reveal any phenotype. Although the original reports on the *Zurich* and *Edinburgh* PrP KO mice (two different targeting strategies to delete PrP, named after the city where the experiments took place) reported "no phenotype", many subsequent studies have revealed that this KO mouse has an abundance of phenotypes, some of which have been contested and many of which are subtle. This review summarizes the recent research in determining the normal function of PrP^C by utilizing the PrP KO mouse. Although many claims to PrP^C function have been generated from the study of cultured cells (Hetz et al., 2003; Roucou et al., 2004), we will mostly confine our discussion to studies utilizing mice: the PrP KO, the deletion of the PrP^C homolog doppel (Dpl), and over-expression transgenics of PrP^C and Dpl. *Prnp* is one of the most frequently knocked out mammalian genes, and a plethora of PrP-deficient mice have been generated with a wealth of strategies. A detailed review of the construction of the various available PrP KO mice exists (Weissmann and Aguzzi, 1999; Weissmann and Flechsig, 2003).

The role of PrP in the immune system, phagocytosis, and as a microbial receptor

Recent reports have suggested a role for PrP^C in cellular internalization pathways, perhaps a function that has been co-opted by microbes. Work from the laboratory of Rafael Linden and colleagues add to the growing list of phenotypes for the PrP KO. *Prnp* null macrophages were found to display increased rates of phagocytosis *in vitro* and *in vivo*, leading to the conclusion that under physiological conditions PrP^C negatively regulates phagocytosis(de Almeida et al., 2005). Studies of microbial pathogenesis in PrP KOs may be connected with a role for PrP^C in phagocytosis or cytokine production. Watarai and colleagues have discovered that the PrP KO is more resistant to infection with the bacterial pathogen *Brucella abortus*

(Aguzzi and Hardt, 2003; Watarai et al., 2003). Localization and biochemical experiments pinpointed bacterial heat shock protein 60 as an interaction partner with PrP^C on the cell surface (Watarai et al., 2003). These results were not confirmed in a different laboratory (Fontes et al., 2005).

Virologists have made use of the PrP KO as well, revealing yet another phenotype likely relating to cellular internalization pathways. In this study, Thackray and Bujdoso demonstrate that PrP KOs are refractory to infection with a neurotropic herpes simplex virus whereas PrP over-expression transgenics (Tga20) were highly susceptible to infection (Thackray and Bujdoso, 2002). Studies of viral titers and maturation markers suggest that viral replication is retarded in PrP KOs in favor of establishing latency. Intriguingly, the viral infection induced neuronal cell death much more dramatically in PrP over-expression transgenics, connecting PrP^C to cell survival pathways (discussed below).

Recent work suggests that PrP^C may play a role in the immunological synapse. Ballerini *et al.*, demonstrated that PrP^C is important in an interaction between T cells and dendritic cell (Ballerini et al., 2006). PrP^C was dispensable on T cells for this interaction but PrP^C on dendritic cells was important in stimulating T cells *in vitro* and in an *in vivo* assay (Ballerini et al., 2006). Another study reports that $\alpha\beta$ T cells are greatly diminished in PrP over-expression transgenic mice, and these mice also display an atrophy of the thymus (Jouvin-Marche et al., 2006). To summarize, PrP^C may be important for host-pathogen interactions, immune synapses and T cell homeostasis, but further studies will be needed to decipher the role of PrP^C in the immune system.

A role for PrP in neuronal excitability

The high level of PrP^C expression in neuronal cells led to an interest in detecting electrophysiological defects in the PrP KO. This topic is no less controversial than any other we have discussed in this review, but the weight of the evidence clearly lies on the side of altered neuronal excitability in PrP KO neurons. Electrophysiological studies of PrP KOs were first under-taken by John Collinge and John Jefferys, who found that CA1 neurons in *Zurich* PrP KOs had faster after-hyperpolarization currents and were impaired in long term potentiation (LTP) (Collinge et al., 1994; Manson JC, 1995). In addition it was shown that both wild-type and a familial mutant human PrP^C were capable of rescuing this electrophysiological phenotype when expressed as transgenes in the PrP KO background (Whittington et al., 1995; Asante et al., 2004). Soon after these findings were reported opposing reports surfaced (Herms et al., 1995; Lledo et al., 1996). Over the ensuing years there have been several other attempts to clarify the electrophysiological phenotype (or lack thereof) in PrP KOs (Curtis et al., 2003; Maglio et al., 2004; Criado et al., 2005). However, only one thing is clear – detection of the electrophysiological phenotype depends on which line of mice is being used, who is investigating, and the age of the PrP KOs being used (Maglio et al., 2006).

The neuronal excitability phenotypes may relate to one of the strongest phenotypes of PrP KOs which presents under the challenge of seizure inducing drugs. *Zurich* PrP KOs are much more susceptible to repeated doses of pentylene tetrazol and kainic acid, both of which induce seizures (Walz et al., 1999). Approximately 50% of PrP KOs died from a single administration of kainic acid while 100% of control animals survived (Walz et al., 1999). This result has been confirmed independently by Rangel, *et al.*, who also note increased neuronal cell death in PrP KOs injected with kainic acid (Rangel et al., 2007). Finally, it is also worth noting that a defect

in neuronal architecture of the hippocampus in *Zurich* PrP deficient mice has been reported and may be relevant to several of the findings discussed above (Colling et al., 1997). Timm stained sections of the hippocampus from PrP KO had more sprouting of axons than did controls in the granule cell layer of the dentate gyrus, and the infrapyramidal region of CA3 region (Colling et al., 1997). This is said to resemble the mossy fiber collateral and terminal sprouting seen in certain human epilepsies.

Behavioral phenotypes: is PrP involved in learning and memory?

If they bear any relevance to real life, the electrophysiological defects described above for the PrP^C null neurons might manifest in the behavior of the PrP KO mouse. The abundant expression of PrP^C in regions important in learning and memory, such as the hippocampus, has lead to a series of behavioral studies aimed at detecting abnormalities in PrP KOs. Initial studies by Charles Weissmann, Hans Peter Lipp, and colleagues did not detect any phenotype of *Zurich* PrP KOs in a long-term study using maze tests (Bueler et al., 1992; Lipp et al., 1998). Further, a study by Roesler *et al.* failed to detect any abnormalities in anxiety nor inhibitory avoidance learning in PrP KOs (Roesler et al., 1999). Cognitive defects have been detected in PrP KOs by Criado and colleagues who found that spatial learning was defective in PrP KOs (Criado et al., 2005). Another study describes PrP KOs as having normal short- and long-term memory at 3 months of age but impairments by 9 months of age (Coitinho et al., 2003). A follow-up study suggested that the interaction of PrP^C and laminin may be key to memory consolidation in rats (Coitinho et al., 2006).

In an attempt to reveal a behavioral phenotype, investigators have challenged PrP KOs in various ways during phenotypic testing. Coitinho *et al.* dosed PrP KO mice with various

psychotropic drugs and interestingly, PrP KOs show a decreased response to the psychotropic drug MK-801, which normally causes increased motor activity (Coitinho et al., 2002). Amphetamine and caffeine induced hyper-locomotion to an equal extent in PrP KOs and controls (Coitinho et al., 2002). Nico *et al.* subjected *Zurich* PrP KOs to acute stress by foot shock or swimming trial and found that PrP KOs showed less anxiety than controls after these treatments (Nico et al., 2005). Another study notes a very subtle increase in locomotor activity in PrP KOs in an open field test (Roesler et al., 1999). This increased locomotor activity has not been observed using extensively backcrossed C57Bl/6 PrP KOs (both *Edinburgh* and *Zurich*) in the home cage using high resolution techniques recently used to study prion disease in detail (Steele et al., 2007), however, our testing conditions are not equivalent to an open field test (ADS and SL, unpublished results).

Diverse neuroprotective properties of PrP

Many studies have claimed that protection against neuronal damage is one of PrP^C's *raison d'être*. Neuroprotection (defined generically as protecting neurons from dysfunction or death) may represent one of the best supported functions of PrP^C. This protection applies to both physiological challenges and to a peculiar yet fascinating paradigm whereby the closest homolog of PrP^C, Dpl, when ectopically expressed in the brain causes loss of Purkinje neurons in the cerebellum but only in a PrP KO background (Sakaguchi et al., 1996).

We will begin our discussion of PrP's protective properties with one of the most agreed upon observations—PrP KOs are much more susceptible to ischemic damage. McLennan and colleagues were the first to document that PrP KOs are more susceptible to stroke (McLennan et al., 2004). They were led to the PrP KO through studying a dramatic upregulation of PrP

expression at sites of stroke in human brains (McLennan et al., 2004). Subsequent studies have replicated and extended these results in acute (Sakurai-Yamashita et al., 2005) and long term models of ischemia (Weise et al., 2006) and even in transgenic rats (Shyu et al., 2005). Interestingly, transgenic over-expression of PrP in the mouse does not protect above wild-type PrP levels (Spudich et al., 2005) while in the rat increasing PrP levels did confer protection. Weise and colleagues note that PrP KOs have lower levels of phosphorylated-Akt both in basal conditions and during ischemic injury, pointing towards a general role of PrP in activation of cell survival pathways (Weise et al., 2006). Other researchers have noted significant increases in the phosphorylation of ERK-1 and -2, STAT-1, and JNK-1 in ischemic PrP KO brains (Spudich et al., 2005). Recently, Gains and colleagues have extended PrP's neuroprotective spectrum. They dosed neonatal PrP KOs and controls with a high dose of ethanol, a paradigm for inducing Bax mediated apoptosis, and noted a dramatic increase in cell death in brains of PrP KOs (Gains et al., 2006). Another brief report documents an enhanced brain injury in PrP KOs after head trauma (Hoshino et al., 2003), however, it is likely that these mice overexpress Dpl and therefore display a confounding effect. The wide-ranging neuroprotective functions of PrP have limitations and these observations of protection in unique models need to be understood in mechanistic detail.

The second well studied paradigm in which PrP exerts a protective function deals with the neurotoxicity induced by its nearest homolog. The exciting and circuitous discovery of Dpl began with conflicting reports on the phenotype of the PrP KO, with two groups reporting no phenotype (Bueler et al., 1992; Manson et al., 1994) and one group reporting a late onset ataxia and Purkinje cell loss in *Nagasaki* PrP KO mice (Sakaguchi et al., 1996; Katamine et al., 1998). Later it was determined by several groups that a previously undescribed tightly linked homolog

of PrP^C was upregulated by the deletion strategy used in the *Nagasaki* PrP KO line. The *Nagasaki* deletion strategy fused PrP's promoter to Dpl, driving expression of Dpl in the brain, where it is not normally expressed (Moore et al., 1999; Li et al., 2000). Subsequent experiments determined that the toxicity induced by ectopic Dpl expression in the PrP KO is abrogated by reintroduction of a single copy of PrP^C (Nishida et al., 1999; Valenti et al., 2001). Interestingly, PrP^C devoid of the octapeptide repeats (amino acids 23-88) is incapable of rescuing Dpl toxicity, suggesting an important role for the N-proximal region of PrP^C in its neuroprotective functions (Atarashi et al., 2003). A similar phenomenon is observed when an artificial deletion mutant of PrP^C, missing amino acids 32-134 is expressed as a transgene in the PrP KO. This trangenic mouse develops a dramatic loss of granular neurons in the cerebellum (Shmerling et al., 1998).

References

Abeliovich A, Schmitz Y, Farinas I, Choi-Lundberg D, Ho WH, Castillo PE, Shinsky N, Verdugo JM, Armanini M, Ryan A, Hynes M, Phillips H, Sulzer D, Rosenthal A (2000) Mice lacking alpha-synuclein display functional deficits in the nigrostriatal dopamine system. Neuron 25:239-252.

Aguzzi A (2006) Prion diseases of humans and farm animals: epidemiology, genetics, and pathogenesis. J Neurochem 97:1726-1739.

Aguzzi A, Haass C (2003) Games played by rogue proteins in prion disorders and Alzheimer's disease. Science 302:814-818.

Aguzzi A, Hardt WD (2003) Dangerous liaisons between a microbe and the prion protein. J Exp Med 198:1-4.

Aguzzi A, Heikenwalder M (2006) Pathogenesis of prion diseases: current status and future outlook. Nat Rev Microbiol 4:765-775.

Ahn K, Kim E, Kwon YA, Kim DK, Lee JE, Jo SA (2006) No association of prion protein gene polymorphisms with Alzheimer's disease in Korean population. Exp Mol Med 38:727-731.

Asante EA, Li YG, Gowland I, Jefferys JG, Collinge J (2004) Pathogenic human prion protein rescues PrP null phenotype in transgenic mice. Neurosci Lett 360:33-36.

Atarashi R, Nishida N, Shigematsu K, Goto S, Kondo T, Sakaguchi S, Katamine S (2003) Deletion of N-terminal residues 23-88 from prion protein (PrP) abrogates the potential to rescue PrP-deficient mice from PrP-like protein/doppel-induced Neurodegeneration. J Biol Chem 278:28944-28949.

Ballerini C, Gourdain P, Bachy V, Blanchard N, Levavasseur E, Gregoire S, Fontes P, Aucouturier P, Hivroz C, Carnaud C (2006) Functional implication of cellular prion protein in antigen-driven interactions between T cells and dendritic cells. J Immunol 176:7254-7262.

Brandner S, Isenmann S, Raeber A, Fischer M, Sailer A, Kobayashi Y, Marino S, Weissmann C, Aguzzi A (1996) Normal host prion protein necessary for scrapie-induced neurotoxicity. Nature 379:339-343.

Brown DR, Qin K, Herms JW, Madlung A, Manson J, Strome R, Fraser PE, Kruck T, von Bohlen A, Schulz-Schaeffer W, Giese A, Westaway D, Kretzschmar H (1997) The cellular prion protein binds copper in vivo. Nature 390:684-687.

Bueler H, Raeber A, Sailer A, Fischer M, Aguzzi A, Weissmann C (1994) High prion and PrPSc levels but delayed onset of disease in scrapie-inoculated mice heterozygous for a disrupted PrP gene. Mol Med 1:19-30.

Bueler H, Aguzzi A, Sailer A, Greiner RA, Autenried P, Aguet M, Weissmann C (1993) Mice devoid of PrP are resistant to scrapie. Cell 73:1339-1347.

Bueler H, Fischer M, Lang Y, Bluethmann H, Lipp HP, DeArmond SJ, Prusiner SB, Aguet M, Weissmann C (1992) Normal development and behaviour of mice lacking the neuronal cell-surface PrP protein. Nature 356:577-582.

Coitinho AS, Roesler R, Martins VR, Brentani RR, Izquierdo I (2003) Cellular prion protein ablation impairs behavior as a function of age. Neuroreport 14:1375-1379.

Coitinho AS, Dietrich MO, Hoffmann A, Dall'Igna OP, Souza DO, Martins VR, Brentani RR, Izquierdo I, Lara DR (2002) Decreased hyperlocomotion induced by MK-801, but not

amphetamine and caffeine in mice lacking cellular prion protein (PrP(C)). Brain Res Mol Brain Res 107:190-194.
Coitinho AS, Freitas AR, Lopes MH, Hajj GN, Roesler R, Walz R, Rossato JI, Cammarota M, Izquierdo I, Martins VR, Brentani RR (2006) The interaction between prion protein and laminin modulates memory consolidation. Eur J Neurosci 24:3255-3264.
Colling SB, Khana M, Collinge J, Jefferys JG (1997) Mossy fibre reorganization in the hippocampus of prion protein null mice. Brain Res 755:28-35.
Collinge J, Whittington MA, Sidle KC, Smith CJ, Palmer MS, Clarke AR, Jefferys JG (1994) Prion protein is necessary for normal synaptic function. Nature 370:295-297.
Criado JR, Sanchez-Alavez M, Conti B, Giacchino JL, Wills DN, Henriksen SJ, Race R, Manson JC, Chesebro B, Oldstone MB (2005) Mice devoid of prion protein have cognitive deficits that are rescued by reconstitution of PrP in neurons. Neurobiol Dis 19:255-265.
Curtis J, Errington M, Bliss T, Voss K, MacLeod N (2003) Age-dependent loss of PTP and LTP in the hippocampus of PrP-null mice. Neurobiol Dis 13:55-62.
de Almeida CJ, Chiarini LB, da Silva JP, PM ES, Martins MA, Linden R (2005) The cellular prion protein modulates phagocytosis and inflammatory response. J Leukoc Biol 77:238-246.
Del Bo R, Scarlato M, Ghezzi S, Martinelli-Boneschi F, Fenoglio C, Galimberti G, Galbiati S, Virgilio R, Galimberti D, Ferrarese C, Scarpini E, Bresolin N, Comi GP (2006) Is M129V of PRNP gene associated with Alzheimer's disease? A case-control study and a meta-analysis. Neurobiol Aging 27:770 e771-770 e775.
Fontes P, Alvarez-Martinez MT, Gross A, Carnaud C, Kohler S, Liautard JP (2005) Absence of evidence for the participation of the macrophage cellular prion protein in infection with Brucella suis. Infect Immun 73:6229-6236.
Gains MJ, Roth KA, LeBlanc AC (2006) Prion protein protects against ethanol-induced Bax-mediated cell death in vivo. Neuroreport 17:903-906.
Herms JW, Kretzchmar HA, Titz S, Keller BU (1995) Patch-clamp analysis of synaptic transmission to cerebellar purkinje cells of prion protein knockout mice. Eur J Neurosci 7:2508-2512.
Hetz C, Maundrell K, Soto C (2003) Is loss of function of the prion protein the cause of prion disorders? Trends Mol Med 9:237-243.
Hoshino S, Inoue K, Yokoyama T, Kobayashi S, Asakura T, Teramoto A, Itohara S (2003) Prions prevent brain damage after experimental brain injury: a preliminary report. Acta Neurochir Suppl 86:297-299.
Jeffrey M, Gonzalez L (2004) Pathology and pathogenesis of bovine spongiform encephalopathy and scrapie. Curr Top Microbiol Immunol 284:65-97.
Jouvin-Marche E, Attuil-Audenis V, Aude-Garcia C, Rachidi W, Zabel M, Podevin-Dimster V, Siret C, Huber C, Martinic M, Riondel J, Villiers CL, Favier A, Naquet P, Cesbron JY, Marche PN (2006) Overexpression of cellular prion protein induces an antioxidant environment altering T cell development in the thymus. J Immunol 176:3490-3497.
Katamine S, Nishida N, Sugimoto T, Noda T, Sakaguchi S, Shigematsu K, Kataoka Y, Nakatani A, Hasegawa S, Moriuchi R, Miyamoto T (1998) Impaired motor coordination in mice lacking prion protein. Cell Mol Neurobiol 18:731-742.
Li A, Sakaguchi S, Atarashi R, Roy BC, Nakaoke R, Arima K, Okimura N, Kopacek J, Shigematsu K (2000) Identification of a novel gene encoding a PrP-like protein expressed

as chimeric transcripts fused to PrP exon 1/2 in ataxic mouse line with a disrupted PrP gene. Cell Mol Neurobiol 20:553-567.
Lindquist S (1996) Mad cows meet mad yeast: the prion hypothesis. Mol Psychiatry 1:376-379.
Lipp HP, Stagliar-Bozicevic M, Fischer M, Wolfer DP (1998) A 2-year longitudinal study of swimming navigation in mice devoid of the prion protein: no evidence for neurological anomalies or spatial learning impairments. Behav Brain Res 95:47-54.
Lledo PM, Tremblay P, DeArmond SJ, Prusiner SB, Nicoll RA (1996) Mice deficient for prion protein exhibit normal neuronal excitability and synaptic transmission in the hippocampus. Proc Natl Acad Sci U S A 93:2403-2407.
Maglio LE, Martins VR, Izquierdo I, Ramirez OA (2006) Role of cellular prion protein on LTP expression in aged mice. Brain Res 1097:11-18.
Maglio LE, Perez MF, Martins VR, Brentani RR, Ramirez OA (2004) Hippocampal synaptic plasticity in mice devoid of cellular prion protein. Brain Res Mol Brain Res 131:58-64.
Manson JC, Clarke AR, Hooper ML, Aitchison L, McConnell I, Hope J (1994) 129/Ola mice carrying a null mutation in PrP that abolishes mRNA production are developmentally normal. Mol Neurobiol 8:121-127.
Manson JC CA, Johnston A, Black C, MacLeod N. (1995) PrP Gene dosage and long term potentiation. Neurodegeneration 4:113-114.
Marc D, Mercey R, Lantier F (2007) Scavenger, transducer, RNA chaperone? What ligands of the prion protein teach us about its function. Cell Mol Life Sci.
McLennan NF, Brennan PM, McNeill A, Davies I, Fotheringham A, Rennison KA, Ritchie D, Brannan F, Head MW, Ironside JW, Williams A, Bell JE (2004) Prion protein accumulation and neuroprotection in hypoxic brain damage. Am J Pathol 165:227-235.
Moore RC, Lee IY, Silverman GL, Harrison PM, Strome R, Heinrich C, Karunaratne A, Pasternak SH, Chishti MA, Liang Y, Mastrangelo P, Wang K, Smit AF, Katamine S, Carlson GA, Cohen FE, Prusiner SB, Melton DW, Tremblay P, Hood LE, Westaway D (1999) Ataxia in prion protein (PrP)-deficient mice is associated with upregulation of the novel PrP-like protein doppel. J Mol Biol 292:797-817.
Nico PB, de-Paris F, Vinade ER, Amaral OB, Rockenbach I, Soares BL, Guarnieri R, Wichert-Ana L, Calvo F, Walz R, Izquierdo I, Sakamoto AC, Brentani R, Martins VR, Bianchin MM (2005) Altered behavioural response to acute stress in mice lacking cellular prion protein. Behav Brain Res 162:173-181.
Nishida N, Tremblay P, Sugimoto T, Shigematsu K, Shirabe S, Petromilli C, Erpel SP, Nakaoke R, Atarashi R, Houtani T, Torchia M, Sakaguchi S, DeArmond SJ, Prusiner SB, Katamine S (1999) A mouse prion protein transgene rescues mice deficient for the prion protein gene from purkinje cell degeneration and demyelination. Lab Invest 79:689-697.
Papassotiropoulos A, Wollmer MA, Aguzzi A, Hock C, Nitsch RM, de Quervain DJ (2005) The prion gene is associated with human long-term memory. Hum Mol Genet 14:2241-2246.
Prusiner SB (1982) Novel proteinaceous infectious particles cause scrapie. Science 216:136-144.
Prusiner SB (1998) Prions. Proc Natl Acad Sci U S A 95:13363-13383.
Prusiner SB (2001) Shattuck lecture--neurodegenerative diseases and prions. N Engl J Med 344:1516-1526.
Rangel A, Burgaya F, Gavin R, Soriano E, Aguzzi A, Del Rio JA (2007) Enhanced susceptibility of Prnp-deficient mice to kainate-induced seizures, neuronal apoptosis, and death: Role of AMPA/kainate receptors. J Neurosci Res.

Richt JA, Kasinathan P, Hamir AN, Castilla J, Sathiyaseelan T, Vargas F, Sathiyaseelan J, Wu H, Matsushita H, Koster J, Kato S, Ishida I, Soto C, Robl JM, Kuroiwa Y (2006) Production of cattle lacking prion protein. Nat Biotechnol.

Riemenschneider M, Klopp N, Xiang W, Wagenpfeil S, Vollmert C, Muller U, Forstl H, Illig T, Kretzschmar H, Kurz A (2004) Prion protein codon 129 polymorphism and risk of Alzheimer disease. Neurology 63:364-366.

Roesler R, Walz R, Quevedo J, de-Paris F, Zanata SM, Graner E, Izquierdo I, Martins VR, Brentani RR (1999) Normal inhibitory avoidance learning and anxiety, but increased locomotor activity in mice devoid of PrP(C). Brain Res Mol Brain Res 71:349-353.

Roucou X, Gains M, LeBlanc AC (2004) Neuroprotective functions of prion protein. J Neurosci Res 75:153-161.

Sailer A, Bueler H, Fischer M, Aguzzi A, Weissmann C (1994) No propagation of prions in mice devoid of PrP. Cell 77:967-968.

Sakaguchi S, Katamine S, Nishida N, Moriuchi R, Shigematsu K, Sugimoto T, Nakatani A, Kataoka Y, Houtani T, Shirabe S, Okada H, Hasegawa S, Miyamoto T, Noda T (1996) Loss of cerebellar Purkinje cells in aged mice homozygous for a disrupted PrP gene. Nature 380:528-531.

Sakudo A, Onodera T, Suganuma Y, Kobayashi T, Saeki K, Ikuta K (2006) Recent advances in clarifying prion protein functions using knockout mice and derived cell lines. Mini Rev Med Chem 6:589-601.

Sakurai-Yamashita Y, Sakaguchi S, Yoshikawa D, Okimura N, Masuda Y, Katamine S, Niwa M (2005) Female-specific neuroprotection against transient brain ischemia observed in mice devoid of prion protein is abolished by ectopic expression of prion protein-like protein. Neuroscience 136:281-287.

Shastry BS (2003) Neurodegenerative disorders of protein aggregation. Neurochem Int 43:1-7.

Shmerling D, Hegyi I, Fischer M, Blattler T, Brandner S, Gotz J, Rulicke T, Flechsig E, Cozzio A, von Mering C, Hangartner C, Aguzzi A, Weissmann C (1998) Expression of amino-terminally truncated PrP in the mouse leading to ataxia and specific cerebellar lesions. Cell 93:203-214.

Shorter J, Lindquist S (2005) Prions as adaptive conduits of memory and inheritance. Nat Rev Genet 6:435-450.

Shyu WC, Lin SZ, Chiang MF, Ding DC, Li KW, Chen SF, Yang HI, Li H (2005) Overexpression of PrPC by adenovirus-mediated gene targeting reduces ischemic injury in a stroke rat model. J Neurosci 25:8967-8977.

Spudich A, Frigg R, Kilic E, Kilic U, Oesch B, Raeber A, Bassetti CL, Hermann DM (2005) Aggravation of ischemic brain injury by prion protein deficiency: role of ERK-1/-2 and STAT-1. Neurobiol Dis 20:442-449.

Steele AD, Jackson WS, King OD, Lindquist S (2007) The power of automated high-resolution behavior analysis revealed by its application to mouse models of Huntington's and prion diseases. Proc Natl Acad Sci U S A 104:1983-1988.

Thackray AM, Bujdoso R (2002) PrP(c) expression influences the establishment of herpes simplex virus type 1 latency. J Virol 76:2498-2509.

Valenti P, Cozzio A, Nishida N, Wolfer DP, Sakaguchi S, Lipp HP (2001) Similar target, different effects: late-onset ataxia and spatial learning in prion protein-deficient mouse lines. Neurogenetics 3:173-184.

Walz R, Amaral OB, Rockenbach IC, Roesler R, Izquierdo I, Cavalheiro EA, Martins VR, Brentani RR (1999) Increased sensitivity to seizures in mice lacking cellular prion protein. Epilepsia 40:1679-1682.

Walz R, Castro RM, Landemberger MC, Velasco TR, Terra-Bustamante VC, Bastos AC, Bianchin M, Wichert-Ana L, Araujo D, Alexandre V, Jr., Santos AC, Machado HR, Carlotti CG, Jr., Brentani RR, Martins VR, Sakamoto AC (2004) Cortical malformations are associated with a rare polymorphism of cellular prion protein. Neurology 63:557-560.

Walz R, Castro RM, Velasco TR, Alexandre V, Jr., Lopes MH, Leite JP, Santos AC, Assirati JA, Jr., Wichert-Ana L, Terra-Bustamante VC, Bianchin MM, Maciag PC, Ribeiro KB, Guarnieri R, Araujo D, Cabalero O, Moura R, Salim AC, Kindlmann K, Landemberger MC, Marques W, Jr., Fernandes RM, Serafini LN, Machado HR, Carlotti CG, Jr., Brentani RR, Sakamoto AC, Martins VR (2003) Surgical outcome in mesial temporal sclerosis correlates with prion protein gene variant. Neurology 61:1204-1210.

Watarai M, Kim S, Erdenebaatar J, Makino S, Horiuchi M, Shirahata T, Sakaguchi S, Katamine S (2003) Cellular prion protein promotes Brucella infection into macrophages. J Exp Med 198:5-17.

Weise J, Sandau R, Schwarting S, Crome O, Wrede A, Schulz-Schaeffer W, Zerr I, Bahr M (2006) Deletion of cellular prion protein results in reduced Akt activation, enhanced postischemic caspase-3 activation, and exacerbation of ischemic brain injury. Stroke 37:1296-1300.

Weissmann C, Aguzzi A (1999) Perspectives: neurobiology. PrP's double causes trouble. Science 286:914-915.

Weissmann C, Flechsig E (2003) PrP knock-out and PrP transgenic mice in prion research. Br Med Bull 66:43-60.

Weissmann C, Bueler H (2004) A mouse to remember. Cell 116:S111-113, 112 p following S113.

Whittington MA, Sidle KC, Gowland I, Meads J, Hill AF, Palmer MS, Jefferys JG, Collinge J (1995) Rescue of neurophysiological phenotype seen in PrP null mice by transgene encoding human prion protein. Nat Genet 9:197-201.

Wickner RB (1994) [URE3] as an altered URE2 protein: evidence for a prion analog in Saccharomyces cerevisiae. Science 264:566-569.

Yu G, Chen J, Yu H, Liu S, Xu X, Sha H, Zhang X, Wu G, Xu S, Cheng G (2006) Functional disruption of the prion protein gene in cloned goats. J Gen Virol 87:1019-1027.

Zuccato C, Ciammola A, Rigamonti D, Leavitt BR, Goffredo D, Conti L, MacDonald ME, Friedlander RM, Silani V, Hayden MR, Timmusk T, Sipione S, Cattaneo E (2001) Loss of huntingtin-mediated BDNF gene transcription in Huntington's disease. Science 293:493-498.

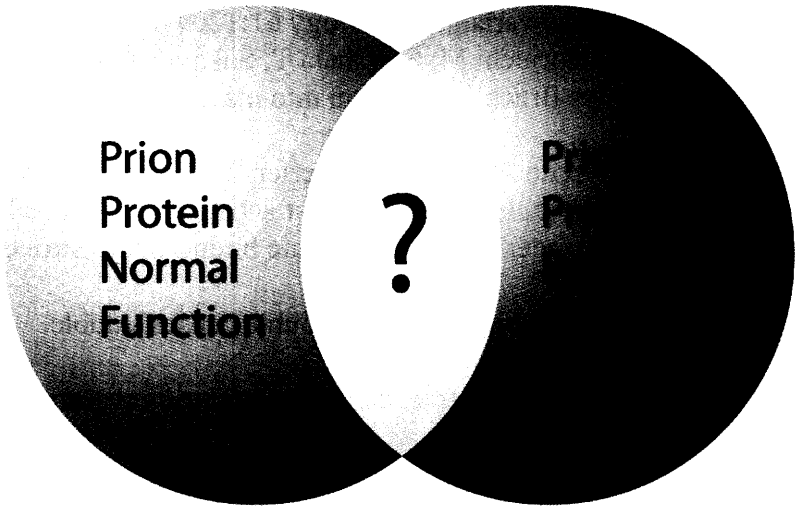

Figure 1 The overlap between the normal function of PrP^{C} and the pathogenic dysfunction of PrP^{Sc} in disease depicted as a Venn diagram. The extent of overlap between the normal function of PrP^{C} and its role in prion disease is open to speculation; the circles could have a much greater or perhaps even less overlap.

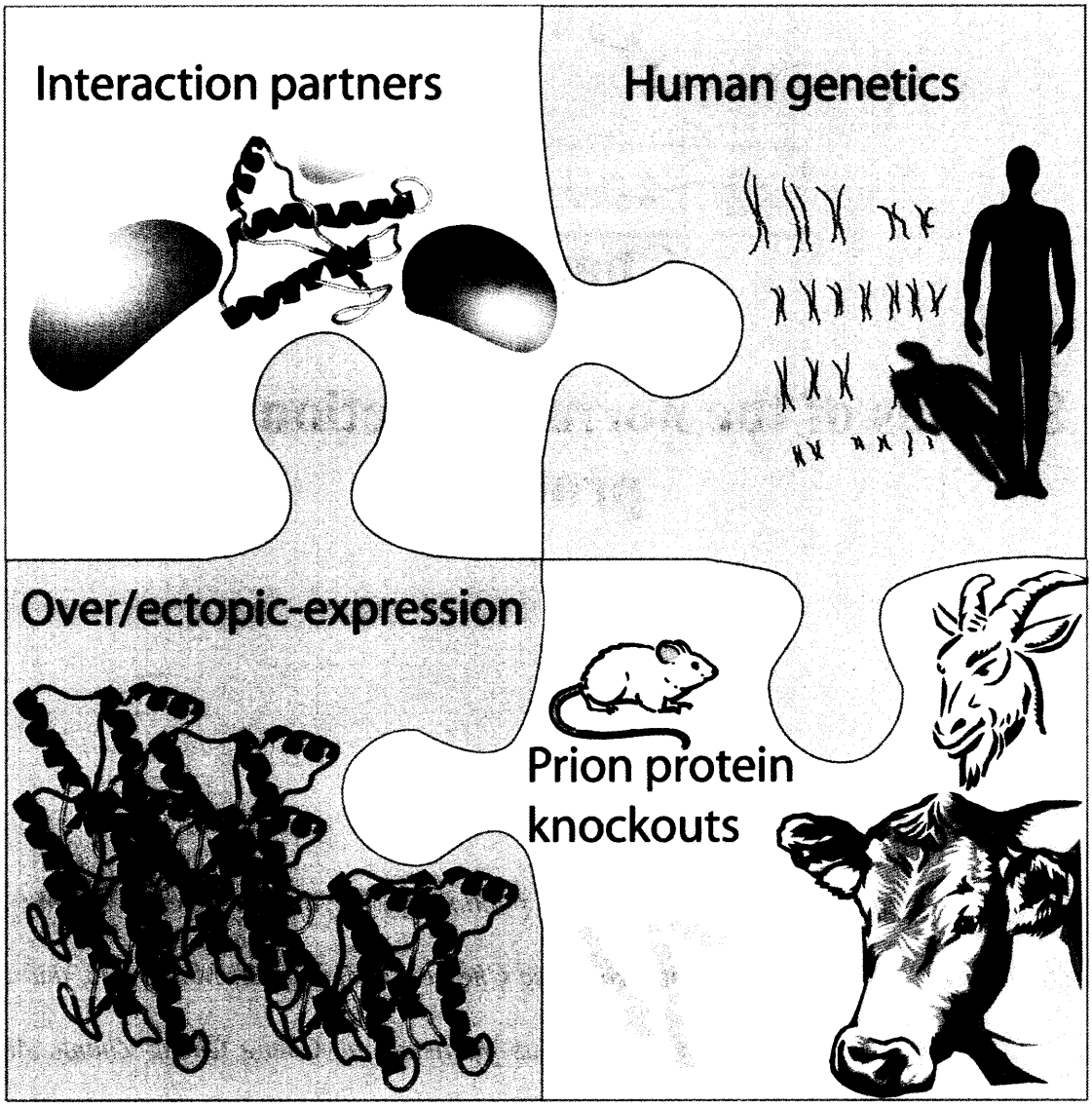

Figure 2 Different approaches to study PrP^C's normal function. There are many ways to approach the study of the normal function of PrP^C, none of which have conclusively demonstrated PrP^C's function. Interacting partners of PrP^C have yielded many interesting candidates, human genetic studies have found associations of PrP^C with diseases beyond prion disease and even to learning and memory, over- and ectopic expression studies constitute another approach to determine the function of PrP^C, and finally—the focus of this review—the PrP KO has given some clues to the function of PrP^C.

Chapter 2

Studies of the normal function of prion protein

Section 1 of this chapter will be submitted for publication by Andrew Steele, Zhipeng Zhou, Walker S. Jackson, Chunni Zhu, Marie-Francoise Chesselet, Michael A. Moskowitz, and Susan Lindquist. Much of Section 2 of this chapter was published by Cheng Cheng Zhang, Andrew Steele, Susan Lindquist, and Harvey Lodish (2006) PNAS *Vol. 103(7): 2184-89. The studies of aged PrP knockout mice will be submitted for publication by Andrew Steele*, Megan Kaba*, Cheng Cheng Zhang, Marian Hester, Mark Fleming, Susan Lindquist and Harvey Lodish. Section 3 of this chapter was published by Andrew Steele*, Jason Emsley*, Hande Ozdinler, Susan Lindquist, and Jeffrey Macklis (2006)* PNAS *Vol. 103(9): 3416-21*

(denotes equal contributors)*

I. PrP deletion in mouse models of neurodegeneration

Introduction

For more than twenty years an aberrant conformation of the prion protein (PrP) has been posited as the causative agent in prion diseases, yet the normal function PrP remains elusive. Numerous studies have suggested a neuroprotective function for PrP (discussed in Chapter 1). The conservation of PrP^C from fish to human (Rivera-Milla et al., 2006) suggests an important role for this protein in biology; however, deletion of PrP^C in the mouse (Bueler et al., 1992) or cow (Richt et al., 2006) does not result in an overt phenotype. Over the years, many phenotypes have been observed in the PrP KO, but most of them are subtle (Steele, 2007). Studies by several groups have demonstrated that PrP KOs are more susceptible to ischemic damage (McLennan et al., 2004; Spudich et al., 2005; Weise et al., 2006). In addition, PrP can protect against toxicity associated with ectopic expression of Doppel as well as truncated PrP mutants (Steele, 2007). Thus, under certain conditions PrP can protect cells and in other conditions (i.e. prion disease) cause neuronal dysfunction and death. Understanding the normal function of PrP may help elucidate the pathogenic chain of events that occur in prion disease.

Neurodegenerative diseases are among the most common affliction of the aged population; millions suffer worldwide from Alzheimer's disease (AD), Parkinson's disease (PD), Tauopathies, and Huntington's disease (HD) (Prusiner, 2001; Shastry, 2003). Neurodegenerative diseases usually manifest as clinically separable disorders where certain regions of the brain deteriorate, but one commonality is the presence of specific misfolded protein(s) (Aguzzi and Haass, 2003; Steele and Yi, 2006). PD is characterized by the aggregation of α-synuclein, a protein of unknown function, in structures called Lewy bodies and neuronal cell loss in *substantia nigra* of the midbrain as well as other areas of the brain (Norris et al., 2004). TP is

characterized by the accumulation of filamentous intraneuronal inclusions of the Tau protein, which interacts with microtubules (Forman et al., 2004). HD is a dominantly heritable, neurodegenerative disease characterized by a polyglutamine repeat expansion in the huntingtin protein and neuronal cell death in the striatum (Landles and Bates, 2004).

We conducted an experiment to answer the question: does the neuroprotective function of PrP extend to a broad spectrum of neurodegenerative diseases? To address this question we crossed transgenic models of Tauopathy, PD, and HD into a PrP KO background and followed the disease progression in comparison to transgenic neurodegenerative disease models with wild-type levels of PrP. We began by confirming the neuroprotective role of PrP in an acute ischemia model, where PrP deletion causes significantly higher levels of damage as measured by lesion volume and behavior (data not shown).

Results

Deletion of PrP in a transgenic model of Parkinson's disease

We utilized a mouse model of Parkinson's disease which over-expresses human α-synuclein driven by a plateled-derived grown factor-beta promoter (Masliah et al., 2000) (Table I). This mouse was reported to have loss of dopamenergic neurons, accumulation of α-synuclein aggregates, and motor dysfunction. However, our assessment of motor performance, using rotarod as conducted in the original description of these mice (Masliah et al., 2000), did not reveal much of a decline in motor performance in PrP WT α-synuclein Tg mice (Figure 1B). For example, the latency to fall off the accelerating rotarod was approximately 150 seconds at 5-8 months and even by 18 months the latency to fall had only decreased to approximately 100 seconds. We noted that there was a large variability in rotarod performance in this mixed genetic

strain (composed of C57Bl/6, DBA/2, and 129/Ola). We also noted a trend that PrP+/- and PrP-/- mice had worse motor performance from 12-18 months, but given the high variability within these groups and the fact that 19-21 months all the groups behaved similarly we concluded that the motor phenotype in the α-synuclein Tg was too weak and/or variable for us to properly address the question of PrP's contribution to this Parkinson's disease model.

We also assessed survival in the α-synuclein Tg with different PrP gene doseages. There were no significant differences between α-synuclein PrP +/+, +/-, or -/- in terms of survival (log rank test, Figure 1B). Most of these mice lived an apparently normal lifespan, although we did not include enough α-synuclein Tg-/- controls to conclusively prove this point.

Deletion of PrP in a transgenic model of Tauopathy

We utilized a transgenic model of tauopathy that expressed mutated human Tau (P301L) driven by a modified murine prion promoter (*Prnp*) promoter (Lewis et al., 2000). P301L Tau Tg mice were mated to PrP KO mice, the F_1 offspring that were PrP+/-, Tau Tg+/- were intercrossed to generate our experimental F_2 progeny. The P301L Tg mice develop a severe motor phenotype, where their hind limbs eventually become completely paralyzed (Lewis et al., 2000). We observed this phenotype but it was extremely variable in onset. The motor performance of the populations of Tau Tg+ PrP+/+, +/-, and -/- mice had a progressive decline in rotarod performance, but the kinetics of this decrease were indistinguishable between all groups of mice (Fig. 2B).

We also followed the survival of the P301L Tau Tg mice with different *Prnp* gene doseages. There were no statistically significant differences in the survival of any of the Tau Tg+

mice with 2, 1, or no copies of PrP (Figure 2A). However, there was a clear difference in survival between Tau Tg+ and Tau Tg-/- mice (both groups with WT levels of PrP) (data not shown).

Deletion of PrP in a transgenic model of Huntington's disease

We also tested whether PrP deletion would alter the phenotype of a mouse model of Huntington's disease. This transgenic mouse "R6/2" expresses the first exon of human Huntingtin with a polyglutamine stretch of approximately 115-150 repeats (CAG codons) (Mangiarini et al., 1996). These mice show severe motor impairments and dramatic weight loss (Mangiarini et al., 1996). We crossed HD Tg+ males (females are infertile) to PrP KO females, then intercrossed the F_1 offspring that were HD Tg+, PrP+/- (males) to HD Tg-, PrP+/- (females) to obtain our experimental F_2 animals.

We assessed survival in the HD Tg+ mice with differing PrP gene dosages. There were no significant differences in the survival of HD Tg+ PrP+/+, +/-, or -/- mice (log rank test) (Fig. 3A). We assessed motor impairment by testing these mice twice per week on an accelerating rotarod. Average values of these two weekly trials suggested that the motor impairment was slightly less severe in PrP null HD Tg+ mice (Fig 3B). This subtle rescue persisted from 6 weeks until 12 weeks, but by 13 weeks and beyond there were no differences in rotarod performance between groups. However, we also assessed other phenotypes of the R6/2 mouse—limb clasping and escaping—but did not note any differences between HD Tg+ PrP+/+ and HD Tg+ PrP-/- mice (Fig. 3C,D). In this test a mouse is held suspended by its tail and healthy mice will typically escape onto the fingers of the experimenter and almost never clasp their fore and hind limbs. HD Tg+ mice progressively develop the clasping phenotype and lose their ability to escape on to the experimenter's fingers, independent of PrP deletion (Fig. 3C,D). We also examined the brains of

HD Tg mice that were PrP+/+ or PrP-/-. Dramatic nuclear aggregates of huntingtin were osbserved by immunohistochemsitry with no notable differences between HD Tg+ PrP+/+ and HD Tg+ PrP-/- (Fig. 3 E,F). Thus, the HD Tg phenotype is mostly unaffected by PrP deletion with the exception of rotarod performance in an early phase of disease.

Transgenic overexpression of PrP in a transgenic model of Huntington's disease

Since we observed a subtle amelioration of the decline in rotarod performance in PrP null HD Tg+, we predicted that over-expression of PrP would enhance the HD Tg phenotype. To test this prediction, we crossed the well characterized PrP over-expression "Tga20" transgenic mouse (which with one copy of the PrP tansgene expresses approximately 4-5 fold more PrP than endogenous) (Fischer et al., 1996) to the R6/2 HD Tg.. We did not observe any effect on the survival of the R6/2 mice whether they expressed PrP at a wild type level or whether they overexpressed PrP (P=0.22, log rank test) (Fig. 4A). The motor performance as measured by rotarod was indistinguishable between HD+ PrP OE Tg+ mice and HD+ PrP OE Tg- mice (Fig. 4B). The clasping and escaping phenotype was also similar between HD mice that overexpress PrP and those that do not (Fig. 4C-D). From these experiments we concluded that PrP overexpression does not affect the HD phenotype.

Discussion

Although our experiment was specifically designed to test whether PrP has a protective function in a panel of neurodegenerative diseases, it also touches upon a broader question of whether there is cross-talk among aggregation prone proteins in neurodegenerative diseases. For example, deletion of Tau caused a remarkable rescue in beta-amyloid mouse model of

Alzheimer's disease (Roberson et al., 2007). Although the connection between beta-amyloid and Tau has a much more firm basis than that of PrP to Tau, alpha-synuclein, or huntingtin, there are several intriguing reports that show striking clinical overlap between prion diseases and other neurodegenerative diseases. Interestingly, a human HD phenocopy (a disease that is clinically indistinguishable from HD) is associated with a mutation in PrP (Nicholl et al., 1995; Moore et al., 2001). This suggests that a mutation in PrP may be sufficient to cause neuronal dysfunction in populations of neurons affected in HD, such as striatal neurons, resulting in the clinical manifestation of HD.

Mutations in PrP are also associated with some PD-like symptoms and neuropathology (Yamazaki *et al.*, 1999). Cases of concomitant CJD and PD have also been reported (Iida *et al.*, 2001). There are reports showing that mutations in PrP manifest clinically as Tauopathy and/or AD-like disorders (Nitrini *et al.*, 1997; Nitrini *et al.*, 2001). Furthermore, the deposition of neurofibrillary tangles of phosphorylated Tau protein, a pathological hallmark of AD, has been noted in many cases of prion disease linked to mutations in PrP or sporadic CJD (Ishizawa et al., 2002; Amano et al., 1992; Ikeda et al., 1994; Yamazaki et al., 1999; Ghetti et al., 1989; Hsiao et al., 1992). Another major pathological hallmark of AD, β-amyloid plaques, has also been found in patients with prion diseases (Barcikowska et al., 1995). Moreover, PrP is found in β-amyloid aggregates in some AD patients (Ferrer et al., 2001). A detailed pathological study attempted to detect co-aggregation of PrP with α-synuclein, Tau and β-amyloid aggregates in humans with prion disease, PD, and AD (Kovacs et al., 2002). PrP-Tau and PrP- α-synuclein co-localize in early inclusions, but do not co-aggregate (Kovacs et al., 2002). While it is possible that misdiagnosis and disease heterogeneity could account for these clinical and pathological reports, PrP could also play a broader role in neurodegenerative diseases than previously appreciated.

In summary, deletion of PrP in a panel of neurodegenerative disease models did not appreciably alter the respective disease phenotypes. The only disease model where we observed a subtle effect was the "R6/2" HD Tg, where there was a delayed impairment of motor performance. However, the other phenotypes of R6/2, such as survival, were unaffected and transgenic overexpression of PrP did not affect the R6/2 phenotype. In addition, we crossed the PrP knockout to a different transgenic model of HD (Schilling et al., 1999) and did not observe any effect on the motor performance or survival of HD model when it was wild type or null for PrP (data not shown). Thus, our tentative conclusion is that PrP does not have a major effect on the progression of disease in the models that we tested.

Materials and Methods

Mouse strains and genotyping:

PrP KO mice (Manson et al., 1994) were crossed once to C57BL/6 for embryo transfer rederivation. Previously they had been maintained on a mixed 129/Ola and C57Bl/10 hybrid background. The genetic background thus represents 129/Ola (original) and C57BL6. The "JNPL3" tau mutant (P301L) (Lewis, et al.) was obtained from Taconic Farms. The PD mouse (Masliah, et al.) was kindly provided by B. Hyman. C57Bl/6xDBA/2. The "R6/2" (Mangiarini et al., 1996) polyglutamine expanded HD mouse was obtained from Jackson Laboratories as ovarian transferred females.

The genotyping DNA was extracted from proteinase K digested tail tips using DNAeasy kit according to manufacturer's instructions (Qiagen). To amplify for PrP and or the KO allele is described in (Steele et al., 2006). To amplify the P301L tau transgene, primers were used 5'TGAACCAGGATGGCTGAGC3' and 5'TTGTCATCGCTTCCAGTCC3'. The R6/2 and

alpha-synuclein mice were genotyped as previously described (Mangiarini et al., 1996; Masliah et al., 2000).

The breeding strategy used to generate experimental mice was to cross PrP KO mice to mice transgenic for mutant Tau, human a-synuclein, and mutant HD transgenes. The F1 progeny that were hemizygous for the PrP KO allele and transgenic for the disease transgene were intercrossed. Expected Mendelian ratios of progeny were obtained from F1 interecrosses of PD and HD mice, but there was a lack of PrP null mice in the Tauopathy crosses perhaps due to a synthetic lethality between an allele in the Tau mouse genetic background and the PrP KO (see appendix)

Behavioral Analysis

HD were weighed, rotarod tested, and clasp tested twice weekly, beginning at 6 weeks of age (+/- 1 week). Mutant Tau Tg mice were tested weekly, beginning at 10 weeks old (+/- 2 weeks) then tested bi-weekly once the mice reached 6 months old. PD mice were tested biweekly, beginning at 6 months old (+/- 2 months). All mice were tested on an Ugo Basile accelerating rotorod, which was modified by placing a rubber bike inner tube on the on the rod to prevent gripping. Mice were placed on the rotarod, then the rotarod was accelerated after 5 seconds for Tau, PD, and HD (R6/2). The amount of time the mice remained on the rotarod was recorded. HD mice were also tested for the 'clasping' phenotype (Mangiarini et al., 1996). Mice were sacrificed when they were moribund as determined in consultation with our veterinary staff. Tauopathy mice developed a severe hindlimb paresis and were sacrificed when they could not ambulate. HD mice were sacrificed when their body condition reached 1-2; many mice were found dead or died when being handled from severe seizures. PD mice were sacrificed when they displayed low body condition.

II. Prion protein promotes the self-renewal of hematopoeitic stem cells during serial transplantation and aging

Introduction

The difficulty in purification and study of hematopoietic stem cells (HSCs) is hampered by our limited understanding of the proteins that are specifically expressed on their surface (Spangrude et al., 1988; Jordan et al., 1990; Rebel et al., 1996). Furthermore, few HSC markers are of functional significance for HSC activity (Chen et al., 2003b). We characterized a novel population of mouse fetal liver cells that support the *ex vivo* expansion of HSCs, and showed that they express abundant amounts of prion protein (PrP) (Zhang and Lodish, 2004). PrP is a highly conserved glycoprotein tethered to cell membranes by a glycosylphosphatidylinositol (GPI) anchor that is expressed on hematopoietic cells as well as in many tissues including brain, heart, and muscle (Aguzzi, 2000; Vostal et al., 2001b). Although it is well established that PrP is the primary component of infectivity in prion diseases (Prusiner, 1998), its normal function(s) remains obscure. Several roles for PrP have been suggested, including copper uptake, cell signaling, cell survival, protection against oxidative stress, cell adhesion, and differentiation (Lasmezas, 2003). However, PrP null mice exhibit no consistent, overt, phenotype other than resistance to infection with prions (Weissmann and Flechsig, 2003). Here we demonstrate that PrP is a novel surface marker for HSCs and is required for their self-renewal, as judged by successive bone marrow transplantations.

Results

PrP is a marker for LT-HSCs.

Preliminary studies showed that 40% of adult mouse bone marrow (BM) cells express PrP on their surface. Over 80% of these PrP^+ cells were erythroid cells as they expressed the glycophorin-related surface protein Ter119 ($Ter119^+$) (data not shown). In Figure 5 the expression of the PrP protein was monitored on the surface of wild-type (WT) mouse BM cell populations that were progressively enriched for HSCs. One way to enrich HSCs is isolation of the side population (SP) fraction of adult bone marrow cells, which is identified by low accumulation of the dye Hoechst 33342 (Goodell et al., 1996). Fig. 5A, plot 4 shows that PrP was expressed on 47.1 ± 5.4 % of SP cells (n = 6).

All HSCs in the SP population express Endoglin (Chen et al., 2003a), an ancillary TGF-ß receptor. Of the $Endoglin^+$ SP cells, 56.4 ± 12.0% also expressed PrP (Table S1 and Fig. 5A, plot 5). Sca-1 is another well-established surface marker for HSCs (Okada et al., 1992). Of the $Sca\text{-}1^+$ SP cells 50.9 ± 12.4% also expressed PrP (Table S1, Fig. 5A, plot 6). Furthermore, virtually all of the PrP^+ SP cells also expressed other cell adhesion molecules that are expressed on HSCs or early hematopoietic progenitors, including CD43, CD44, CD49D, and CD49E (Table S1, Fig. 5A, plots 7-10, respectively). In contrast, CD11A and CD62L, antigens not expressed on HSCs (Orschell-Traycoff et al., 2000), were expressed on only 27% (= 13/(13+34)) and 9% (= 4/(4+41)), respectively, of the PrP^+ SP cells (Fig. 5A, plots 11-12).

To further test PrP expression on the HSC enriched populations, we took advantage of two other features of HSCs. First, HSCs are lineage negative (Lin^-), that is, they do not express surface markers of differentiated erythroid, myeloid, or lymphoid cell lineages. Second, all HSCs do express the surface markers Sca-1 and Endoglin (Chen et al., 2003a) and thus are Lin^- $Sca\text{-}1^+$

Endoglin$^+$. Fig. 5B, plot 3, shows that, Lin$^-$Sca-1$^+$Endoglin$^+$ cells comprised 0.03% (= 0.05 x 0.006) of total BM cells; of these cells, 85.7% expressed surface PrP (plot 4). In contrast, of the non-HSC Lin$^-$Sca-1$^+$Endoglin$^-$ cell population (Chen et al., 2003a), only 22.8% expressed surface PrP (plot 5). Since one in eighteen Lin$^-$Sca-1$^+$ Endoglin$^+$ cells is a LT-HSC (Chen et al., 2003a), the expression of PrP on Lin$^-$Sca-1$^+$ Endoglin$^+$ cells, together with PrP co-expression on SP stained Sca-1$^+$ and Endoglin$^+$ cells, suggested that PrP might be a surface marker for LT-HSCs.

The ability to reconstitute the hematopoietic system of lethally irradiated mice is the hallmark of LT-HSCs. To determine if LT-HSCs indeed express surface PrP, we affinity-purified fractions from enriched BM HSC populations that do or do not express PrP on their surface, followed by reconstitution assays (Fig. 6). To examine the HSC activity of the donor cells in reconstitution analyses, lethally irradiated recipient mice were co-transplanted with both the donor cells to be tested and WT BM competitors. The competitor cells serve as an internal control and as a supply of hematopoietic cells until the transplanted stem cells can generate sufficient mature lymphoid and myeloid cells for survival. Donor and recipient mice are genetically identical except for the CD45 surface protein that is found on nucleated peripheral blood cells and that is not involved in hematopoiesis or stem cell activity; donor cells carried the marker CD45.2, while recipient mice and supportive cells expressed CD45.1.

In the study in Figure 6A, total adult CD45.2 BM cells were sorted according to their cell surface expression of PrP. PrP$^+$ and PrP$^-$ fractions were mixed separately with 1 x10^5 CD45.1 total BM cells and injected into lethally irradiated CD45.1 recipients. 1 x 10^5 PrP$^-$ donor cells exhibited a small measure of reconstitution at 4 weeks post-transplantation, which primarily measures short-term (ST)-HSC activity (Fig. 6A, Bar 1). In contrast, at 6 months post-transplant there were no peripheral blood cells derived from these donor PrP$^-$ cells (Bar 3), showing that

BM cells that do not express the prion protein lack LT-HSC activity. In contrast, 2 x 10^4 PrP^+ BM cells supported both ST and LT engraftment, as assayed by reconstitution of peripheral blood cells (Fig. 6A, Bars 2, 4). PrP^+ donor cells repopulated both lymphoid and myeloid compartments (Fig. 6B).

Next, HSC enriched $Lin^-Sca\text{-}1^+$ BM cells were sorted according to their expression of PrP. Of Lin^- cells, 0.8% and 5.2% are $Sca\text{-}1^+PrP^+$ and $Sca\text{-}1^+PrP^-$, respectively (data not shown). Competitive transplantation of 500 isolated $Lin^-Sca\text{-}1^+PrP^-$ cells resulted in significant repopulation after 3 weeks (Fig. 6C, Bar 1) but none after 4 months (Bar 3). In contrast, injection of only 100 $Lin^-Sca\text{-}1^+PrP^+$ CD45.2 donor BM cells resulted in significant reconstitution after both 3 weeks and 4 months (Bars 2 and 4, respectively). Each of the 5 recipient mice were engrafted, with frequencies of 5.1%, 1.4%, 27.6%, 2.5%, and 1.4% of peripheral blood cells. Thus, starting with a purified $Lin^-Sca\text{-}1^+$ HSC population, the subfraction of cells that express PrP on their surface contain all LT-HSCs.

Fig. 6D further shows that all LT-HSCs express PrP on their surface. SP cells were sorted based on PrP expression. SP cells that did not express PrP contained no LT-HSC activity while those that expressed PrP had significant activity (Fig. 2D). Thus, adult BM LT-HSC activity resides in the PrP^+ but not in the PrP^- fractions of both Lin^-Sca1^+ and SP populations. In the transplantation experiments in panels A and C we used 5 fold more PrP^- cells than PrP^+ cells. From the data in Panel A we conclude that the presence of surface PrP protein distinguishes those Lin^- $Sca\text{-}1^+$ cells that contain the LT-HSCs from those that do not. The ability of PrP^+ SP cells to repopulate all recipients coupled with no detectable LT-HSC activity in the PrP^-SP population (Fig. 6D) similarly suggests that all LT-HSCs express PrP. We conclude that PrP is a

marker for LT-HSCs. Like other LT-HSC markers, PrP expression is not exclusive to that cell type.

PrP is important for renewal of HSCs during serial transplantation or 5-fluorouracil stress

We asked whether PrP expression had a functional role in HSCs by utilizing mice ablated for PrP. The PrP null and WT control mice used in the first studies (Figs. 7 and 8) were backcrossed onto the C57BL/6J background 4 times (termed N4). First, we analyzed the nature and number of hematopoietic cells from WT and PrP null littermates (Manson et al., 1994). The hematocrits, hemoglobin levels, and total red and white blood cell levels in peripheral blood were similar in the PrP null and control mice (Table S2). Furthermore, BM cells were reacted with various lineage-specific antibodies and the cells were analyzed by flow cytometry; we found no differences in staining profiles between the two types of animals (data not shown), consistent with prior observations (Genoud et al., 2004). We assayed PrP null and WT BM cells for colony-forming units (CFUs) to look for defects in progenitor numbers or activities. PrP null and control BM had similar numbers of multipotential granulocyte/ erythroid/ monocyte/ megakaryocyte progenitors (CFU-GEMM), granulocyte/ monocyte progenitors (CFU-GM), erythroid progenitors (BFU-E), and B lymphoid (CFU-Pre-B) progenitors (Fig. 7A). In addition, the surface expression of seven important hematopoietic surface antigens on BM SP cells isolated from PrP null and WT mice was similar, as detected by flow cytometry analysis (Table S3). Thus, PrP deficient BM has normal levels of progenitors and terminally differentiated hematopoietic cells.

To determine whether PrP has a role in activity of HSCs, we used competitive reconstitution assays (Ito et al., 2003). Fig. 3B shows the competitive repopulation results pooled

from 3 independent experiments. 2 x 10^6 PrP null or WT CD45.2 BM cells were mixed with an equal number of competitor CD45.1 BM cells and transplanted into lethally irradiated CD45.1 recipients. If the PrP null or control WT donor CD45.2 BM cells functioned equivalently to the CD45.1 competitor, one would expect 50% of the peripheral blood cells in the recipient to express the CD45.2 protein. Indeed, both WT and PrP null donor cells exhibited about 50% reconstitution of peripheral blood 4 months post-transplant (Fig. 7B, Bars 1 and 2). This suggests that freshly isolated BM from PrP null and WT mice have similar HSC numbers and activities. We tested the serial engraftment capacity of PrP null HSCs by pooling BM cells from primary transplanted recipients and transplanting them into lethally irradiated secondary CD45.1 recipients. After 4 months, peripheral blood of the secondary recipients was analyzed for expression of the donor CD45.2 marker (Fig. 7B, Bars 3-4). Cells derived from original WT CD45.2 BM comprised 60 ± 4% of the nucleated peripheral blood cells. In contrast, cells derived from the original PrP null CD45.2 BM comprised only 29 ± 7% of the peripheral blood, a significantly lower number ($p < 0.005$, t-test) than observed with WT donors. The lineage profiles of the primary and secondary transplanted PrP null BM were normal (data not shown). Tertiary transplantations were carried out in the same manner. Again cells derived from the original PrP null BM showed significantly less engraftment than their WT counterparts (Bars 5-6, $p < 0.05$, t-test). Since the contribution of PrP null HSCs to the reconstitution of lethally irradiated recipients steadily decreased with each transplantation, relative to WT HSCs, we infer that PrP null HSCs have impaired self-renewal capabilities as analyzed by long-term serial transplantation.

Because the competitor CD45.1 cells used in the transplants in Figure 3B may have had untoward effects on the CD45.2 WT or PrP null cells, we carried out serial transplantation

without competitors. To this end 1 x 10^6 BM cells isolated from three PrP null or WT littermates were transplanted into lethally irradiated CD45.1 recipients. As expected all of the recipients survived (Fig. 7C, bars 1-2). Four months later, 5 x 10^5 BM cells from these primary recipients were pooled and transplanted into secondary recipients, and the same procedure was repeated in tertiary transplantations. After the secondary transplant 86% of the mice receiving WT BM survived, whereas only 57% of those receiving PrP null BM did (Fig. 7C, bars 3-4). A more striking difference in survival between PrP null and WT repopulated mice was noted following tertiary transplantation: 67% of transplanted mice receiving WT BM survived whereas none of the mice transplanted with null BM did (Fig. 7C, bars 5-6). In all cases flow cytometry analysis of the transplanted mice confirmed that the recipient BM derived exclusively from the donor cells (data not shown). The defect in the ability of PrP null BM to repopulate during serial transplantation was confirmed in a separate experiment in which a higher number of cells (1 x10^6 cells) from the secondary transplant were used to transplant lethally irradiated tertiary recipients. The survival curve confirmed the dramatically lower repopulation potential of PrP null BM after the tertiary transplantation (Fig. 7D, $p < 0.0001$, log-rank test).

Since the PrP null mice used in these studies were only backcrossed four times into the C57BL/6J background, it remained possible that some genetic difference linked to the PrP locus was responsible for the observed differences in serial transplantation. Thus, in the experiment depicted in Figure 3C, Bars 7-9, we used a retroviral vector to introduce PrP into the PrP null BM cells isolated from the secondary transplanted recipients. The efficiency of infection was 30-50% (Fig. S1); specifically, 1 x 10^6 cells were infected and transplanted into lethally irradiated recipients. Consistent with the data in bar 5, none of the mice transplanted with BM infected by the control GFP vector survived (Fig. 7C, bar 7). In contrast, half of the mice transplanted with

the same BM but expressing exogenous PrP survived (Fig. 7C, bar 8 and fig. S2, $p < 0.05$, log-rank test). In another control experiment, the same BM cells were infected with a retrovirus encoding a mutant PrP with deletion of amino acids 23-72, the segment that contains the N-terminal octapeptide repeats (Roucou et al., 2004). None of the mice transplanted with BM expressing this mutant PrP protein survived (Fig. 7C, bar 9 and fig. S2). This deletion might also remove amino acids that may be essential for the internalization or the proper signal peptide processing (Sunyach et al., 2003; Taylor et al., 2005) and further study is needed to characterize the nature of PrP sequence critical for supporting PrP's HSC engraftment. However, this complementation experiment demonstrates that full-length PrP supports hematopoietic engraftment during long-term transplantation. It will be interesting to further study whether the hematopoietic rescue is PrP dose dependent, and whether overexpression of PrP in WT bone marrow gains better serial engraftment capacity.

The competitive reconstitution experiment in Figure 3E confirms our conclusion that the defects observed in the PrP null BM during serial transplantations indeed are due to defects in HSC renewal. BM from the initially transplanted mice used in Figure 7C, bars 1 and 2, was mixed with 5×10^5 freshly isolated BM cells from WT CD45.1 mice and transplanted into irradiated WT CD45.1 recipients. Consistent with impaired survival of HSCs, the PrP null cells showed $4.4 \pm 0.8\%$ repopulation as short-term (ST)-HSC activity (6 weeks) and $2.2 \pm 0.5\%$ repopulation as LT-HSC activity (5 months). Both figures were significant lower than that obtained from their WT counterparts ($23.8 \pm 4.0\%$ and $6.1 \pm 1.0\%$ respectively, Fig. 7E, $p < 0.05$, t-test).

As noted, the experiments depicted in Figure 3 were performed using PrP null and WT mice that were backcrossed to C57 BL/6J background 4 times. To confirm the notion that PrP is

important for hematopoietic engraftment under stress we also used mice backcrossed 6 times (termed N6). Similar HSC frequencies (Figs. S3A and S3B) and activities (fig. S3C, bars 1-2) were observed in freshly isolated N6 PrP null and WT BM cells as well as in purified BM SP cells. In parallel, we infected freshly isolated PrP null BM cells with PrP/GFP or control GFP retrovirus and collected the GFP positive cells by flow cytometric sorting. Again, there was no significant difference in HSC activities between the PrP infected and GFP infected BM measured by competitive reconstitution (Fig. S3C, bars 3-4). These results confirm that PrP is not required for the HSC activity in normal unstressed mice.

We further compared the HSC activities of N6 PrP null and WT BM after the stress of serial transplantation. As for Fig. 7E, we transplanted N6 PrP null or WT BM cells without competitors into irradiated recipients. Three months later, the transplanted BM cells were collected and their HSC activities were measured by competitive reconstitution. PrP null BM cells showed 2.2 ± 0.9% engraftment, significantly lower than that from WT cells, which had 5.9 ± 1.4% engraftment (fig. S3D, bars 1-2, $p < 0.05$, t-test). In parallel we infected N6 PrP null BM cells with either a PrP/ GFP or control GFP retrovirus population, isolated the GFP positive population, and then transplanted the cells without competitors into irradiated recipients. Three months later, the transplanted BM cells were collected and their HSC activities were measured in secondary transplants by competitive reconstitution (Fig. S3D, bars 3-4). Consistent with the results in bars 1-2, the expression of PrP increased the HSC activity of prion null BM (bar 3: 1.8 ± 0.4% engraftment by control GFP infected cells, bar 4: 4.8 ± 1.9% engraftment by PrP infected cells, $p < 0.05$, t-test). We conclude that while the absence of PrP does not affect HSC activity in normal unstressed mice, it is important for renewal of HSC activity that occurs under the stress of serial bone marrow transplantation.

To further test the notion that PrP deficiency leads to a defect in the stress response of hematopoietic cells, we treated mice with 5-fluorouracil (5-FU), which is toxic to cycling cells and accelerates the entry of HSCs into the cell cycle (Cheng et al., 2000). Isogenic WT mice reconstituted with either PrP null or control BM were treated with 5-FU at one month post transplantation. The survival of mice repopulated with PrP null BM was significantly lower than those reconstituted with wild-type cells (Fig. 8A, $p < 0.05$, log-rank test). Repeated experiments showed similar results (data not shown).

We verified that PrP was still expressed on the surface of wild-type HSCs after 5-FU stress; in this experiment, BM cells from 5-FU treated wild-type mice were sorted into PrP^+ and PrP^- fractions. Competitive repopulation assays showed that, as in normal BM, PrP^+ cells contain all the HSC activity (Fig. 8B). The 5-FU- treated mice used in the study in Panel A were wild type in all tissues except for their hematopoietic system, which was of either wild-type or PrP null origin. Thus the difference in survival after 5-FU treatment is due only to the presence or absence of the PrP on hematopoietic stem or early progenitor cells. Therefore, consistent with its role of supporting sustained LT-HSC self-renewal in serial transplantation, PrP protects hematopoietic cells from exhaustion by toxic agents such as 5-FU.

Aged PrP Knockouts Have Decreased Repopulating Potential

Based on our results with serial transplantation analysis, we hypothesized that aged PrP KOs would have a decreased HSC number as they aged, since during the aging process HSCs are constantly self-renewing. We aged PrP KO and WT controls to 16 to 20 months then performed competitive reconstitution analysis also including young (2 to 4 month old) PrP WT and KO bone marrow in parallel. We observed that young PrP WT and KO mice had similar

reconstituting activity, consistent with our prior observations (Fig. 7). On the other hand, the aged PrP KOs had a diminished repopulating potential, reconstituting only half as well as aged expected (data is normalized to young WT) ($P<0.01$, Student's T test) whereas aged WT BM was equal to young BM in reconstituting lethally irradiated recipients (Figure 9). In addition to examining repopulating activity, we also performed a complete blood count on peripheral blood from young PrP WT, young PrP KO, aged PrP WT, and aged PrP KO mice. Almost all parameters were indistinguishable between all groups of mice (young and old, PrP WT and PrP KO), such as red blood cell counts (shown in Fig. 10B). However, the aged PrP KO mice had a depletion of white blood cells ($P<0.05$, Student's T test). Future studies will examine which types of white blood cells are depleted.

Discussion

Previous work showed that several types of blood cells express PrP, albeit at vastly different levels: lymphocytes, dendritic cells, monocytes, granulocytes, erythrocytes, platelets, certain lymphoid precursors, and $CD34^+$ cells, which in humans are an enriched stem/progenitor cell population (Dodelet and Cashman, 1998; Liu et al., 2001; Vostal et al., 2001a; Risitano et al., 2003). However, it was unknown whether PrP is expressed on HSCs with repopulating activity, and there was no indication of a possible function of PrP in any of these cells. We demonstrated that PrP is located on the surface of HSCs and supports their engraftment during serial transplantation. Thus, using antibodies to PrP, together with other HSC markers, it may be possible to devise novel protocols for purifying human HSCs.

Other GPI-anchored proteins, including Sca-1 (Ito et al., 2003) and possibly CD59 (Hill et al., 1996) are also expressed on HSCs. Similar to PrP, Sca-1 is also required for HSC self-

renewal (Ito et al., 2003). Like other GPI-anchored proteins (Horejsi et al., 1999), PrP has been reported to localize to lipid rafts in the plasma membrane (Naslavsky et al., 1997) and it might regulate certain signaling proteins that are also concentrated in these domains. Indeed, PrP has been reported to be involved in activation of Fyn tyrosine kinase (Mouillet-Richard et al., 2000) and to interact with laminin, the laminin receptor, and stress-inducible protein 1, as well as other proteins (Lasmezas, 2003). Like the GPI- anchored alpha subunit of the ciliary neurotrophic factor receptor (Stahl et al., 1994), PrP might be the co-receptor for a hormone affecting HSC activity, possibly concentrating this as yet unidentified molecule on the cell surface and/or presenting it to the signaling receptor(s). In this function PrP might protect HSCs from apoptosis or sustain their long-term self-renewal. Alternatively, PrP might interact with proteins in the BM extracellular matrix or on the surface of stromal cells, and possibly support retention of transplanted HSCs within the BM microenvironment. Our work opens an avenue of investigation that may illuminate the details of the normal function of PrP in cell biology.

Materials and Methods

Mouse strains and genotyping

CD45.1 and CD45.2 C57BL/6 mice were purchased from the Jackson Laboratory or the National Cancer Institute. The PrP knockout mice (Manson et al., 1994) were provided by Drs. R. Race and B. Chesebro (RML), and backcrossed to C57 BL/6J CD45.2 mice at least 4 times or 6 times (indicated in text and figure legends) to obtain PrP null and WT control littermates. To genotype mice, DNA was extracted from proteinase K- digested tail tips using a DNAeasy kit according to the manufacturer's instructions (Qiagen). The PrP and/or neomycin (neo) insert was

amplified in a 4-primer PCR using primers 5'TCATCCCACGATCAGGAAGATGAG3' and 5'ATGGCGAACCTTGGCTACTGGCTG3' for PrP and 5'TTGAGCCTGGCGAACAGTTC3' and 5'GATGGATTGCACGCAGGTTC3' for the neomycin insert. The cycling conditions were 94° C for 3 minutes, followed by 30 cycles of 94 ° C for 30 seconds, 62 ° C for 30 seconds, and 72 ° C for 1 min, followed by a final extension of 72 ° C for 10 minutes.

Flow cytometry

Donor BM cells were isolated from 7-10 week old mice. Anti-PrP mAb (SAF-83, Cayman Chemical, Ann Arbor, MI) was FITC-conjugated using the Quick-Tag FITC conjugation kit (Roche). Its specificity was verified by its inability to bind to PrP null cells and its specific binding to cell lines expressing transfected prion protein (data not shown).

SP cells were stained with Hoechst 33342 dye as described (Goodell et al., 1996). In Fig. 1A, Hoechst stained cells were then co-stained with anti-PrP-FITC and PE conjugated anti-Sca-1, CD43, CD44, CD49D, CD49E, CD11A, or CD62L antibodies (BD Pharmingen). When Endoglin was detected, Hoechst 33342 stained cells were subsequently stained with anti-Endoglin mAb (BD Pharmingen), anti-rat-PE, and anti-PrP-FITC. In Fig. 1B, the cells were stained first with anti-Endoglin mAb (BD Pharmingen) followed by anti-rat-PE/CY5.5 (eBioscience), a biotinylated antibody cocktail recognizing multiple hematopoietic lineage markers (StemCell Technologies), as well as streptavidin-APC, anti-PrP-FITC, and anti-Sca-1-PE (BD Pharmingen). In Fig. 2, cells were stained with anti-PrP-FITC (Fig. 2A and Fig. 2B), or biotinylated multilineage antibody cocktail followed by streptavidin-APC, anti-PrP-FITC, and anti-Sca-1-PE (Fig. 2C). In Fig. 2D, the staining was the same as in Fig. 1A, plot 4.

The peripheral blood analysis after reconstitution was performed as described previously (Zhang and Lodish, 2004). Peripheral blood cells were stained with anti-CD45.2-FITC, and anti-

CD45.1-PE. Anti-Thy1.2-PE, anti-B220-PE, anti-Mac-1-PE, anti-Gr-1-PE, and anti-Ter119-PE monoclonal antibodies (BD Pharmingen) were used for detecting specific hematopoietic lineages. FACS analyses were performed on a FACSCalibur® instrument. Cells were sorted in a MoFlo® cell sorter. The purity of sorted cells was typically higher than 90%.

Reconstitution analysis

The reconstitution protocol was essentially as described (Zhang, 2004 #29). Briefly, the indicated numbers of CD45.2 donor cells were injected directly, or after mixing with 1 x 10^5 or 2 x 10^5 or 5 x 10^5 (as indicated) freshly isolated CD45.1 competitor BM cells, intravenously into a group of 6 to 9 week old CD45.1 mice that had been irradiated with a total dose of 10 Gy. To measure reconstitution of transplanted mice, peripheral blood or BM was collected by at the indicated times post-transplant and the presence of $CD45.1^+$ and $CD45.2^+$ cells in lymphoid and myeloid compartments were measured. The calculation of CRUs in limiting dilution experiments was conducted as described (Zhang and Lodish, 2004), using L-Calc software (StemCell Technologies).

Colony assays

PrP null or WT BM cells were diluted to $2x10^5$/ml in IMDM with 2% FBS, and then were seeded into methylcellulose medium M3434 (StemCell Technologies Inc) for CFU-GEMM, CFU-GM, and BFU-E colony formation, or into M3630 (StemCell Technology Inc) for CFU-pre-B colonies, according to the manufacturer's protocols.

Retrovirus Infection

Mouse PrP (Δ23-72) was constructed by ligating the PCR products of PrP1-23 and 72-254 and inserting into XZ201 (a MSCV-IRES-GFP vector, gift from Dr. Xiaowu Zhang, Whitehead Institute, Cambridge, MA). Mouse PrP or PrP (Δ23-72) cDNA was cloned upstream of the internal ribosomal entry site (IRES) in XZ201. The retroviral plasmids were transfected using lipofectamine 2000 (Invitrogen) into BOSC packaging cells. The resulting retroviral supernatant was collected 48 hours later and was used for infection. To this end BM cells were resuspended in viral supernatants (2×10^5 cells/mL) with 6 μg/ml polybrene and centrifuged at 2000 rpm for 90 min before culturing for 24 hours in StemSpan (StemCell Technologies, Inc.) in the presence of 10 μg /ml heparin, 10 ng/mL SCF, 20 ng/ml TPO, 20 ng/ml IGF-2, and 10 ng/ml FGF-1 (Zhang and Lodish, 2005). Cells were then resuspended in viral supernatant for another round of infection. Cells were then used directly for transplantation or cultured for another 4 days before sorting.

5-Fluoruracil challenge

In Fig. 8A, 5×10^5 PrP null or wild-type BM cells were used to reconstitute 10 Gy-irradiated CD45.1 C57BL/6 mice; there were 11 mice in each group. At 1 month post-transplant, 5-FU was administered i.p. at a dose of 150 mg/kg weekly for 2 weeks. The survival rates of the two groups were analyzed using a log-rank test (GraphPad Prism). In Fig. 4B, a single dose of 150 mg/kg body weight of 5-FU was injected i.p. into CD45.2 C57BL/6 mice (n = 3). After 3 days, the BM was pooled and subjected to FACS staining and sorting before competitive repopulation (n = 5).

III. Prion protein positively regulated neural precursor proliferation during developmental and adult mammalian neurogenesis

Introduction

The mammalian prion protein (PrP^c) has been intensively studied for its role in mammalian neurodegenerative disorders such as Creutzfeldt-Jakob disease and the transmissible spongiform encephalopathies (Prusiner, 1998; Aguzzi and Heikenwalder, 2006). Suggested roles for PrP^c, an N-linked glycoprotein tethered to the cell membrane by a GPI anchor, include cell signaling, survival, adhesion, and differentiation (Steele, 2007). Despite these putative roles for PrP^c, mice that are null for PrP^c exhibit no consistent, overt phenotype other than resistance to infection with prions, the infectious agent in the transmissible spongiform encephalopathies (Bueler et al., 1993). Recent work has shown that PrP^c induces polarization in synapse development as well as in neuritogenesis in embryonic hippocampal neuron cultures (Kanaani et al., 2005; Lopes et al., 2005). PrP^c is also up-regulated following focal cerebral ischemia (Weise et al., 2006) and PrP^c over-expression reduces the extent of neuronal loss following ischemic insult, suggesting that PrP^c might confer a neuroprotective effect in certain contexts (Shyu et al., 2005). Recent studies have also shown that PrP^c is expressed on the surface of long-term repopulating hematopoietic stem cells (HSC) and that PrP^c null mice have limited HSC self-renewal (Zhang et al., 2006).

Given the role of PrP^c in HSCs and its abundant expression in the developing and adult mammalian central nervous system (CNS), we investigated the role of PrP^c in neural development and in adult neurogenesis, which occurs constitutively in the dentate gyrus (DG) of the hippocampus and in the olfactory bulb from precursors in the subventricular zone (SVZ)/rostral migratory stream (RMS) (Emsley et al., 2005). We performed analyses of PrP^c

knockout (KO), wild-type (WT), and over-expresser (OE) mice to investigate loss- and gain-of-function. Using immunocytochemistry, *in vitro* analyses of embryonic neural precursor cultures, *in vivo* cell birth-dating approaches, and morphometry, we find that PrP^c expression is neuronal specific in differentiated neural cells, and that it increases multipotent neural precursor differentiation *in vitro* and proliferation in neurogenic regions *in vivo*. Our results describe, for the first time, an important role for the normal prion protein in neurogenesis of the developmental and adult mammalian CNS.

Results

Prion protein (PrP^c) expression increases as neurons mature, but it is not detected in astroglia or oligodendroglia

We investigated PrP^c protein expression in the developing and mature CNS, both *in vitro* and *in vivo*. PrP genotypes were confirmed by PCR, and PrP^c protein expression was verified by Western blots (Fig. 11A); the specificity of the PrP^c polyclonal antibody used for immunohistochemistry was confirmed by abundant staining in PrP OE brain and a lack of staining in PrP^c KO brain (Fig. 11B,C). *In vivo*, we observed that PrP^c is expressed most strongly immediately adjacent to the proliferative region of the subventricular zone (SVZ), but not in mitotic cells (Fig. 12,B). We also find that PrP^c expression increases in fully differentiated, mature neurons. Both *in vivo* and *in vitro*, PrP^c is found in increasing amounts as neuronal differentiation progresses: lowest in a subset of nestin-positive multipotent neural precursors; more in beta-III tubulin (TuJ1)- and doublecortin (Dcx)-positive immature neurons and in Hu (RNA binding protein)-positive early postmitotic neurons; and highest in mature neurons identified by NeuN and MAP-2 expression. *In vivo*, PrP^c is found at highest levels in mature

neurons (Fig. 2C) but it is not detected in astroglia (Fig. 12D). Similarly, PrP^c expression *in vitro* is highest in mature, MAP-2-positive neurons (Fig. 12E), but it is not expressed in recently generated S100β-positive astroglia (Figure 12F) or O4-positive oligodendroglia (data not shown).

PrP^c levels directly correlate with differentiation of multipotent neural precursors *in vitro*

We isolated multipotent neural precursors from PrP^c knockout (KO), wildtype (WT), and over-expresser (OE) embryonic (E13.5) mice to investigate the developmental role of PrP^c in proliferation and subsequent production of differentiated neurons and glia (Johe et al., 1996). Embryonic neural precursors express the intermediate filament protein nestin and, following withdrawal of basic fibroblast growth factor (bFGF) (Kilpatrick and Bartlett, 1993), nestin-positive precursors give rise to immature neurons, followed by astroglia, and then oligodendroglia (Reynolds et al., 1992; Richards et al., 1992; Panchision et al., 1998).

We find that PrP^c levels are positively correlated with differentiation of nestin-positive multipotent neural precursors. One day after inducing differentiation of neural precursors (termed "1 day *in vitro*" (1 DIV)), approximately 75% of WT cells express nestin (Figures 13A). Over the next several days *in vitro*, during which nestin-positive precursors produce neurons, astroglia, and oligodendroglia, the number of such precursors declines so that, by 7 DIV, only a very low percentage (< 5%) remains. In contrast, nestin-positive multipotent precursors derived from PrP^c null mice remain undifferentiated for much longer, whereas those derived from OE mice leave their multipotent state more rapidly than they do in WT cultures (Figure 13A). For example, three days after inducing differentiation (3 DIV), 48 ± 2% of cells in PrP^c KO cultures are still multipotent precursors, compared with 34 ± 2% in PrP^c WT and 17 ± 1% in PrP^c OE

cultures (standard error of the mean (SEM), $P < 0.001$). However, by 7 DIV, the multipotent precursor populations are depleted in all three conditions. Taken together, these results suggest that PrP^c levels directly increase the rate of multipotent precursor differentiation.

PrP^c increases the rate of neuronal differentiation in a dose-dependent manner

Concomitant with its positive effect on the differentiation of multipotent neural precursors, PrP^c increases the production of mature neurons (Fig. 13B). For example, five days after induction of differentiation (5 DIV), 26 ± 1% of cells are MAP-2-positive neurons in PrP^c OE cultures, compared with 18 ± 2% in PrP^c WT (SEM; $P < 0.05$) and 14 ± 1% in PrP^c KO cultures (SEM; $P < 0.001$). The proportion of mature neurons in PrP^c KO animals remains lower than in WT and OE conditions, even after 7 DIV. However, PrP^c KO derived multipotent neural precursors are still capable of generating neurons, suggesting a delay in differentiation rather than a failure to differentiate (Fig. 13B). In marked contrast with its direct effect on neuronal differentiation, PrP^c has no effect on gliogenesis; after 3 DIV, for example, the percentage of S100β-positive astroglia is 27 ± 4%, 24 ± 2%, and 25 ± 3% in PrP^c KO, WT, and OE cultures, respectively.

PrP^c increases cellular proliferation *in vivo*

In the adult CNS, both the SVZ and DG contain multipotent neural precursors. We investigated the effect of PrP^c levels on proliferation in these regions by quantifying the number of mitotic cells one hour after giving PrP^c KO, WT, and OE mice pulse labels of the thymidine analog BrdU.

PrP^c levels increase cellular proliferation in both adult neurogenic regions. In the SVZ, PrP^c OE mice have significantly more proliferating cells compared with WT or KO mice; specifically, PrP^c OE mice have an average of 79 ± 3 cells in each of 101 counted regions of the SVZ (n= 9 mice), compared with PrP^c WT (65 ± 2 cells in 209 counted regions, n = 9) and PrP^c KO mice (60 ± 3 cells in 83 counted regions, n = 11) ($P < 0.01$) (Fig. 14A). Similarly, in the DG, PrP^c OE and WT mice have significantly more proliferating cells compared with KO mice; PrP^c OE mice have an average of 8 mitotic cells (in each of 188 counted regions of the DG, n = 9), as do PrP^c WT mice (in each of 154 counted regions, n = 9), compared with PrP^c KO mice, which have an average of 6 cells (in each of 160 counted regions, n = 11) ($P < 0.001$) (Fig. 14B).

PrP^c levels do not influence the gross morphology of the adult CNS

Others have reported that there is no notable difference in the mature CNS of mice expressing normal, reduced, or higher levels of PrP^c (Bueler et al., 1992; Bueler et al., 1993; Fischer et al., 1996). These reports used methods such as hematoxylin and eosin staining (Bueler et al., 1993). Given the subtle differences in cellular proliferation in PrP^c KO, WT, and OE brains, we re-examined the CNS morphology in greater detail by morphometric studies using the cellular label cresyl violet and Fluoromyelin staining. From every 6^{th} thin section from adult, age-matched mouse brains, we performed blinded analyses of the size and overall structure of several selected CNS regions, including the cortex, hippocampus, thalamus, cerebellum, and brain stem. Similarly, we analyzed the size and density of major fiber tracts such as the corpus callosum, medial forebrain bundle, and anterior commissure. We find no morphological differences among any of the experimental groups (data not shown); these observations confirm

that, regardless of PrP^c level during development and adulthood, a morphologically normal CNS is formed.

Neurogenesis in the DG is unchanged by PrP^c level

Given the positive effect of PrP^c on proliferation in the SVZ and DG, and the low level of proliferation in the DG of PrP^c KO mice in particular, we investigated whether deletion of PrP^c leads to a net reduction in adult hippocampal neurogenesis. We injected mice with pulse labels of BrdU over a two day period, and assessed the number of newborn immature and mature neurons 3, 7, and 14 days after the last BrdU injection. We find that PrP^c levels do not influence the number of immature (TuJ1-positive) neurons produced in the SVZ or DG, nor do they change the net number of new neurons produced in the DG. For example, 14 days after the last BrdU injection, there is an average of 5 BrdU/NeuN-positive neurons per DG counted in each of PrP^c KO (n = 4 mice), WT (n = 6), and OE mice (n = 4). Therefore, although PrP^c levels increase proliferation in the DG, they have no detectable effect on the ultimate number of neurons that are produced.

Environmental enrichment of PrP knockout and overexpression transgenic mice

To examine whether we would observe stronger phenotypes of PrP deletion or overexpression we sought to challenge the adult neurogenesis system. Environmental enrichment is the best known method to dramatically increase adult neurogenesis (Kempermann et al., 1997). We placed groups of n=6-8 female mice that were either PrP KO, PrP WT, or PrP OE in standard or enriched housing conditions. Enriched housing conditions included a running wheel, a red dome, multiple cotton nestlets, corn husks, and the presence of at least 6 female mice. Mice

were housed in enriched or standard conditions for 40 days, and injected once daily with BrdU (50mg/kg) from days 35-40. After 28 additional days of either enriched or standard housing conditions, all mice were sacrificed. Their brains were sectioned and stained for BrdU and NeuN. We quantified BrdU labeled cells and BrdU/NeuN double labeled cells in the DG of the hippocampus. We observed that in unenriched conditions, the PrP OE mouse had higher basal levels of cellular proliferation in the DG ($P<0.001$, T test) (Fig. 15). During enriched conditions, all groups of mice (PrP KO, WT, and OE) had dramatically enhanced BrdU labeling compared to unenriched groups, but there were no significant differences among the enriched groups. We next measured net neurogenesis by comparing the number of BrdU/NeuN double labed cells in the DG. In unenriched conditions, PrP OE mice had increased neurogenesis in the DG ($P<0.01$, T test) (Fig. 16). This observation was not made in our prior experiment, but could be due to differences in labeling protocols. During enriched conditions, there was a dramatic increase in neurogenesis, indepent of PrP levels (Fig. 16). All enriched groups were significantly elevated over unenriched groups ($P<0.001$, T test) (Fig. 16).

Discussion

We have presented evidence here, from multiple modes of analysis, that PrP^c expression positively influences both developmental and adult mammalian neurogenesis. We find that 1) PrP^c is expressed most strongly immediately adjacent to the proliferative region of the SVZ, but not in mitotic cells; 2) PrP^c expression increases in mature neurons, but is not detectable in astroglia or oligodendroglia; 3) PrP^c levels directly correlate with neuronal differentiation from multipotent neural precursors *in vitro*; 4) PrP^c significantly increases cellular proliferation *in vivo*, in both the SVZ and DG; 5) the ultimate number of neurons produced in the

DG is elevated in PrP^c overexpression transgenics under normal laboratory conditions (dependent on BrdU dosing protocol), and 6) PrP^c levels do not influence the gross morphology of the murine CNS.

Cell type expression of PrP^c in the brain remains controversial, with claims that it is exclusively neuronal or else that it is ubiquitously expressed in many glial and neuronal cell types throughout the CNS (Ford et al., 2002). It has been shown, however, that in disease states PrP^c is strongly expressed in astrocytes, which are also capable of replicating prions after neuronal PrP^c expression is turned off post-natally in transgenic mice (Mallucci et al., 2003). Our studies used a PrP^c-specific (goat polyclonal) antibody to label PrP^c-positive cells, which were then analyzed with high magnification, three-dimensional confocal image reconstructions; our *in vivo* and *in vitro* analyses demonstrate that PrP^c is expressed strongly in neurons but it is not detectable in astroglia or oligodendroglia. Neuronal expression begins with very low levels of PrP^c in nestin-positive multipotent neural precursors, followed by increasing levels from immature neurons on through to mature, integrated neurons. This restricted pattern of neuronal PrP^c expression in the developing and adult CNS strongly suggests that PrP^c has an ongoing and active role in neurogenesis throughout life.

We have shown that PrP^c has a positive effect on cellular proliferation in the adult SVZ and DG, indicated by increased proliferation in the SVZ of PrP^c OE mice and by a paucity of proliferation in the DG of PrP^c KO mice. However, despite the fact that proliferation in the DG is reduced in PrP^c KO mice, there is neither a corresponding reduction in the number of newborn neurons nor a change in the gross morphology of the hippocampus. These results support the concept that cellular proliferation rates alone do not determine the net level of neurogenesis

(Emsley et al., 2005). The number of surviving newborn neurons in the adult depends on multiple factors, and PrP^c is likely only one such factor involved in this complex process.

It is possible that the neurogenic niche of the DG produces and maintains only a finite number of new neurons, and that cell death acts in part to regulate these numbers. The absolute number of proliferating cells in the DG in our studies was low, making it unlikely that significant differences in cell death could be detected using methods such as TUNEL. The number of new neurons that can be integrated into the adult DG partially depends upon local environmental support, including the provision of neurotrophic factors critical for survival of newly generated neurons. Because environmental enrichment increases net neurogenesis in the DG via increased neurotrophic factor production (Kempermann et al., 1997), future studies on the role of PrP^c in adult neurogenesis could determine whether such enrichment or even response to injury would increase the possibility that PrP^c OE mice would generate and maintain more neurons than their WT or KO counterparts. It is important to note, for example, that under normal laboratory conditions the hematopoietic compartment of PrP^c KO mice is indistinguishable from that of WT mice; however, under the stress of serial transplantation or myelotoxic injury, hematopoietic stem cells from PrP^c KO mice perform poorly when compared to WT controls (Zhang et al., 2006). When we challenged the neurogenic system with environmental enrichment we did not observe a diminished potential of PrP KOs to upregulate either proliferation or neurogenesis. Thus, environmental enrichment can overwhelm a small genetically determined proliferation defect.

A role for the normal prion protein in development was proposed in 1992, when its expression at different embryonic stages was described (Manson et al., 1992). Embryonic multipotent neural precursor cultures are a simple model with which to study cellular

proliferation and differentiation. We found that cellular PrP^c levels positively correlate with neuronal differentiation from multipotent neural precursors, in that nestin-positive precursors derived from PrP^c null mice remain multipotent for a longer period of time, whereas higher PrP^c levels significantly increase neuronal differentiation. Although the rate of neuronal production in PrP^c KO cultures is significantly lower than in the other groups, precursors from KO mice are still capable of generating neurons, indicating a delay in differentiation, rather than a failure to differentiate. Whether these differences are related to neuronal survival *in vitro* is not yet known. However, it is evident that PrP^c has no effect on the rate of gliogenesis, indicating that its effects on differentiation are specific to neurons.

Taken together, these results suggest that PrP^c might play a role as a switch from uncommitted, multipotent precursors toward the generation of neurons. Our observations about neural development are further supported by recent studies of neuronal maturation, which demonstrated that folded recombinant PrP^c added to cultured rat hippocampal neurons induces neuronal differentiation and process outgrowth (Kanaani et al., 2005; Lopes et al., 2005). Studies such as these indicate that *in vitro* neural cell preparations are effective systems with which to study the role of PrP^c in discrete stages of neuronal development, and to determine what mechanisms might compensate for the lack of PrP^c in precursors and their neuronal progeny.

The downstream signaling pathway of PrP^c is of great interest for studies of the normal and disease-associated isoforms of PrP^c. For example, recent work demonstrated that transgenic mice expressing PrP^c lacking a GPI anchor are refractory to development of a prion disease phenotype, despite dramatic CNS accumulation of misfolded PrP (Chesebro et al., 2005). One intriguing interpretation of this result is that cell surface-bound PrP^c is required to transmit a toxic signal to neurons (Aguzzi, 2005). This raises the possibility that PrP^c is normally a signal

transducer, and in disease states this signal transduction goes awry. Elucidation of the signaling pathways through which PrP^c influences neurogenesis, along with an understanding of the pathways involved in other key cellular processes, will provide insight into how PrP^c misfolding leads to devastating neurodegenerative diseases. Further *in vivo* and *in vitro* studies of the role of PrP^c in developmental and adult neurogenesis will contribute to our understanding of the biological function of normal PrP^c, and could inform studies aimed toward identifying and counteracting the devastating sequelae of prion diseases.

Materials and Methods

Mouse strains and genotyping

Adult mice were housed and all procedures were performed according to institutional and NIH guidelines. All surgical and euthanasia procedures were performed using Avertin anesthesia. PrP^c KO mice (25) were kindly provided by Drs. R. Race and B. Chesebro on a mixed 129/Ola and C57Bl/10 background and were backcrossed to C57Bl/6J for at least 6-10 generations to obtain PrP^c KO and WT control littermates. The PrP^c OE transgenic "Tg20" mice (Fischer et al., 1996) were obtained from the European Mutant Mouse Archive on a mixed C57Bl/6 and 129S7/Sv hybrid background and null for PrP^c. These mice were backcrossed to C57Bl/6J for 5-6 generations and the KO allele was bred out to yield mice that were WT at the endogenous *Prnp* locus and contained one copy of the PrP^c OE transgene. For genotyping, DNA was extracted from proteinase K-digested tail clippings by isopropanol precipitation; genotyping for PrP^c KO and OE was performed as follows: the PrP and/or neomycin insert was amplified in a 4-primer PCR reaction using primers 5'TCATCCCACGATCAGGAAGATGAG3' and 5'ATGGCGAACCTTGGCTACTGGCTG3' for PrP and 5'TTGAGCCTGGCGAACAGTTC3'

and 5'GATGGATTGCACGCAGGTTC3' for the neomycin insert. Cycling conditions were 94 °C for 3 minutes, 30 cycles at 94 °C for 30 seconds, 62 °C for 30 seconds, and 72 °C for 1 min, followed by a final extension at 72 °C for 10 minutes.

Western blotting

Protein was quantified using a BCA protein assay kit (Pierce). Briefly, 20ug of protein from whole brain homogenates of PrP^c KO, WT, and OE mice was electrophoresed in 15% Tris-HCl gels (Biorad) and transferred to nitrocellulose membranes at 25V for 10 hours at 4 °C. Membranes were blocked in 3% milk; the primary antibody SAF-32 was used at 0.2ug/mL (Cayman Chemicals) for detection of PrP^c, while anti-beta-tubulin served as a loading control. Rat anti-mouse HRP conjugated secondary antibody (Jackson ImmunoResearch Labs) was used at 1:10,000. Supersignal (Pierce) was used for detection (Figure 1A).

BrdU administration

For cell proliferation studies, the thymidine analog 5-Bromo-2'-deoxyuridine (BrdU; Sigma) was administered as a pulse label (one injection i.p., 200 mg/kg body weight, in sterile saline). Animals used for cell proliferation studies were perfused one hour after BrdU administration. For cell differentiation studies, BrdU was administered as four pulse labels (four i.p. injections, 12 hours apart, 100 mg/kg, in sterile saline). Animals used for cell differentiation studies were perfused 3, 7, or 14 days after the last BrdU administration.

Tissue collection and histology

Animals were deeply anesthetized with an overdose of Avertin and were transcardially perfused with cold 0.1 M PBS followed by cold 4% paraformaldehyde (PFA) in 0.1 M PBS. Brains were postfixed in 4% PFA at 4 °C for 16 hours. Coronal sections of 30 μm thickness were cut on a Leica VT 1000S vibrating microtome and stored in 0.1M PBS/0.025% sodium azide.

All immunocytochemical procedures were performed on a minimum of every 6th tissue section. Sections were rinsed in 0.1M PBS, and blocked in 0.3% bovine serum albumin (BSA)/8% serum (e.g. goat) in 0.3% PBS-Triton X-100 (PBS-T). The following primary antibodies were used: PrP^c (goat polyclonal, 1:500, abcam), Dcx (guinea pig polyclonal, 1:500, Chemicon), GFAP (mouse monoclonal, 1:400, Sigma), GFP (rabbit polyclonal, 1:500, Chemicon), NeuN (mouse monoclonal, 1:500, Chemicon), and TuJ1 (mouse monoclonal, 1:500, CoVance). For BrdU staining, tissue sections were treated for 2 hours at room temperature (RT) in 2M HCl prior to application of the primary antibody (rat monoclonal, 1:400, Harlan).

Primary antibodies were applied overnight at 4 °C in blocking solution, followed by a series of PBS rinses and incubation in appropriate secondary fluorescent antibodies (1:500; Alexa 488, 546; Molecular Probes) in blocking solution at RT for 2-4 hours. In most cases, a nuclear counterstain (DAPI, 1:5,000 in 0.1 M PBS) was used. Specificity of the PrP^c antibody was confirmed with immunocytochemistry on tissue from PrP^c OE and KO mice.

Neural precursor cell cultures

Timed matings were established between PrP^c KO x PrP^c KO, PrP^c OE (homozygous for the Tg20 transgene) x WT, and WT x WT male and female mice. E13.5 embryos were collected in ice-cold Hank's Balanced salt solution (HBSS) supplemented with glucose (Gibco); the telencephalon was microdissected out and the meninges were removed in sterile conditions. Single cell suspensions were prepared with trituration and plated on poly-ornithine/fibronectin coated plates (Sigma). Briefly, cells were kept in a proliferative state for two days in DMEM/F-12 with 1%N2, 1%B27, 1% penicillin/streptomycin (P/S), and 20ng/ml bFGF. Neural precursors were selectively lifted off the plates in the presence of HNH buffer (HBSS supplemented with $NaHCO_3$ and HEPES as described previously (11). Single cells were plated (80,000

cells/coverslip) on poly-ornithine/fibronectin coated glass coverslips and cultured in differentiation medium (DMEM/F-12, 1%N2, 1%B27, 1% P/S, and 1% fetal calf serum) (26). Differentiation was induced by bFGF withdrawal and defined as "day *in vitro* 0" (0 DIV); coverslips were collected at 0, 1, 3, 5, and 7 DIV. Cells were fixed with 4% PFA for 10 minutes at RT, washed with 0.1M PBS, and kept at 4 °C.

Differentiated neural precursor cultures were detected immunocytochemically as described above. Primary antibodies used for *in vitro* analyses were PrP^c (goat polyclonal, 1:1000, abcam), Dcx (guinea pig polyclonal, 1:750, Chemicon), MAP-2 (mouse monoclonal, 1:1000, Sigma), nestin (mouse monoclonal, 1:300, Chemicon), NeuN (mouse monoclonal, 1:500, Chemicon), O4 (mouse monoclonal IgM, 1:400, gift of P. Follet), S100□ (mouse monoclonal, 1:1000, Sigma), followed by PBS rinses and incubation in appropriate secondary fluorescent antibodies (1:500; Alexa 488, 546; Molecular Probes) in blocking solution at RT for 2-4 hours. In most cases, a nuclear counterstain (DAPI, 1:5000 in 0.1 M PBS) was used.

Data and image analysis

Tissue sections and cells were viewed on a Nikon E1000 microscope equipped with an X-Cite 120 fluorescence illuminator unit (EXFO). Images were acquired with a Retiga EX cooled CCD camera (QImaging) and analyzed with OpenLab image analysis software (Version 3.5). Confocal images were acquired with a BioRad Radiance Rainbow laser scanning confocal microscope equipped for spectral imaging and mounted on a Nikon E800 microscope. Three-dimensional image reconstructions were analyzed using BioRad LaserSharp 2000 (Version 5.1), LaserVox 3-D (Version 1.0), and Imaris 4.1.3 (Bitplane) rendering software. All confocal images were produced from z-stacks, and all cell counts and measurements were made using NIH ImageJ software.

All cell counts were performed in a blinded fashion, with the counter unaware of the experimental condition being assessed. For *in vivo* analyses, cells were only counted if a full nucleus was present in the section (e.g., for nuclear labels such as NeuN), or if the cell body and its process could be visualized in the same section (e.g., for cells positive for TuJ1). For *in vitro* analyses, each coverslip was observed under 40X magnification, and from each coverslip 10 independent areas were randomly selected for quantification. For each experimental condition, 3-5 coverslips were analyzed, and each experiment was repeated in 2-3 separate litters of each genotype.

References

Aguzzi A (2000) Prion diseases, blood and the immune system: concerns and reality. Haematologica 85:3-10.

Aguzzi A (2005) Cell biology. Prion toxicity: all sail and no anchor. Science 308:1420-1421.

Aguzzi A, Haass C (2003) Games played by rogue proteins in prion disorders and Alzheimer's disease. Science 302:814-818.

Aguzzi A, Heikenwalder M (2006) Pathogenesis of prion diseases: current status and future outlook. Nat Rev Microbiol 4:765-775.

Bueler H, Aguzzi A, Sailer A, Greiner RA, Autenried P, Aguet M, Weissmann C (1993) Mice devoid of PrP are resistant to scrapie. Cell 73:1339-1347.

Bueler H, Fischer M, Lang Y, Bluethmann H, Lipp HP, DeArmond SJ, Prusiner SB, Aguet M, Weissmann C (1992) Normal development and behaviour of mice lacking the neuronal cell-surface PrP protein. Nature 356:577-582.

Chen CZ, Li L, Li M, Lodish HF (2003a) The endoglin(positive) sca-1(positive) rhodamine(low) phenotype defines a near-homogeneous population of long-term repopulating hematopoietic stem cells. Immunity 19:525-533.

Chen CZ, Li L, Li M, Lodish HF (2003b) The endoglin(positive) sca-1(positive) rhodamine(low) phenotype defines a near-homogeneous population of long-term repopulating hematopoietic stem cells. Immunity 19:525-533.

Cheng T, Rodrigues N, Shen H, Yang Y, Dombkowski D, Sykes M, Scadden DT (2000) Hematopoietic stem cell quiescence maintained by p21cip1/waf1. Science 287:1804-1808.

Chesebro B, Trifilo M, Race R, Meade-White K, Teng C, LaCasse R, Raymond L, Favara C, Baron G, Priola S, Caughey B, Masliah E, Oldstone M (2005) Anchorless prion protein results in infectious amyloid disease without clinical scrapie. Science 308:1435-1439.

Dodelet VC, Cashman NR (1998) Prion protein expression in human leukocyte differentiation. Blood 91:1556-1561.

Emsley JG, Mitchell BD, Kempermann G, Macklis JD (2005) Adult neurogenesis and repair of the adult CNS with neural progenitors, precursors, and stem cells. Prog Neurobiol 75:321-341.

Fischer M, Rulicke T, Raeber A, Sailer A, Moser M, Oesch B, Brandner S, Aguzzi A, Weissmann C (1996) Prion protein (PrP) with amino-proximal deletions restoring susceptibility of PrP knockout mice to scrapie. Embo J 15:1255-1264.

Ford MJ, Burton LJ, Li H, Graham CH, Frobert Y, Grassi J, Hall SM, Morris RJ (2002) A marked disparity between the expression of prion protein and its message by neurones of the CNS. Neuroscience 111:533-551.

Forman MS, Trojanowski JQ, Lee VM (2004) Neurodegenerative diseases: a decade of discoveries paves the way for therapeutic breakthroughs. Nat Med 10:1055-1063.

Genoud N, Behrens A, Miele G, Robay D, Heppner FL, Freigang S, Aguzzi A (2004) Disruption of Doppel prevents neurodegeneration in mice with extensive Prnp deletions. Proc Natl Acad Sci U S A 101:4198-4203. Epub 2004 Mar 4198.

Goodell MA, Brose K, Paradis G, Conner AS, Mulligan RC (1996) Isolation and functional properties of murine hematopoietic stem cells that are replicating in vivo. J Exp Med 183:1797-1806.

Hill B, Rozler E, Travis M, Chen S, Zannetino A, Simmons P, Galy A, Chen B, Hoffman R (1996) High-level expression of a novel epitope of CD59 identifies a subset of CD34+ bone marrow cells highly enriched for pluripotent stem cells. Exp Hematol 24:936-943.

Horejsi V, Drbal K, Cebecauer M, Cerny J, Brdicka T, Angelisova P, Stockinger H (1999) GPI-microdomains: a role in signalling via immunoreceptors. Immunol Today 20:356-361.

Ito CY, Li CY, Bernstein A, Dick JE, Stanford WL (2003) Hematopoietic stem cell and progenitor defects in Sca-1/Ly-6A-null mice. Blood 101:517-523. Epub 2002 Aug 2029.

Johe KK, Hazel TG, Muller T, Dugich-Djordjevic MM, McKay RD (1996) Single factors direct the differentiation of stem cells from the fetal and adult central nervous system. Genes Dev 10:3129-3140.

Jordan CT, McKearn JP, Lemischka IR (1990) Cellular and developmental properties of fetal hematopoietic stem cells. Cell 61:953-963.

Kanaani J, Prusiner SB, Diacovo J, Baekkeskov S, Legname G (2005) Recombinant prion protein induces rapid polarization and development of synapses in embryonic rat hippocampal neurons in vitro. J Neurochem 95:1373-1386.

Kempermann G, Kuhn HG, Gage FH (1997) More hippocampal neurons in adult mice living in an enriched environment. Nature 386:493-495.

Kilpatrick TJ, Bartlett PF (1993) Cloning and growth of multipotential neural precursors: requirements for proliferation and differentiation. Neuron 10:255-265.

Landles C, Bates GP (2004) Huntingtin and the molecular pathogenesis of Huntington's disease. Fourth in molecular medicine review series. EMBO Rep 5:958-963.

Lasmezas CI (2003) Putative functions of PrP(C). Br Med Bull 66:61-70.

Lewis J, McGowan E, Rockwood J, Melrose H, Nacharaju P, Van Slegtenhorst M, Gwinn-Hardy K, Paul Murphy M, Baker M, Yu X, Duff K, Hardy J, Corral A, Lin WL, Yen SH, Dickson DW, Davies P, Hutton M (2000) Neurofibrillary tangles, amyotrophy and progressive motor disturbance in mice expressing mutant (P301L) tau protein. Nat Genet 25:402-405.

Liu T, Li R, Wong BS, Liu D, Pan T, Petersen RB, Gambetti P, Sy MS (2001) Normal cellular prion protein is preferentially expressed on subpopulations of murine hemopoietic cells. J Immunol 166:3733-3742.

Lopes MH, Hajj GN, Muras AG, Mancini GL, Castro RM, Ribeiro KC, Brentani RR, Linden R, Martins VR (2005) Interaction of cellular prion and stress-inducible protein 1 promotes neuritogenesis and neuroprotection by distinct signaling pathways. J Neurosci 25:11330-11339.

Mallucci G, Dickinson A, Linehan J, Klohn PC, Brandner S, Collinge J (2003) Depleting neuronal PrP in prion infection prevents disease and reverses spongiosis. Science 302:871-874.

Mangiarini L, Sathasivam K, Seller M, Cozens B, Harper A, Hetherington C, Lawton M, Trottier Y, Lehrach H, Davies SW, Bates GP (1996) Exon 1 of the HD gene with an expanded CAG repeat is sufficient to cause a progressive neurological phenotype in transgenic mice. Cell 87:493-506.

Manson J, West JD, Thomson V, McBride P, Kaufman MH, Hope J (1992) The prion protein gene: a role in mouse embryogenesis? Development 115:117-122.

Manson JC, Clarke AR, Hooper ML, Aitchison L, McConnell I, Hope J (1994) 129/Ola mice carrying a null mutation in PrP that abolishes mRNA production are developmentally normal. Mol Neurobiol 8:121-127.

Masliah E, Rockenstein E, Veinbergs I, Mallory M, Hashimoto M, Takeda A, Sagara Y, Sisk A, Mucke L (2000) Dopaminergic loss and inclusion body formation in alpha-synuclein mice: implications for neurodegenerative disorders. Science 287:1265-1269.

McLennan NF, Brennan PM, McNeill A, Davies I, Fotheringham A, Rennison KA, Ritchie D, Brannan F, Head MW, Ironside JW, Williams A, Bell JE (2004) Prion protein accumulation and neuroprotection in hypoxic brain damage. Am J Pathol 165:227-235.

Moore RC, Xiang F, Monaghan J, Han D, Zhang Z, Edstrom L, Anvret M, Prusiner SB (2001) Huntington disease phenocopy is a familial prion disease. Am J Hum Genet 69:1385-1388.

Mouillet-Richard S, Ermonval M, Chebassier C, Laplanche JL, Lehmann S, Launay JM, Kellermann O (2000) Signal transduction through prion protein. Science 289:1925-1928.

Naslavsky N, Stein R, Yanai A, Friedlander G, Taraboulos A (1997) Characterization of detergent-insoluble complexes containing the cellular prion protein and its scrapie isoform. J Biol Chem 272:6324-6331.

Nicholl D, Windl O, de Silva R, Sawcer S, Dempster M, Ironside JW, Estibeiro JP, Yuill GM, Lathe R, Will RG (1995) Inherited Creutzfeldt-Jakob disease in a British family associated with a novel 144 base pair insertion of the prion protein gene. J Neurol Neurosurg Psychiatry 58:65-69.

Norris EH, Giasson BI, Lee VM (2004) Alpha-synuclein: normal function and role in neurodegenerative diseases. Curr Top Dev Biol 60:17-54.

Okada S, Nakauchi H, Nagayoshi K, Nishikawa S, Miura Y, Suda T (1992) In vivo and in vitro stem cell function of c-kit- and Sca-1-positive murine hematopoietic cells. Blood 80:3044-3050.

Orschell-Traycoff CM, Hiatt K, Dagher RN, Rice S, Yoder MC, Srour EF (2000) Homing and engraftment potential of Sca-1(+)lin(-) cells fractionated on the basis of adhesion molecule expression and position in cell cycle. Blood 96:1380-1387.

Panchision D, Hazel T, McKay R (1998) Plasticity and stem cells in the vertebrate nervous system. Curr Opin Cell Biol 10:727-733.

Prusiner SB (1998) Prions. Proc Natl Acad Sci U S A 95:13363-13383.

Prusiner SB (2001) Shattuck lecture--neurodegenerative diseases and prions. N Engl J Med 344:1516-1526.

Rebel VI, Miller CL, Thornbury GR, Dragowska WH, Eaves CJ, Lansdorp PM (1996) A comparison of long-term repopulating hematopoietic stem cells in fetal liver and adult bone marrow from the mouse. Exp Hematol 24:638-648.

Reynolds BA, Tetzlaff W, Weiss S (1992) A multipotent EGF-responsive striatal embryonic progenitor cell produces neurons and astrocytes. J Neurosci 12:4565-4574.

Richards LJ, Kilpatrick TJ, Bartlett PF (1992) De novo generation of neuronal cells from the adult mouse brain. Proc Natl Acad Sci U S A 89:8591-8595.

Richt JA, Kasinathan P, Hamir AN, Castilla J, Sathiyaseelan T, Vargas F, Sathiyaseelan J, Wu H, Matsushita H, Koster J, Kato S, Ishida I, Soto C, Robl JM, Kuroiwa Y (2006) Production of cattle lacking prion protein. Nat Biotechnol.

Risitano AM, Holada K, Chen G, Simak J, Vostal JG, Young NS, Maciejewski JP (2003) CD34+ cells from paroxysmal nocturnal hemoglobinuria (PNH) patients are deficient in surface expression of cellular prion protein (PrPc). Exp Hematol 31:65-72.

Rivera-Milla E, Oidtmann B, Panagiotidis CH, Baier M, Sklaviadis T, Hoffmann R, Zhou Y, Solis GP, Stuermer CA, Malaga-Trillo E (2006) Disparate evolution of prion protein

domains and the distinct origin of Doppel- and prion-related loci revealed by fish-to-mammal comparisons. Faseb J 20:317-319.
Roberson ED, Scearce-Levie K, Palop JJ, Yan F, Cheng IH, Wu T, Gerstein H, Yu GQ, Mucke L (2007) Reducing endogenous tau ameliorates amyloid beta-induced deficits in an Alzheimer's disease mouse model. Science 316:750-754.
Roucou X, Gains M, LeBlanc AC (2004) Neuroprotective functions of prion protein. J Neurosci Res 75:153-161.
Schilling G, Becher MW, Sharp AH, Jinnah HA, Duan K, Kotzuk JA, Slunt HH, Ratovitski T, Cooper JK, Jenkins NA, Copeland NG, Price DL, Ross CA, Borchelt DR (1999) Intranuclear inclusions and neuritic aggregates in transgenic mice expressing a mutant N-terminal fragment of huntingtin. Hum Mol Genet 8:397-407.
Shastry BS (2003) Neurodegenerative disorders of protein aggregation. Neurochem Int 43:1-7.
Shyu WC, Lin SZ, Chiang MF, Ding DC, Li KW, Chen SF, Yang HI, Li H (2005) Overexpression of PrPC by adenovirus-mediated gene targeting reduces ischemic injury in a stroke rat model. J Neurosci 25:8967-8977.
Spangrude GJ, Heimfeld S, Weissman IL (1988) Purification and characterization of mouse hematopoietic stem cells. Science 241:58-62.
Spudich A, Frigg R, Kilic E, Kilic U, Oesch B, Raeber A, Bassetti CL, Hermann DM (2005) Aggravation of ischemic brain injury by prion protein deficiency: role of ERK-1/-2 and STAT-1. Neurobiol Dis 20:442-449.
Stahl N, Boulton TG, Ip N, Davis S, Yancopoulos GD (1994) The tails of two proteins: the scrapie prion protein and the ciliary neurotrophic factor receptor. Braz J Med Biol Res 27:297-301.
Steele AD, Yi CH (2006) Neuromuscular denervation: Bax up against the wall in amyotrophic lateral sclerosis. J Neurosci 26:12849-12851.
Steele AD, Emsley JG, Ozdinler PH, Lindquist S, Macklis JD (2006) Prion protein (PrPc) positively regulates neural precursor proliferation during developmental and adult mammalian neurogenesis. Proc Natl Acad Sci U S A 103:3416-3421.
Steele AD, Lindquist, S., and Aguzzi, A. (2007) The prion protein knockout mouse: a phenotype under challenge. Prion 1.
Sunyach C, Jen A, Deng J, Fitzgerald KT, Frobert Y, Grassi J, McCaffrey MW, Morris R (2003) The mechanism of internalization of glycosylphosphatidylinositol-anchored prion protein. Embo J 22:3591-3601.
Taylor DR, Watt NT, Perera WS, Hooper NM (2005) Assigning functions to distinct regions of the N-terminus of the prion protein that are involved in its copper-stimulated, clathrin-dependent endocytosis. J Cell Sci 118:5141-5153.
Vostal JG, Holada K, Simak J (2001a) Expression of cellular prion protein on blood cells: potential functions in cell physiology and pathophysiology of transmissible spongiform encephalopathy diseases. Transfus Med Rev 15:268-281.
Vostal JG, Holada K, Simak J (2001b) Expression of cellular prion protein on blood cells: potential functions in cell physiology and pathophysiology of transmissible spongiform encephalopathy diseases. Transfus Med Rev 15:268-281.
Weise J, Sandau R, Schwarting S, Crome O, Wrede A, Schulz-Schaeffer W, Zerr I, Bahr M (2006) Deletion of cellular prion protein results in reduced Akt activation, enhanced postischemic caspase-3 activation, and exacerbation of ischemic brain injury. Stroke 37:1296-1300.

Weissmann C, Flechsig E (2003) PrP knock-out and PrP transgenic mice in prion research. Br Med Bull 66:43-60.

Zhang CC, Lodish HF (2004) Insulin-like growth factor 2 expressed in a novel fetal liver cell population is a growth factor for hematopoietic stem cells. Blood 103:2513-2521.

Zhang CC, Lodish HF (2005) Murine hematopoietic stem cells change their surface phenotype during ex vivo expansion. Blood 105:4314-4320.

Zhang CC, Steele AD, Lindquist S, Lodish HF (2006) Prion protein is expressed on long-term repopulating hematopoietic stem cells and is important for their self-renewal. Proc Natl Acad Sci U S A 103:2184-2189.

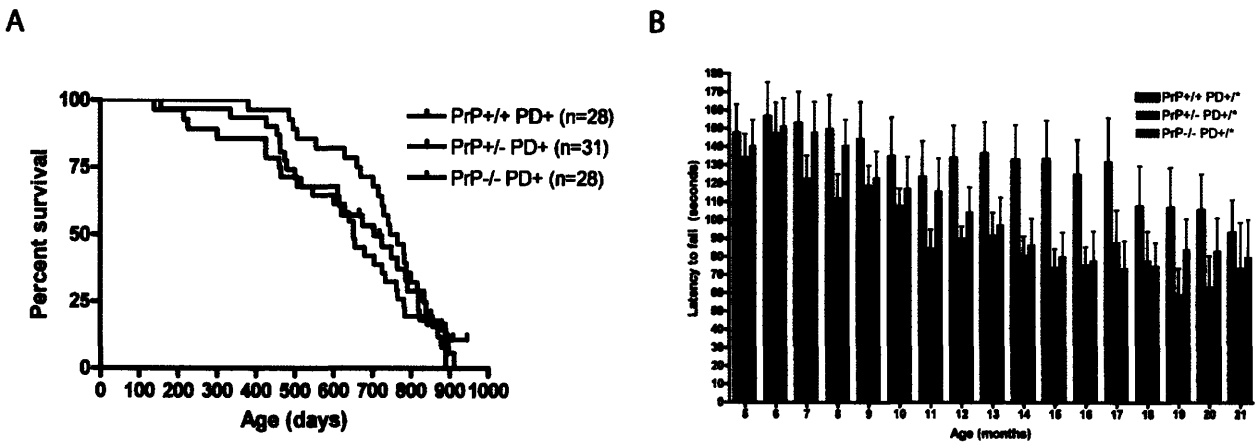

Figure 1 PrP deletion does not appreciably alter the phenotype of α-synuclein Tg mice. Survival analysis did not show a significant differences between PrP+/+, PrP+/-, and PrP-/- alpha-synuclein overexpression Tg mice (log rank test) (A). Motor performance was assessed on an accelerating rotarod; however, the motor performance did not decline much over the timepoints tested, from 5 months of age to 21 months of age (B).

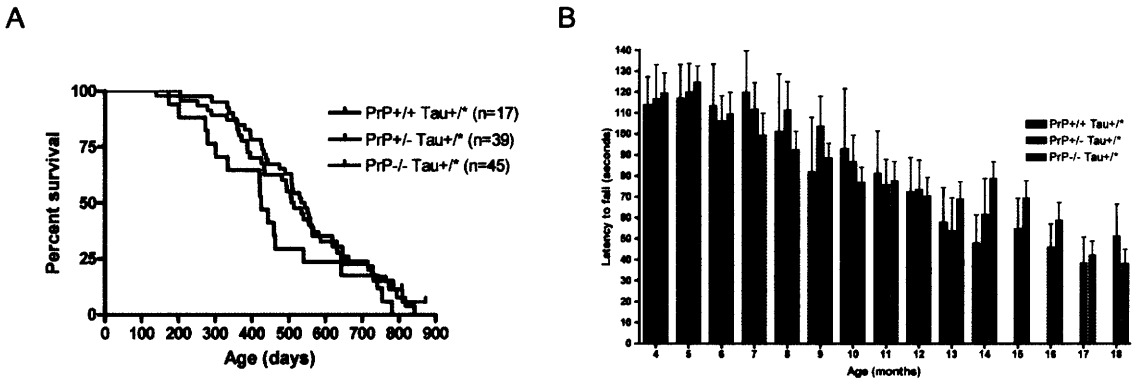

Figure 2 PrP deletion does not appreciably alter the phenotype of P301L Tau Tg mice. Survival analysis did not show a significant differences between PrP+/+, PrP+/-, and PrP-/- P301L Tau Tg mice (log rank test) (A). Motor performance was assessed on an accelerating rotarod; however, there were no significant differences among the experimental groups (B).

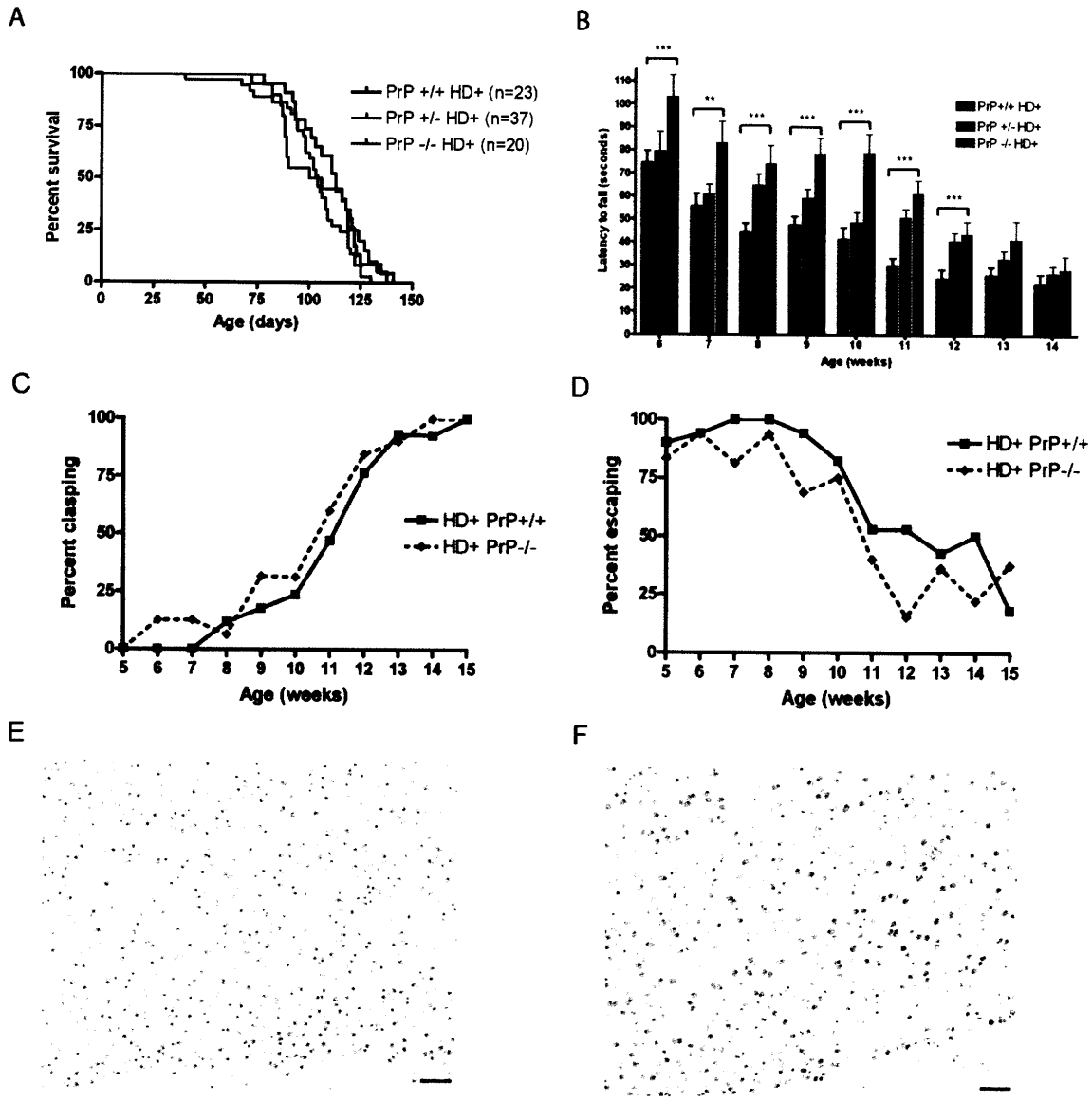

Figure 3 Deletion of PrP in the R6/2 transgenic model of Huntington's disease. Survival of R6/2 HD mice was not altered by deletion of PrP (A). Rotarod performance of PrP-/- HD Tg+ mice was improved over that of PrP+/- or PrP+/+ HD Tg+ until the later points of disease (12-14 weeks) (B). Clasping (C) and escaping (D) were not altered by PrP deletion in HD Tg+ mice (HD Tg- mice all escape [100% escape at all timepoints] and never clasp [0% at all timepoints]. Accumulation of nuclear aggregates is shown in (E) and (F).

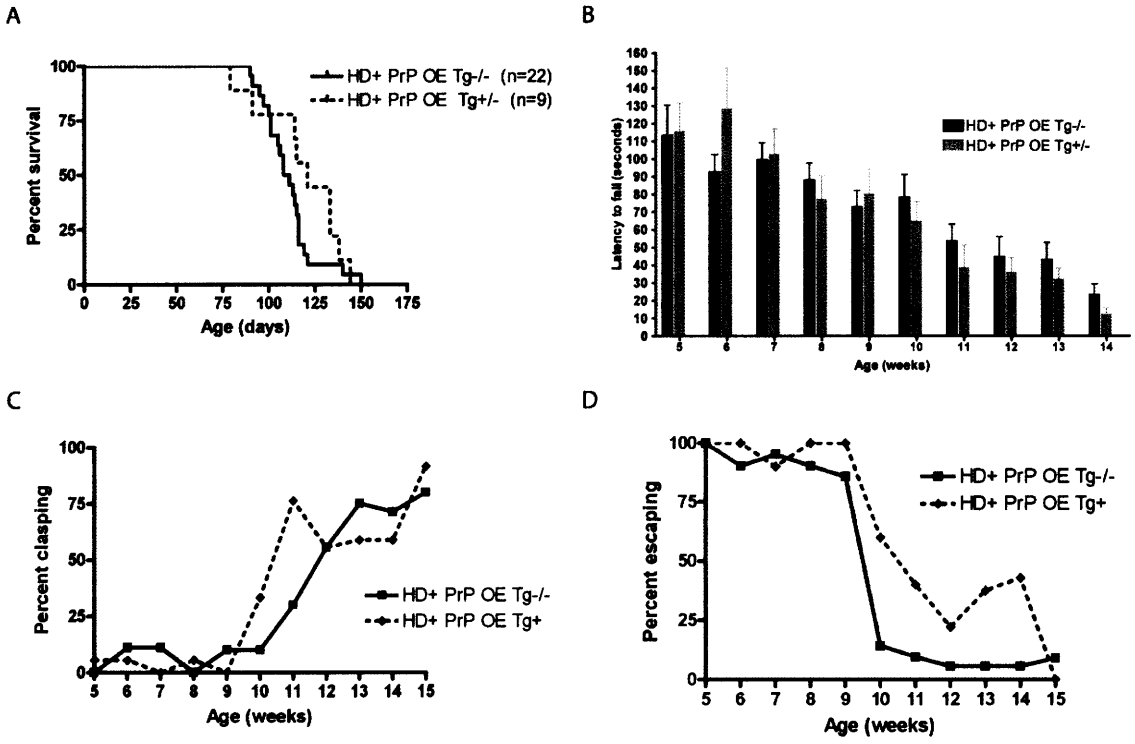

Figure 4 Overexpression of PrP in the R6/2 transgenic model of Huntington's disease. Survival of R6/2 HD mice was not altered by overexpression of PrP (log rank test) (A). Rotarod performance of HD Tg+ PrP Tg-/- and PrP Tg+ was indistinguishable (B). Clasping (C) and escaping (D) were not altered by PrP overexpression HD Tg+ mice (HD Tg- mice all escape [100% escape at all timepoints] and never clasp [0% at all timepoints].

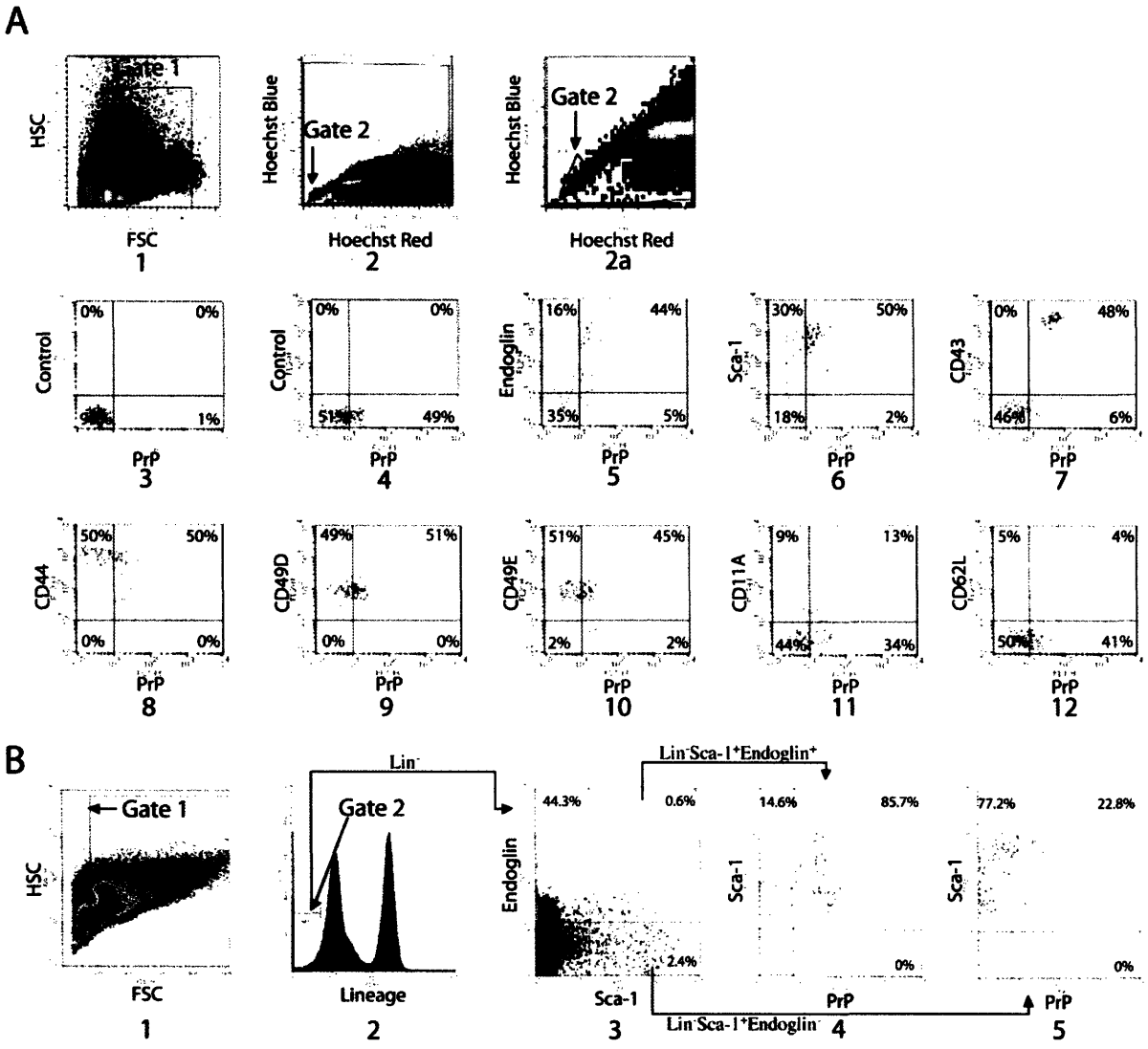

Figure 5 PrP is expressed on bone marrow populations enriched in HSC activity. (A) Freshly isolated BM cells were stained with Hoechst 33342 dye and the SP fraction was gated (gates 1 and 2) to analyze the expression of PrP. In plot 1, forward scatter (FSC) and side scatter (SSC) is used to gate on hematopoietic cells. Hoechst Red and Hoechst Blue (plots 2 and 2a, gate 2 was set as 0.02% of total cells) represent two fluorescence emission wavelengths used to detect the SP cells. Plot 2a is an expansion of the gate 2 region of plot 2. PrP null BM SP cells served as a negative control for PrP antibody staining (plot 3). WT BM SP cells were stained for PrP (plots 4-12) together with isotype control (plot 4), Endoglin (plot 5), Sca-1 (plot 6), CD43 (plot 7), CD44 (plot 8), CD49D (plot 9), CD49E (plot 10), CD11A (plot 11), or CD62L (plot 12), respectively. (B) Total BM cells were stained with anti-Endoglin followed sequentially by anti-rat-PE/CY5.5, a cocktail of biotinylated lineage-specific antibodies, and streptavidin-APC, anti-PrP-FITC, and anti-Sca-1-PE. Plot 1 shows the gate of FSC and SSC channels. The lowest 5% of APC-stained cells (i.e. Lin^-) were gated (plot 2). Plot 3 shows the staining of the gated Lin^- cells with Sca-1 and Endoglin and plot 4, the staining of the gated Lin^- $Sca\text{-}1^+$ $Endoglin^+$ cells with PrP. Plot 5 shows the staining of the gated Lin^- $Sca\text{-}1^+$ $Endoglin^-$ cells with PrP.

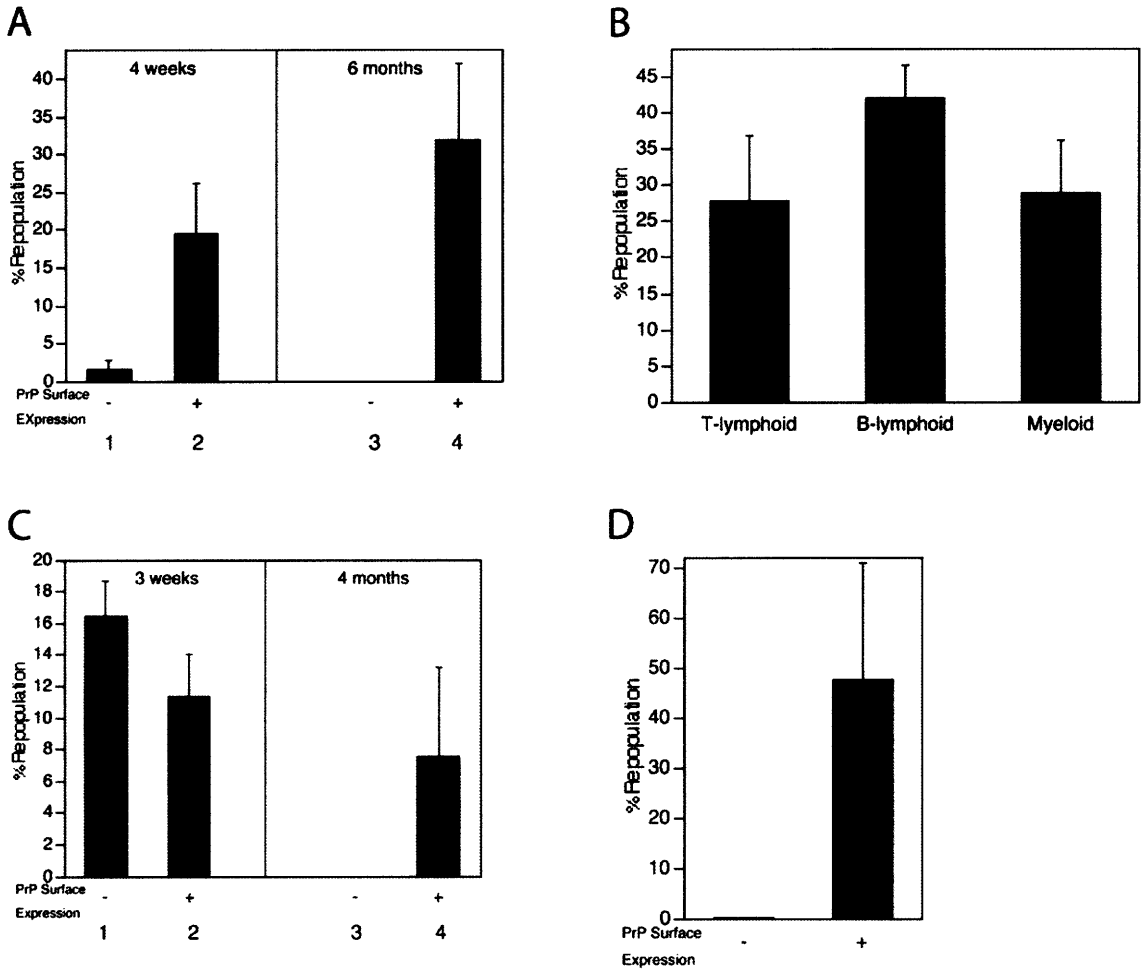

Figure 6. All LT repopulating bone marrow HSC cells express surface PrP. 1 x 10^5 PrP^- or 2 x 10^4 PrP^+ CD45.2 donor BM cells (panel A), or 2 x 10^4 PrP^+ CD45.2 donor BM cells (panel B), or 500 sorted $Lin^-Sca\text{-}1^+PrP^-$ or 100 $Lin^-Sca\text{-}1^+PrP^+$ CD45.2 donor BM cells (panel C), or 500 isolated SP PrP^- or 250 SP PrP^+ donor BM cells (panel D) were mixed with 1 x 10^5 competitor CD45.1 cells and transplanted into lethally irradiated CD45.1 mice (n = 4-5). Donor CD45.2 contribution at 4 weeks and 6 months post-transplant (A). Multilineage contribution at 6 months post-transplant (B). Donor contribution at 3 weeks and 4 months post-transplant (C). Donor contribution at 4 months post-transplant (D).

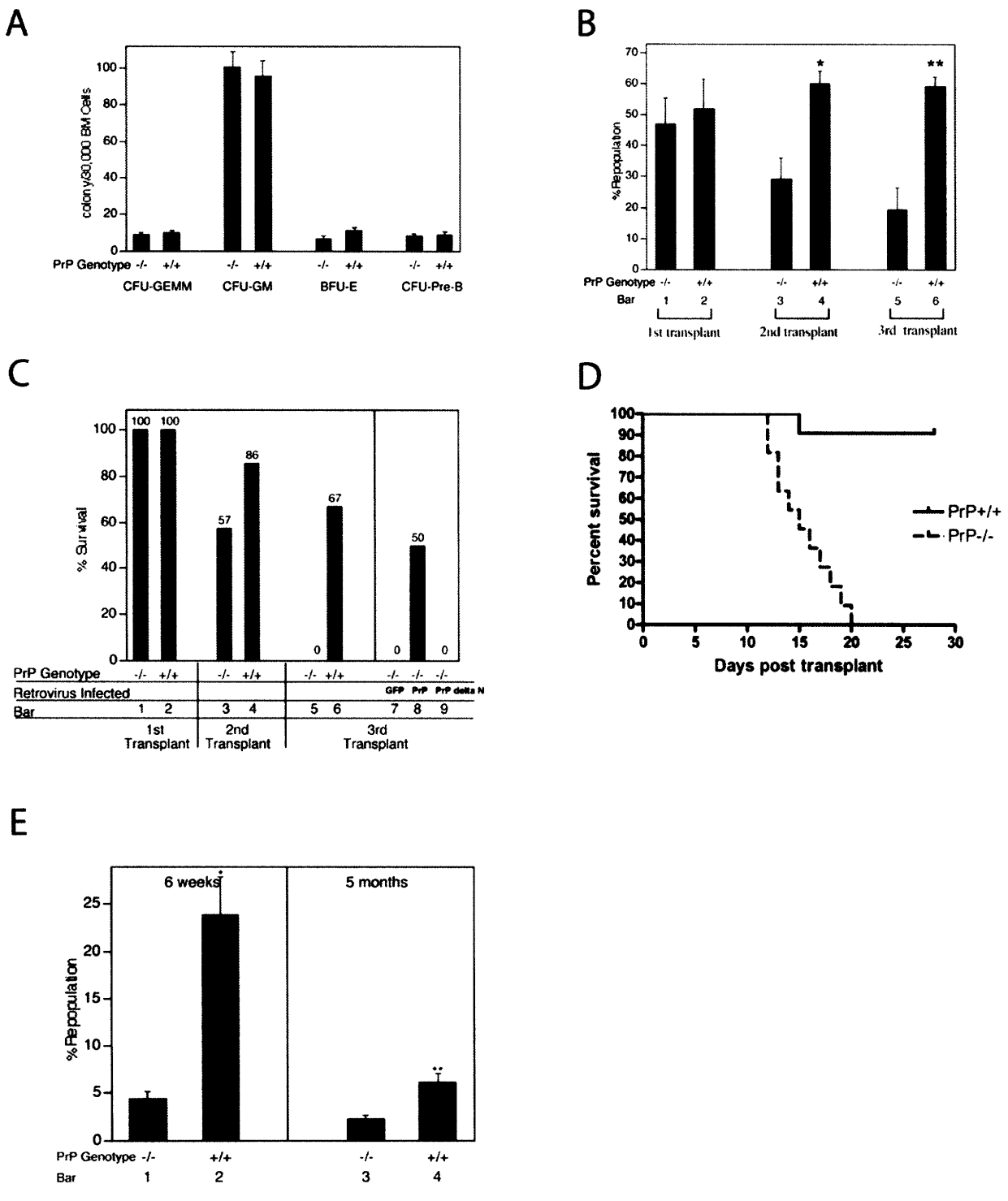

Figure 7 Ectopic expression of PrP rescues the impaired self-renewal of PrP null stem cells during serial transplantation. (A) Colony assays for erythroid, lymphoid, and myeloid progenitors in PrP null and WT BM. Total BM cell populations were plated in methylcellulose medium M3434 (StemCell Technology, Vancouver, Canada) for quantifying CFU-GEMM, CFU-GM, and BFU-E colonies, and in M3630 (StemCell Technology, Vancouver, Canada) for quantifying CFU-Pre-B colonies.

(B) Serial transplantation of PrP null and WT BM with competitor bone marrow cells. 2 x 10^6 donor CD45.2 PrP null or littermate control BM cells were mixed with 2 x 10^6 CD45.1 WT BM cells and transplanted into lethally irradiated CD45.1 recipients (n = 6). The extent of chimerism in peripheral blood (Bars 1, 2) was analyzed 4 months post-transplant. In the experiment in Bars 3-4, BM cells from the primary transplanted mice were pooled and 2 x 10^6 cells were injected directly into each of 5 lethally irradiated CD45.1 recipients. The fraction of donor CD45.2 cells in the peripheral blood of these transplanted mice was analyzed 4 months later. The process was repeated for the tertiary transplants (bars 5-6). This is a combined result of three independent experiments from a total of initial 6 null or wild type control mice. * significantly different from bar 3 value, $p < 0.005$; ** significantly different from bar 5 value, $p < 0.005$.
(C) Serial transplantation of PrP null and WT BM cells without competitors; rescue of HSC activity in PrP null cells by PrP expression. 1 x 10^6 PrP null or WT BM CD45.2 cells, pooled from 3 donors, were transplanted into lethally irradiated CD45.1 recipients without competitors. Recipients were monitored daily for survival for more than 30 days (bars 1-2, n = 6). These mice were sacrificed after 4 months. From them 5 x 10^5 BM cells were collected and transplanted into new irradiated recipients (bars 3-4, n = 7). The process was repeated an additional time for tertiary transplants (bars 5-6, n = 12).
In parallel 1 x10^6 PrP null BM cells isolated from the surviving secondary transplant recipients, as shown in bar 3, were infected by retroviruses encoding GFP, PrP, or PrP Δ23-72, and injected into irradiated recipients (bars 7-9, n = 7-8). Plotted is the fraction of surviving mice 50 days after each bone marrow transplant. See fig. S2 for details of animal survival.
(D) 1 x 10^6 BM from the secondary transplanted mice shown in bars 3 and 4 of Fig. 3C were transplanted into the lethally irradiated recipients. Survival data were plotted as Kaplan-Meier curves (n = 11 for each group, $p < 0.0001$, log-rank test).
(E) Competitive transplantation demonstrates impaired renewal of PrP null HSC activity during successive bone marrow transplants. Here 5 x 10^5 PrP null or WT BM collected from primary transplanted mice 4 months post-transplant (without competitors, as in panel C bars 1-2) were mixed with 5 x 10^5 CD45.1 freshly isolated BM cells and transplanted into lethally irradiated recipients. Peripheral blood engraftment at 6 weeks and 5 months post-transplant is shown (n = 4). * significantly different from bar 1 value, $p < 0.005$; ** significantly different from bar 3 value, $p < 0.05$.

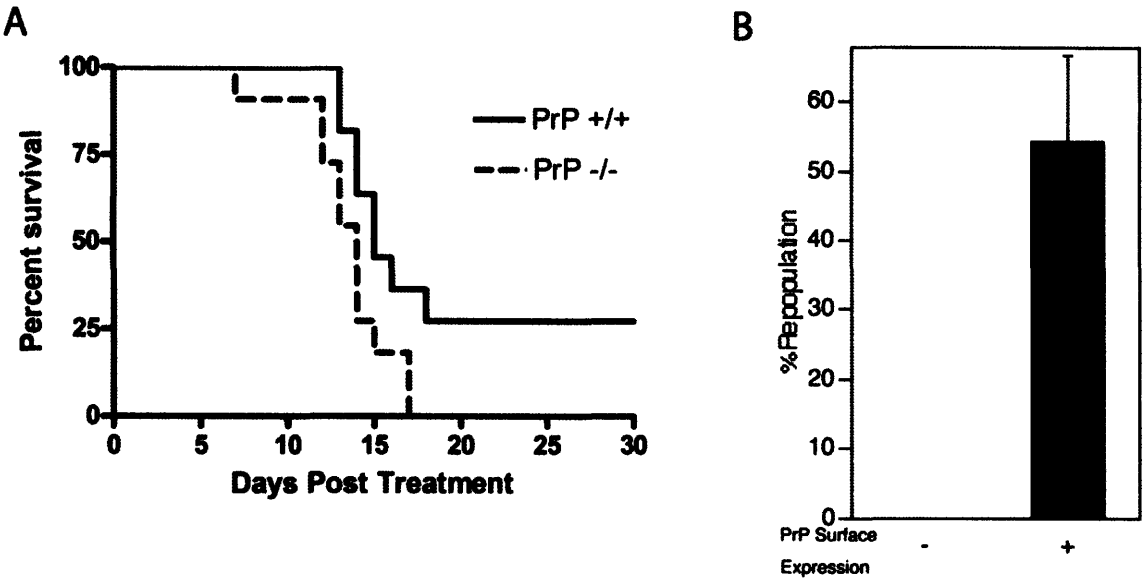

Figure 8 **PrP null HSCs are more sensitive than normal to myelotoxic injury.** (A) 5 x 10^5 CD45.2 PrP null or wild-type BM cells, pooled from three littermates, were transplanted into lethally irradiated CD45.1 recipients, respectively. One month post-transplant, 11 recipient mice from each group were treated with 150 mg/kg 5-FU i.p. weekly for 2 weeks. The survival of these two groups was analyzed using a log-rank nonparametric test ($p = 0.0307$, $n = 11$ in each group) and expressed as Kaplan-Meier survival plot. (B) 150 mg/kg 5-FU was administered i.p. to 3 wild-type CD45.2 mice. After 3 days, the BM of these treated mice was pooled and fractionated according to PrP expression. 1 x 10^5 PrP^+ or 1 x 10^6 PrP^- total BM cells was transplanted, together with 2 x10^5 competitor CD45.1 wild-type BM cells, into lethally irradiated CD45.1 recipients. The level of chimerism in the peripheral blood of the recipients was analyzed 4 months later ($n = 5$).

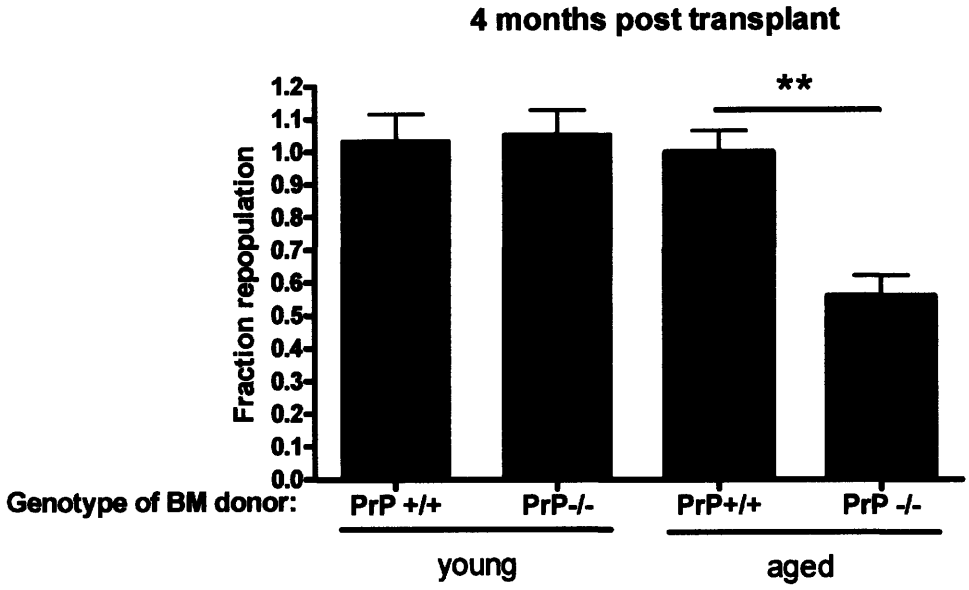

Figure 9 Aged PrP knockout bonemarrow (16-20 months old) shows diminished repopulating activity in a competitive reconstitution analysis. These data were pooled from two separate experiments and normalized to young PrP+/+ samples ($P<0.01$, Student's T test)

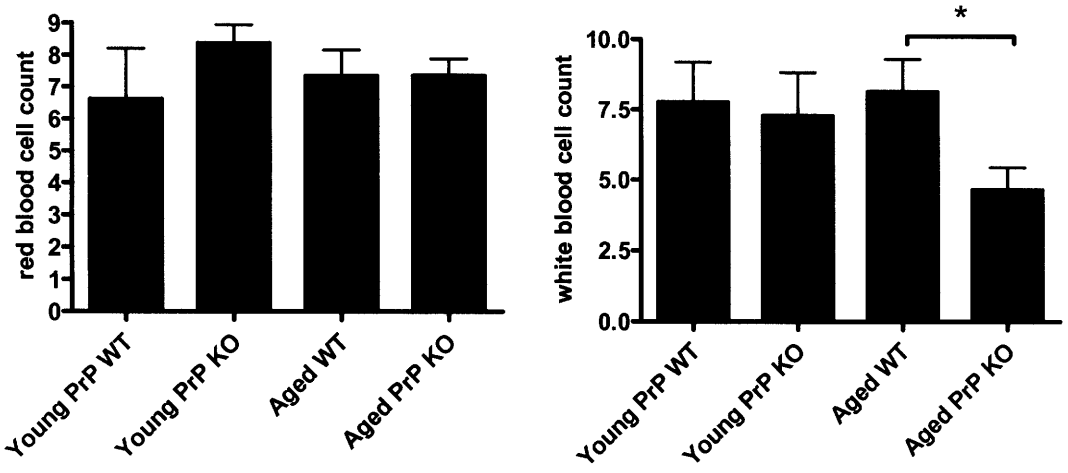

Figure 10 Complete blood count analysis from peripheral blood of young and old PrP WT and KO mice. Red blood cell counts were equivalent between you and old mice irrespective of PrP genotype. For young PrP WT n=5, young PrP KO n=4, aged WT n=12, aged KO n=9. * denotes $P<0.05$, Student's T test.

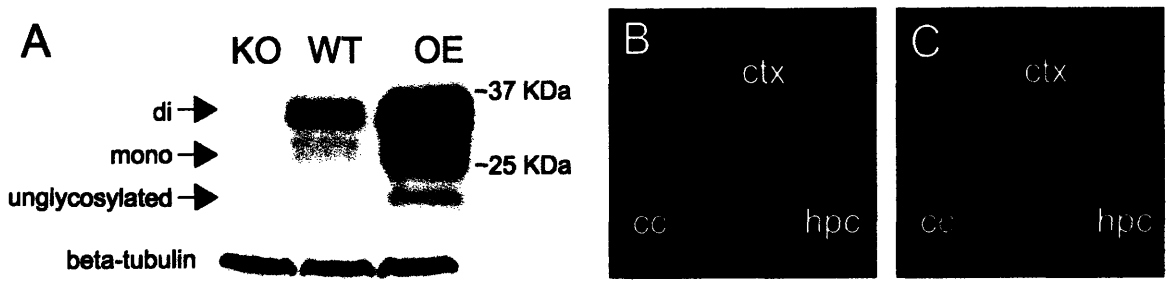

Figure 11 Confirmation of PrP protein expression and *in vivo* antibody specificity. (A) The absence of PrP^c in KO mouse brain and its over-expression in PrP^c OE transgenic mice was confirmed by Western blots of whole brain homogenate using a monoclonal antibody against the PrP^c protein. The uppermost, middle, and lower bands of the PrP^c blot (upper panel) correspond to di-, mono-, and un-glycosylated PrP^c, respectively. The blot was re-probed with an antibody against beta-tubulin to demonstrate equal loading (bottom panel). (B and C) Specificity of the polyclonal antibody against PrP^c was confirmed in 30 μm sections of adult brain from PrP^c OE (B) and PrP^c KO (C) mice at equal exposures. cc, corpus callosum; ctx, cortex; hpc, hippocampus.

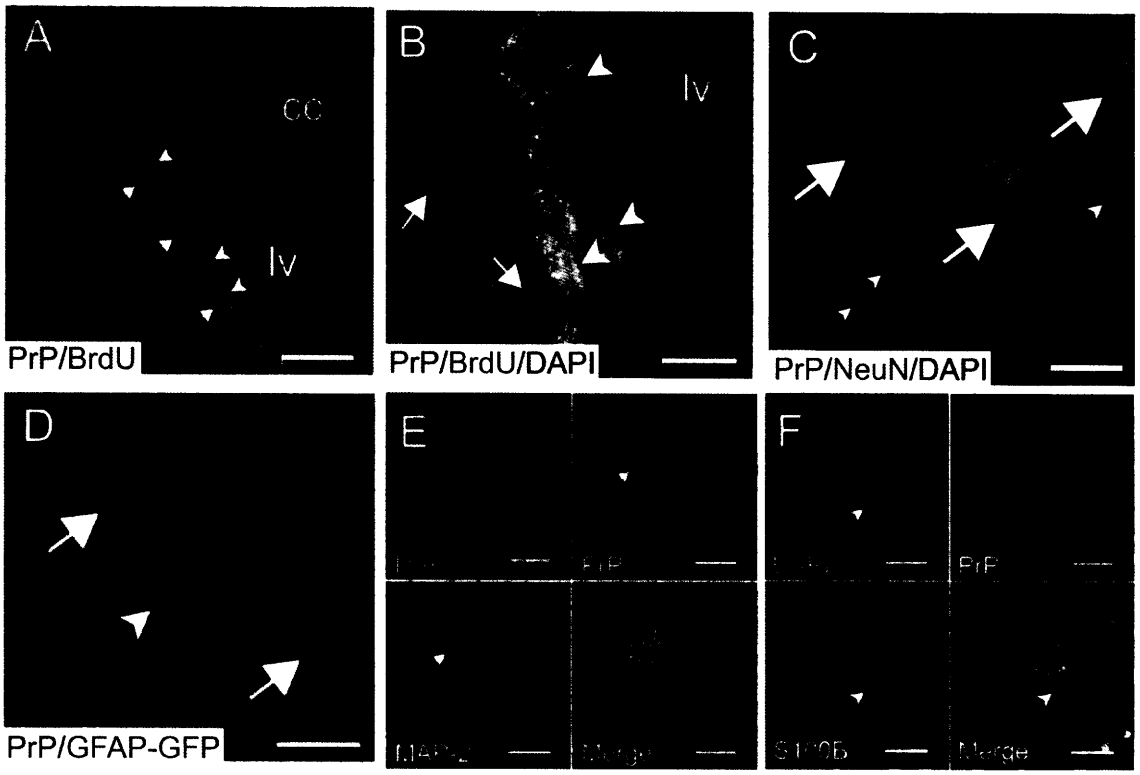

Figure 12 PrP^c is expressed in neurogenic regions and is strongly expressed in neurons *in vivo* and *in vitro*. (A) Proliferation in the SVZ of the adult mouse detected with BrdU (green, arrowheads). PrP^c-positive cells (red, arrows) are found adjacent to the neurogenic region. (B) A close-up of the SVZ region shown in (A), indicating that PrP^c (red, arrows) is not expressed in proliferating cells (green, arrowheads), but instead is expressed in cells just lateral to those proliferating in the SVZ. (C and D) Three-dimensional confocal reconstructions of the CNS *in vivo*. (C) PrP^c (red in all micrographs) is strongly expressed in mature NeuN-positive neurons (green, arrows). Note the lack of PrP^c in surrounding DAPI stained cells with small compact nuclei consistent with glia (arrowheads). (D) PrP^c is not expressed in GFAP-positive astroglia identified by a human GFAP (hGFAP) promoter driving expression of eGFP (arrowhead, green). PrP^c-positive, GFAP-negative cells (arrows) surround the astrocyte. (E and F) Embryonic neural precursor cultures. (E) PrP^c (red, arrows), is most strongly expressed in MAP-2-positive neurons (green), whereas it is not detected in S100β-positive astroglia (F, arrowheads, green). DAPI nuclear counterstain (blue) in Figures *B, C, E,* and *F*. Scale bar in A, 100 μm; in B, 10 μm; in C and D, 25 μm; in E and F, 100 μm. cc, corpus callosum; lv, lateral ventricle.

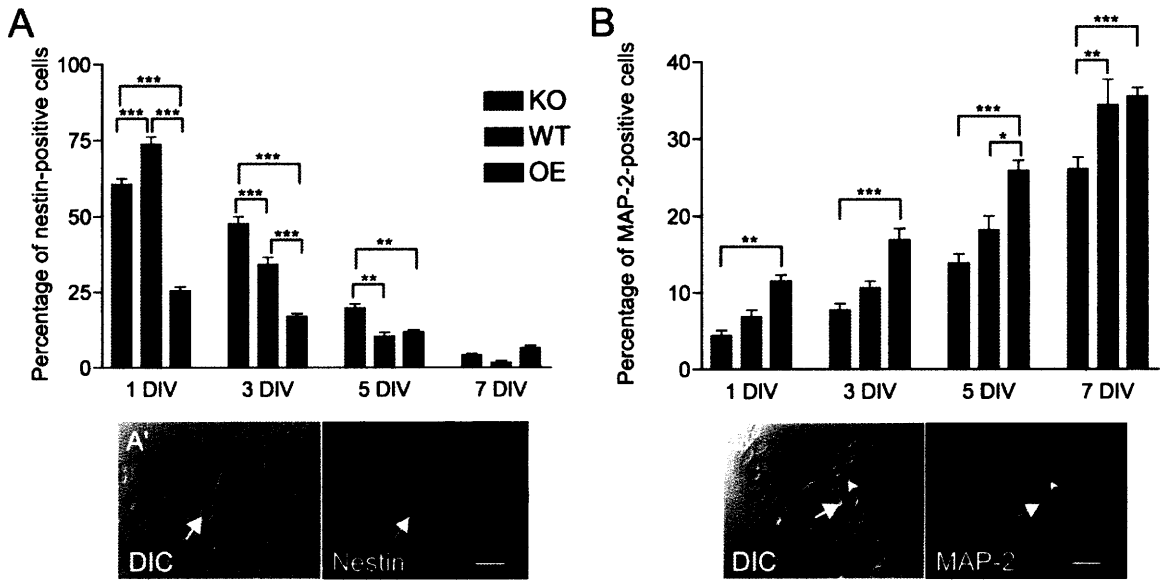

Figure 13 PrP^c levels increase differentiation of embryonic neural precursors in vitro. (A) Neural precursors derived from PrP^c KO embryos remain as uncommitted multipotent precursors (A', nestin-positive, arrow) for a longer period than do precursor derived from WT and, especially, OE embryos. Three days after induction of precursor differentiation via removal of bFGF (3 DIV), there are significant differences between the percentage of nestin-positive precursors derived from KO, WT, and OE embryos. PrP^c OE precursors differentiate from their multipotent state more rapidly than do those from KO and WT mice, even at 1 DIV. By 7 DIV, there are no significant differences among any of the three groups. (B) Differentiation and maturation into a neuronal phenotype (B', MAP-2-positive; cell body, arrow; cell process, arrowhead) occurs at a significantly slower rate in PrP^c KO-derived precursors than in WT, and differentiation is significantly more rapid in PrP^c OE-derived precursors. PrP^c KO precursors are still capable of producing neurons, indicating a delay in neuronal production rather than a failure to differentiate. Scale bar in A' and B', 50 μm. (*, $P < 0.05$; **, $P < 0.01$; ***, $P < 0.001$).

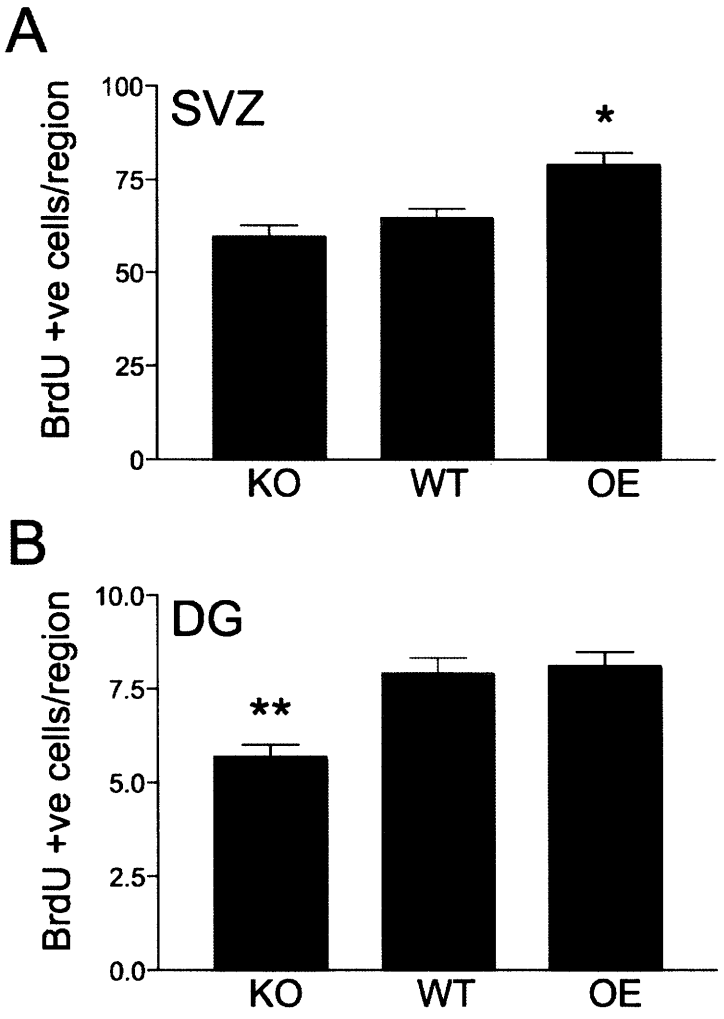

Figure 14 PrP^c increases proliferation *in vivo*. *(A)* One hour after a pulse label of BrdU, PrP^c OE mice have significantly more proliferating cells in the SVZ than in PrP^c KO or WT mice. *(B)* In the DG, PrP^c KO mice have significantly fewer proliferating cells than do WT or OE mice. (*, $P < 0.01$; **, $P < 0.001$).

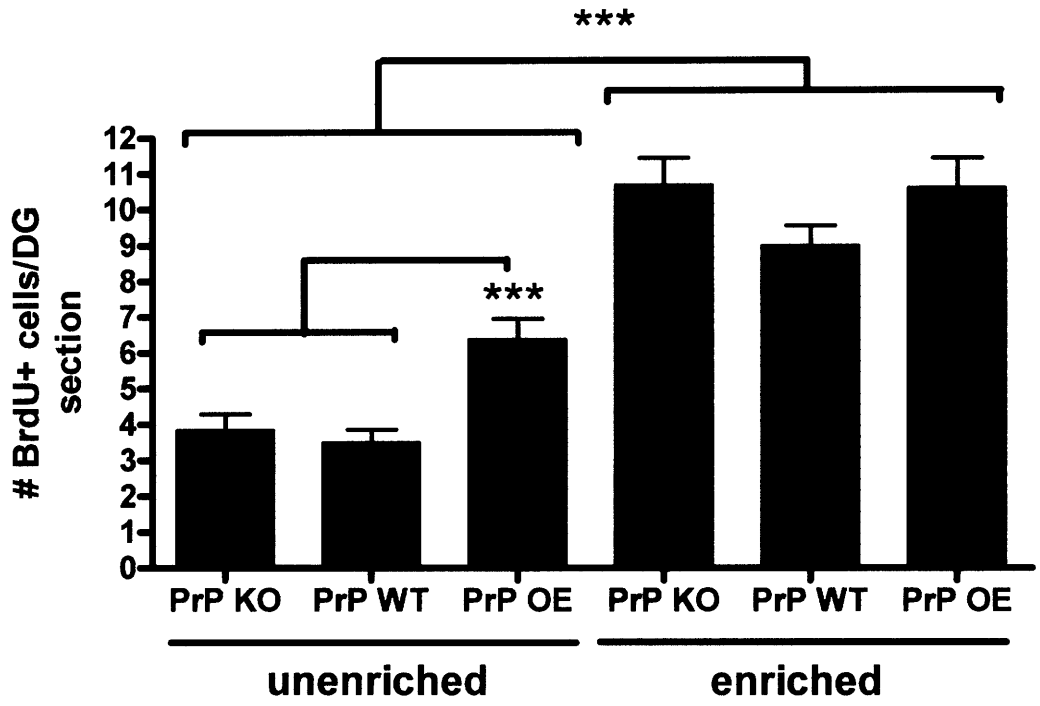

Figure 15 Cellular proliferation was measured by BrdU administration immunohistochemistry in sections of the dentate gyrus of PrP KO, WT, or OE mice under normal housing conditions or environmentally enriched housing conditions. Mice were either normally housed or environmentally enriched for 35 days then administered BrdU for 5 days (50mg/kg) and sacrificed 28 days after the last BrdU injection. Under basal housing conditions, PrP OE mice had a higher level of cellular proliferation ($P<0.001$, T test) compared with PrP KO or WT. (Note that this was not observed in the prior figure where we pulse labeled BrdU for 1 hour which is a different BrdU dosing protocol). During environmental enrichment there is a dramatic increase in the number of BrdU positive cells per DG section in all genotypes. All enriched samples are significantly elevated over unenriched samples ($P<0.001$, Students T test), but there were no significant among the enriched groups.

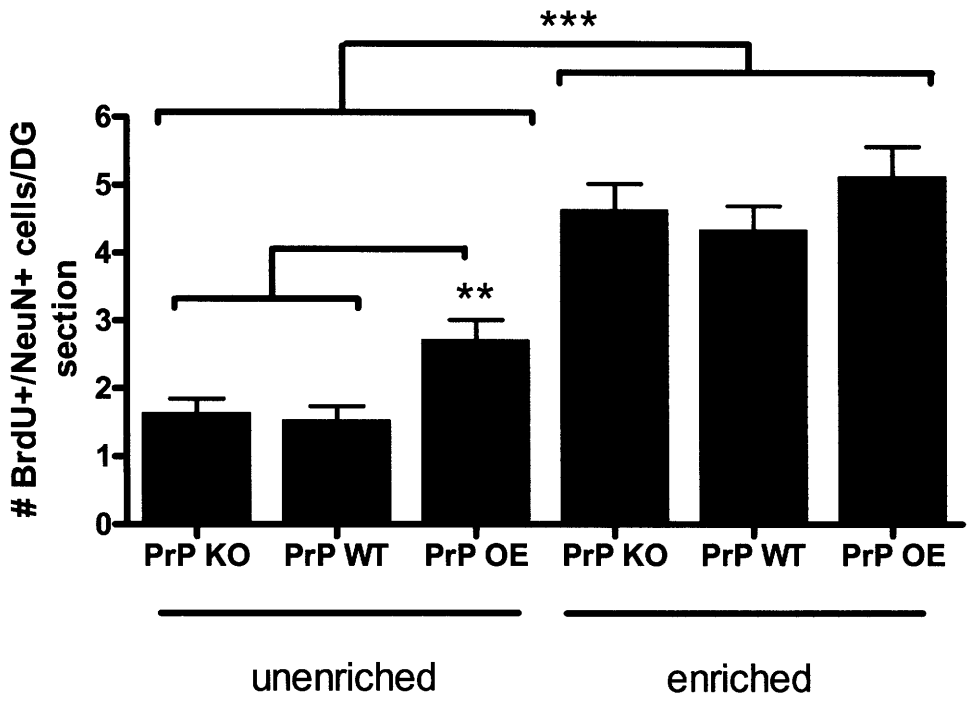

Figure 16 Neurogenesis was measured by combined BrdU and NeuN labeling of serial sectioned dentate gyrus of PrP KO, WT, or OE mice under normal housing conditions or environmentally enriched housing conditions (as described in prior legend). Under basal housing conditions, PrP OE mice had a higher level of cellular proliferation ($P<0.001$, T test) compared with PrP KO or WT. During environmental enrichment there is a dramatic increase in the number of BrdU positive cells per DG section in all genotypes. All enriched samples are significantly elevated over unenriched samples ($P<0.001$, Students T test), but there were no significant among the enriched groups.

Appendix

Supplemental Material

Author Contributions:

Section 1 (PrP deletion in mouse models of neurodegeneration):

I designed and performed the mouse crosses and phenotypic analysis with assistance from Walker Jackson and Susan Lindquist. Artur Topolszki was responsible for most of the mouse breeding and genotyping. Chunni Zhu and Marie-Francoise Chesselet (UCLA) performed huntingtin aggregate staining in Figure 3.

Section 2 (Prion protein promotes the self-renewal of hematopoeitic stem cells during serial transplantation and aging):

Cheng Cheng Zhang was the leader of all experiments presented in this section with the exception of the aged PrP knockout mouse studies, which I led. I assisted Cheng Cheng more heavily (intellectually and physically) in the work related to PrP function presented in Figures 7 and 8 and contributed only a little to Figures 5 and 6. Megan Kaba assisted with the reconstitution studies of the aged PrP knockout mice and the retroviral rescue experiment and Mark Fleming's laboratory (Children's Hospital, Harvard Medical School) performed the complete blood count. Susan Lindquist and Harvey Lodish provided intellectual input in the design and interpretation of this work.

Section 3 (Prion protein positively regulated neural precursor proliferation during developmental and adult mammalian neurogenesis):

Jason Emsley and I led this project jointly. I presented him with the idea that PrP might be involved in adult neurogenesis and he provided all the expertise to help test this hypothesis. Hande Ozdinler preformed the *in vitro* precursor differentiation assay with timed pregnant matings that I had set up. Jason Emsley performed all confocal microscopy experiments. I conducted the environmental enrichement experiment and Artur Topolszki sectioned all of the brains (he also genotyped all the mice used in this study). Ashley Palmer performed all the cell counts used to generate the graphs in Figures 15 and 16. Jeffrey Macklis and Susan Lindquist provided intellectual guidance in this project.

Preliminary evidence for a synthetic lethal genetic element with prion protein deletion

When I intercrossed PrP KOs with the mouse model of tauopathy I did not obtain expected Mendelian ratios of PrP null progeny from the F1 intercross of xx in the F2 generation. A table summarizing these results is below:

		Predicted	Observed	
	fraction expected	# mice	# mice	fraction observed
PrP +/+	0.25	83.3	109	0.33
PrP +/-	0.5	165.5	199	0.6
PrP -/-	0.25	83.3	25	0.08
		total pups screened:	333	

X square test for PrP genotypes
8.82066E-13

One possible interpretation of these results is that there was a synthetic lethality between PrP deletion and an allele in the mutant Tau transgenic background (which is composed of C57BL/6, DBA/2, and Swiss-Webster). The data are consistent with this hypothetical synthetic lethal allele being lethal when it is present in one or two copies but only lethal when combined with PrP deletion. This effect was independent of the mutant Tau transgene. To address this possibility, I crossed PrP KOs to each of the inbred strains—C57BL/6, DBA/2, and Swiss-Webster—that constitute the genetic background of the Tau transgenic mice. However, I obtained expected Mendelian ratios of PrP knockout in each of the genetic backgrounds tested. It is possible that the effect that I observed when crossing to the mutant Tau transgenic mouse was a more complex multigenic interaction.

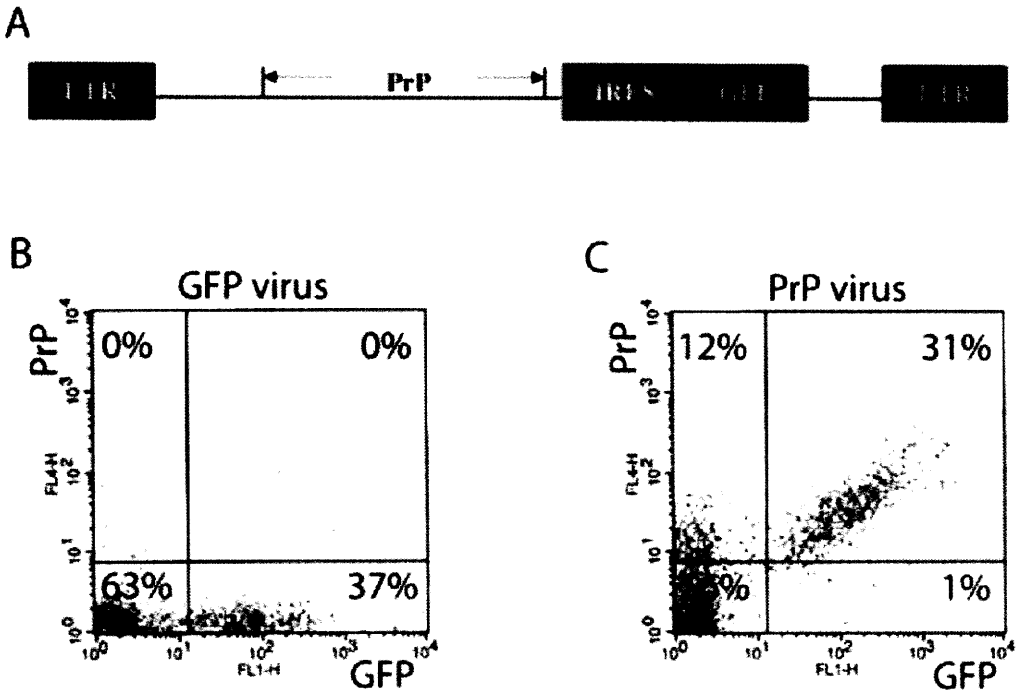

Supp. Fig. 1 Retrovirus infection of PrP-null bone marrow (BM) cells. (*Upper*) A schematic description of the retroviral expression vector for mouse PrP. In the lower panels, PrP-null BM collected from secondary transplanted recipients, as in Fig. 3*C* bar 3, were infected by PrP or control GFP retrovirus. 48 h later, cells were stained with a Lin^{+}-PE antibody mixture, and anti-PrP followed by anti-mouse-APC. Lin^{-} cells were gated to show the expression of GFP and specific staining of PrP in all of the GFP-positive cells in the right panel.

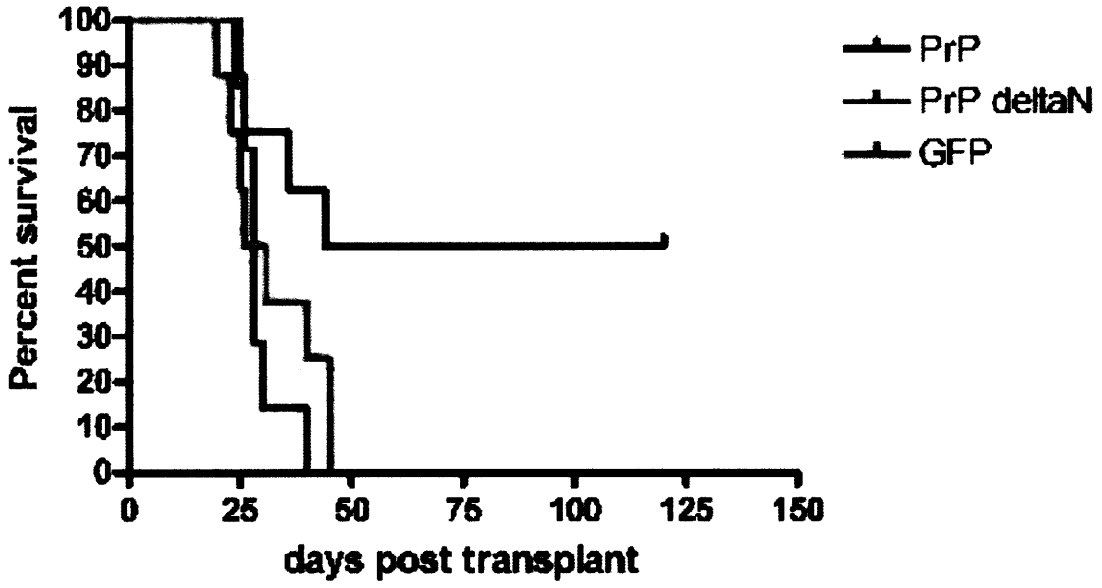

Supp. Fig. 2 Retrovirus transduction of PrP protein into PrP bone marrow (BM) cells rescued lethally irradiated mice that were transplanted with the PrP-null BM after the secondary BMT, shown as survival curves. The same survival data as shown in bars 7-9 in Fig. 3C were plotted as Kaplan-Meier curves (n = 7-8 for each group, $P < 0.05$, log-rank test).

Table 1. Expression of antigens on PrP^+ and PrP^- subfractions of BM SP cells

Antigen name	Endo	Sca-1	CD43	CD44	CD49d	CD49e	CD11a	CD62L
% PrP-positive cells in $antigen^-$ fraction	56.4 ± 12.0	50.9 ± 12.4	48.6 ± 23.0	36.1 ± 11.4	46.0 ± 10.0	49.9 ± 7.1	45.0 ± 10.0	29.1 ± 10.5
% PrP-positive cells in $antigen^-$ fraction	18.8 ± 5.0	18.2 ± 8.3	31.3. ± 19.7	4.2 ± 5.1	17.8 ± 21.8	25.6 ± 15.7	51.5 ± 9.6	56.5 ± 9.4

Antigen expression was determined by flow cytometry. Data represent the mean percentage of PrP-positive cells ± SEM: $n = 3–5$.

Table 2. Peripheral blood analysis of WT and PrP-null mice

Hematologic parameter	$PrP^{+/+}$	$PrP^{-/-}$
WBC count, per mm^3	7.4 ± 1.4	7.9 ± 2.4
RBC count, $\times 10^6$ per mm^3	8.0 ± 1.3	9.2 ± 0.4
Hct, %	47.1 ± 5.9	49.0 ± 3.0
Hgb, g/dL	14.9 ± 0.5	14.5 ± 0.5
Plt count, per mm^3	790.7 ± 62.0	952.7 ± 157.1
Percentage of WBC count		
Neutrophil, %	12.7 ± 2.7	15.0 ± 1.9
Lymphocytes, %	84.7 ± 2.5	80.3 ± 1.1
Monocytes, %	2.0 ± 1.2	1.3 ± 0.4

Mice were backcrossed to the C57BL/6J strain six times. Four- to 5-week-old mice were used. Analysis was performed by the Diagnostic and Comparative Pathology Laboratory at MIT; $n = 3$.

Chapter 3

Automating mouse home cage behavior analysis and application to the study of neurodegenerative disease

This chapter was published by Andrew Steele, Walker Jackson, Oliver King, and Susan Lindquist in Proceedings of the National Academy of Science *(2007) Vol. 104(6): 1983-1988*

Introduction

The value of mouse models for human diseases has created a keen need for high throughput behavioral analyses, as has the ambitious goal of systematic characterization of the complete mouse genome (Auwerx et al., 2004; Brown et al., 2005). Variability in standard behavioral tests hinders comparative studies (Crabbe et al., 1999; Arndt and Surjo, 2001; Kafkafi et al., 2005) and most sample "snapshots" of behavior. Anxiety caused by being handled by the researcher complicates interpretation and obscures subtle phenotypes. Testing behavior during the daytime may not reflect normal behavior, as mice are nocturnal animals. Finally, manual data collection has inherent investigator bias and high labor costs. Automated analysis of mouse behavior will be vital for elucidating the genetic determinants of behavior, for comprehensive analysis of human disease models, and for assessing the efficacy of various therapeutic strategies and their unexpected side effects.

We tested and helped develop a novel conceptual framework for analysis of mouse behavior by evaluating and improving a beta version of HomeCageScan (HCS), a video-based behavior recognition platform. The original version of the software functioned only in proof-of-principle experiments: short recordings of a single mouse. It proved unable to give any meaningful phenotypic data in the laboratory setting. By working reiteratively with the software designers (Clever Systems Inc.) we overcame numerous video recording and hardware problems, increased the throughput of the system, and refined behavioral definitions. Further details of the modifications to the system are described in the Supplemental Methods section. In the end the system provided very high resolution analysis and allowed us to characterize behavior with equally high resolution during the entire light and dark phases, with virtually no intervention by the investigator. We explored the benefits of video-based behavior recognition by conducting

high resolution automated mouse behavior analysis (AMBA) of the home cage (HC) behaviors of two mouse models of neurodegenerative disease, Huntington's disease (HD) and infectious prion disease (PrD).

HD is an autosomal dominant disorder caused by the expression of huntingtin protein with an expanded glutamine repeat (1993). Degeneration of the striatum and cortex leads to severe psychological and motor abnormalities, ending in death (Vonsattel and DiFiglia, 1998). The 'R6/2' mouse is the most widely used HD model, showing an early, severe disease phenotype, with declines in motor performance, cognitive abilities, weight and premature death (Mangiarini et al., 1996). Prion diseases (PrD's) have different etiologies and affect distinct regions of the brain. Acquired genetically, spontaneously, or through exposure to infectious material (Prusiner, 1998), their hallmark features are the misfolding of the prion protein (PrP), dementia, severe ataxia and death. The most common and robust PrD model involves infecting wild-type mice with established 'strains' of prions. Prion-infected mice exhibit hunched posture, ataxia, tail rigidity, priapism, and death (Kingsbury et al., 1983). Behavioral abnormalities such as disturbances in food intake and activity vary depending on the mouse strain as well as the prion strain (Dell'Omo et al., 2002; Cunningham et al., 2005). The diversity of PrD symptoms provide excellent candidates for higher resolution behavioral analysis.

High resolution AMBA enabled us to characterize models of HD and PrD in unprecedented detail and to discover novel disease phenotypes. Using a systems approach to data analysis, we describe unique behavioral signatures for each disease. Combinatorial behavioral metrics allowed earlier assignment of disease onset. This approach will be extremely useful for phenotypic discovery and as an entry point to more specific behavioral tests.

Results

Experimental setup

Previously reported behavior acquisition platforms reduce the mouse to a point in space or count the number of breaks of laser beams. Both give very limited information. HCS employs video images collected at a rate of 30 frames per second in the HC and software algorithms to categorize a diverse set of mouse behaviors. The software extracts the image of the mouse as it moves and automated recovery tools adapt to changes in lighting and bedding. Information on the sequence of postures and position of body parts is used to deduce behaviors by comparisons with pre-trained data sets. For example, "walking" comprises the mouse being in a particular posture and performing a concerted movement of torso and limbs that changes the position of the mouse along the horizontal axis. For "eat" the snout must cross the plane of the food bin with a reared (forelimbs off the ground) posture. For "chew", which is scored after "eat", the mouse moves into a vertically huddled position with its paws in front the snout. Detailed definitions of behaviors are in the Supplemental Methods.

We recorded control and diseased mice and assessed the accuracy of AMBA by viewing and surveying individual videos for approximately 20 mice for 3-4 hours each. Initially, HCS recorded one mouse at a time. We increased the throughput of the system from one cage to four cages by adding extra cameras. HCS initially also mis-scored behaviors so frequently that we could detect no differences between wild-type mice and those suffering from neurodegenerative disease. We worked reiteratively with Clever Systems Inc to improve ease of use, data transfer capabilities, and most importantly, the accuracy of scored behaviors through numerous modifications to the algorithms and re-testings.

The final accuracy assessment was conducted by inspecting approximately 100 instances of each behavior (according to HCS) in a 24 hour video of a single wild-type C57Bl/6 mouse (summary in Supplementary Table I). For 9 of 17 behaviors, ≥90% of the instances identified by HCS agreed with manual assessments. For example, 100/100 behaviors identified by HCS as "hang upside down" were confirmed, 67/70 for "rest," and 95/100 for "walking." For "hang vertical," 75/100 instances identified by HCS were confirmed. However, most errors were for related activities. The 25 behaviors that HCS misidentified as "hang vertical" were all due to "rearing". Both require the animal to be in a vertical posture. For the former, the forelimbs touch the wire rack and the hindlimbs lift off the ground; for the latter hindlimbs remain in contact with the ground. A small fraction of behaviors (1-2% of recording time) were unassigned due to failure of the software to recognize the mouse or a behavior (Figs. 6S and 7S for HD and PrD, respectively). The former often occurred immediately after light/dark transitions. The mis-scoring of behaviors was generally unbiased between wild-type and diseased mice, except for the later timepoints for PrD when the mice move very rapidly and erratically.

Home cage behavioral abnormalities in Huntington's disease mice

Standard methods for detecting the HD transgenic (Tg) phenotype are weight loss, clasping, and declining performance in rotarod and grip strength tests (Mangiarini et al., 1996; Hockly et al., 2003). In other laboratories and in our own these metrics did not reliably detect disease onset until 9-11 weeks (Carter et al., 1999; Hockly et al., 2003). Recently earlier detection has been achieved by examining running-wheel activities (Hickey et al., 2005). We recorded the behaviors of seven HD Tg mice, and seven gender-matched littermate controls, from a side-view of the HC (Fig. 5) for two 24-hour periods weekly, beginning 5-6 weeks of age

until 11-13 weeks, the terminal phase. High resolution AMBA demonstrated many abnormalities in HD Tg behaviors, many of which were previously unknown. Relative to controls, time spent "resting" progressively declined in HD Tgs (Fig. 1A). (The behavior we have defined as "resting" roughly approximates "sleep", but because we have not validated it with electroencephalogram analysis, we use the more general term "rest".) Commensurate with less time spent resting, awakening events were dramatically increased in HD Tgs with transgenic mice awakening from rest as much as 2.5-fold more than controls (Fig. 1B). "Twitching", defined as a movement during rest, was elevated in HD mice at the earliest time point tested and this difference was maintained throughout (Fig. 1C). This difference in resting and awakening between HD Tgs and controls was one of the earliest behavioral abnormalities detected and remained significantly different from 6 weeks onwards for awaken and at 6 time points for rest (Fig. 1A and B). The early detection of rest abnormalities highlights the remarkable sensitivity of AMBA to clearly and unambiguously detect subtle phenotypic changes before more obvious disease onset at 9-10 weeks of age.

High resolution AMBA also revealed decreased exploratory behaviors in HD Tgs. For example, distance traveled provided a robust metric of overall activity and motor performance. By 9 weeks there was a 30% percent decline in the distance traveled by HD Tgs (Fig. 1D). AMBA also detected hyper-grooming in HD Tg mice. At 5 weeks, HD Tgs groom for ~15% of their time increasing steadily to 25% at terminal stages of disease (Fig. 1E). Control mice showed stable week-to-week grooming behavior, 12-14% of total time (Fig. 1E). HD Tgs groomed more frequently than controls rather than grooming for longer bouts (data not shown).

Consistent with previously reported motor abnormalities, high resolution AMBA also quantified defects in behaviors requiring significant grip strength and coordination. Hanging

vertically was reduced in HD Tgs even at the earliest time point tested, 5 weeks, declining approximately 100-fold by 10 weeks (Fig. 1F). Despite considerable variation in hanging behaviors of diseased and control mice, statistically significant differences between HD Tgs and controls were detected at the early age of 8 weeks. Stretching was similar for HD Tgs and controls until 9 weeks when stretching severely declined for HD Tgs (Fig. 1G). This is consistent with their advancing disease 'hunched' posture (Mangiarini et al., 1996) and by 13 weeks HD Tgs rarely stretched (0.003% +/- 0.001 SEM of total time compared to 0.074% +/- 0.02% SEM in Wt controls). Jumping, another complex motor behavior, showed a dramatic decline in HD Tgs (Fig. 1R). Despite large inter-mouse variability of this behavior among controls, a significant difference appeared in HD Tgs by 10 weeks. Alterations in many other behaviors were detected, such as remain low, pause, walk, turn, sniff, rear, eat, chew, drink, and hang upside down (Fig. 6).

Home cage behavioral abnormalities in prion diseased mice

Standard methods for detecting PrD rely on subjective assessments that are not readily quantified: ruffled coat, hunched posture, priapism, and ataxia (Kingsbury et al., 1983). Consistent with a multitude of reports from other laboratories, when we injected mice with prions harvested from brains of infected animals, these symptoms were easily and reliably detected only 3-4 weeks before the endpoint of disease (5.5-6.0 m.p.i.). For AMBA, we recorded eight similarly infected C57Bl/6 males and eight mock-inoculated controls for two 24-hour periods monthly or twice monthly until the terminal phase, 5.5 months post inoculation (m.p.i). AMBA detected alterations in PrD mice behavior much earlier than previously reported and detected many novel phenotypes.

By 3.5 m.p.i. prion-infected animals exhibited a significant decrease in resting and at the final stages of disease PrD mice rested only half as much as mock-injected mice (Fig. 1I). Awakening from rest showed a significant increase in early stages of PrD at 3, 3.5, and 4 m.p.i., and then decreased in the late stages of disease of 5-5.5 m.p.i. (Fig. 2J). Movement during rest, or twitching, was significantly reduced from a very early time point, 3 m.p.i. (Fig. 1K). Thus, rest abnormalities were one of the most sensitive metrics of disease onset for PrD and HD.

Unexpectedly, PrD mice showed an enormous increase in activity concomitant with overt disease onset. Beginning at 4.5 m.p.i., they traveled 1378 (+/- 411 SEM) meters compared to 96 (+/- 5 SEM) meters in controls (Fig. 1L). PrD mice showed a sharp decline in grooming; by advanced disease (5.5 m.p.i.), they spent half as much time grooming as controls (Fig. 1M). In sharp contrast to HD Tg mice, the exploratory activities sniffing and rearing were highly elevated in PrD mice at 3.5 m.p.i. and this increase persisted until the final time point at 5.5 m.p.i. (Fig. 1N and O). Despite ataxia and imbalance, PrD mice spent significantly more time jumping than controls from 4.5 to 5.5 m.p.i. (Fig. 1P). These behavioral alterations occurred at very early time points, long before classic symptoms developed. Many other behavioral alterations were detected, such as remain low, pause, walk, turn, eat, chew, drink, stretch, hang upside down, and hang vertical (Fig. 7).

Behaviors of Huntington's and prion disease mice in the light and dark phase

Data collection over 24 hours allowed us to examine behaviors with respect to the light and dark phase, when mice are normally more active. Wild-type mice were most active during the first half of the dark phase as demonstrated by decreased rest and increased hanging vertical

behaviors (Fig 2A and C, respectively). In the second half of the dark phase resting increased and hanging vertical decreased for wild-type mice (Fig. 2A and C).

At 6 weeks, HD Tgs slept a similar amount of time as controls during the dark phase (Fig. 2A); however, even at this early stage, HD Tgs slept less during the light phase. This difference in rest during the light phase was observed again at a later stage of disease (Fig. 3B). HD Tgs spent slightly less time hanging vertical than did control mice during the dark cycle at 6 weeks, but during the light cycle the hanging behavior was the same (Fig. 2C). By 11 weeks, the difference in hang vertical behavior with respect to light and dark cycles was much more profound (Fig. 2D). The HD Tgs showed a statistically significant decrease in hanging vertical throughout the entire dark phase. Thus, these behavioral alterations observed in HD Tgs were often observed only in light or dark phases.

PrD mice also showed remarkable changes in behaviors, distinct from HD Tgs, with respect to light and dark phases. Resting was similar between PrD and control mice at 2 m.p.i., prior to disease symptoms (Fig. 2E). Resting for both PrD and control mice was fairly constant throughout the light and dark phase, with a slight increase for both in the light phase (Fig. 2E). At 5 m.p.i., PrD mice barely rested during the dark phase in striking contrast to controls whereas little difference was observed in rest during the light phase (Fig 2F). Upon first entering a new cage, both PrD and control mice spent time walking indicative of exploring the new cage (Fig. 2G). In PrD and control mice at 2 m.p.i., walking was uniformly distributed during the light and dark phases (Fig. 2G). However, by 5 m.p.i., PrD mice showed a profoundly different pattern of walking; during the dark phase, PrD mice walked approximately ten fold more than controls (Fig. 4H).

Systems approach to defining disease phenotypes

The behavioral changes in both HD and PrD mice were marked compared to control mice and were distinct between diseases. To examine the HD and PrD phenotypes globally with respect to time, we employed an approach pioneered in other high-throughput high-resolution technologies such as microarray analysis. The assessment of each phenotype for each time point is represented by a box in a grid. Different colors represent behaviors that increase (yellow) or decrease (blue), with black indicating no change. Different intensities of color were used to represent different degrees of phenotypic change. To generate the phenotypic array displayed in Figure 3, data were normalized by dividing mean diseased mouse values by mean control mouse values. In Figure 8, the array is shown in terms of P-values, with 5 behaviors significantly different between HD and control mice at the early time point of 6 weeks and 8 behaviors for PrD at 3.5 m.p.i.. This style of representation yields a comprehensive disease signature of HD and PrD mice and demonstrates strikingly different easily comprehended symptomologies for these diseases at a single glance.

To define disease onset effectively we took a systems-level approach—which considers the interdependencies between parts of a whole—to analyze the behavioral phenotypes. Examining combinations of behaviors rather than single behaviors in isolation allowed for early detection of disease onset. We used logistic regression to construct diagnostic rules based on linear combinations of the different behaviors. We constructed diagnostic rules independently for the 9 time points in the disease progression of HD Tg mice and 8 time points for PrD mice. These rules typically involved 1-7 behaviors. The rules perfectly separated HD Tgs from controls at 6 weeks and subsequent time points, and separated PrD mice from controls beginning at 3.5 m.p.i.. The rule sufficient for diagnosing HD Tgs at week 7 encompassed the combination

of awaken, groom, and sniff behaviors (Fig. 4A). The rule for predicting PrD and control mice at 4 m.p.i utilized awaken and twitch behaviors (Fig. 4B). The hyperplanes in Figures 4A and B are the boundaries between the regions of behavior-space in which mice are classified as diseased and the regions in which they are classified as controls. Note that in Figure 4A none of the single features awaken, groom, or sniff separates HD mice from control mice, but a linear combination of the three features successfully predicts diseased mice. We used L_1 regularization to control over-fitting (Tibshirani, 1996), the details of which can be found in Supplemental Methods. Detailed results of cross-validation at all time points are given in Supplementary Table 2.

Discussion

We have established a novel, rigorous system for characterizing behavioral abnormalities in the mouse and have employed it to demonstrate a contrasting array of behavioral changes in HD and PrD mouse models. Despite intense study of both models, many of these behavioral alterations were previously unreported, such as hyper-grooming in HD Tgs and increased activity in PrD mice. We detected significant abnormalities in HD Tgs for most behaviors examined. Many behavioral abnormalities were observed at the reported age of disease onset for the HD Tgs, at 9-11 weeks (Mangiarini et al., 1996; Carter et al., 1999; Lione et al., 1999; Morton et al., 2005). However, the sensitivity of high resolution AMBA detected statistically significant differences as early as 6 weeks for five behaviors despite the limited sample size (n=7 Wt and n=7 HD Tg; Fig. 1; Fig. 8). In addition, we detected differences in some exceedingly rare behaviors, such as stretching (Fig. 1G), with high accuracy. With current testing paradigms for HD Tgs, a large sample size is often required for drug trials (Hockly et al., 2003). High resolution behavioral analysis such as provided by HC monitoring should reduce this number,

cost and labor particularly for mutants or models that are difficult to breed (Mangiarini et al., 1996).

Our analysis of HC behaviors showed that the HD and PrD models reflect human symptomology better than previously appreciated. Most of the behavioral testing of HD mice is focused on their robust motor phenotypes (Hickey et al., 2005), yet HD patients often present with psychological symptoms (Vonsattel and DiFiglia, 1998) and some cognitive defects have been described in HD Tgs (Lione et al., 1999; Murphy et al., 2000). Our analysis of HC activity revealed substantial psychological abnormalities in HD Tgs, such as hyper-grooming, decreased resting, and altered patterns of behavior with respect to the light-dark cycle. The rest-wake abnormalities that we observed in HD Tgs have also been reported as a clinical phenotype in human HD patients, who suffer from sleep disturbances (Morton et al., 2005). Increased drinking behavior in HD Tgs may mirror the diabetes that is characteristic of HD patients (Hurlbert et al., 1999). In addition we detected decreases in motor and exploratory phenotypes of HD Tgs. High resolution AMBA was equally valuable in phenotyping PrD mice. They were distinguishable from controls at 3.5 m.p.i., with subtle phenotypic changes later followed by more dramatic changes (Fig. 3B). The increased activity observed during prion infection is unprecedented. Mice undergoing calorie restriction, which radically increases the activity of mice, showed a ~5 fold increase in distance traveled (Chen et al., 2005). PrD mice travel nearly 15-fold more distance at 4.5 m.p.i.. For PrD mice we established a previously undocumented rest disturbance phenotype which is likely of relevance to a genetic form of PrD in humans known as fatal familial insomnia (Prusiner, 1998) and to sleep abnormalities in Creutzfeldt-Jakob disease (Landolt et al., 2006).

Since the HC provides an unperturbed laboratory environment for mice it has the potential to reduce the variability observed in many types of behavioral testing. Our approach

presents some disadvantages. Minimal bedding was used to reduce obstruction of the mouse, which eliminates the instinctive behaviors dig and forage. Also, since we cannot discriminate two mice in the same cage, mice must be singly housed during testing. High resolution AMBA will never replace the cleverly designed, highly specific behavioral tests employed to assess particular physical and behavioral deficits. But our approach offers advantages including automated data collection, minimal labor, and unbiased interpretation of video data. In this study we have measured 18 parameters from a procedure requiring minimal handling. Our approach and other automated behavioral measurement technologies will be of vital importance in detection and quantification of phenotypes in the rodent. The ability to detect a multitude of behavioral alterations and robustly diagnose both HD and PrD mice by 6 weeks and 3.5 m.p.i, respectively, will greatly aid in testing therapeutics on these mouse models of human disease.

Materials and Methods

Mouse strains and prion inoculations

All experiments were approved by the MIT Committee on Animal Care. The HD line was obtained from Jackson Laboratories (Bar Harbor, Maine) as ovarian transferred females. This line is maintained on a mixed C57Bl/6J and CBA genetic background and ovarian transplanted females were crossed with wild-type males of the same mixed genetic background to generate the mice used in this study. The PCR genotyping protocol is described elsewhere (Hockly, 2003 #26). C57Bl/6 males were purchased from Taconic and injected intracranially with 30□l of 0.1% uninfected mouse brain homogenate or 0.1% RML scrapie-infected mouse brain homogenate containing approximately 5.5 log ID_{50} / 30ul. Food and water were provided *ad libitum* and mice were singly housed for the duration of the study while being maintained on a 12:12 light-dark

cycle. During video recording, dim (25 Watt) red lights were used for recording in the dark phase. Since red light can entrain circadian rhythms of rodents (McCormack, 1980 #61), it is possible that entrainment effects were caused by our nighttime recording conditions.

Video Recording Setup

Four JVC digital video cameras (model number GR-D93) were mounted perpendicular to the cages (Fig. 5). The cameras input into a Pelco video processor connected to a Dell Dimension computer with an ATI All-In-Wonder video card. Video data was analyzed by HomeCageScan software (Clever Systems Inc, Reston, Virginia) using a Dell Dimension 450 computer. During recording, mice were housed in standard cages, using minimal bedding (80ml) to minimize mounding, which can obscure the mouse. The cage was changed after the first 24 hours of recording. Mice were recorded for 2 consecutive days per week for the duration of the HD Tg lifespan. With very few exceptions data presented in the figures are from 46-49 hours of recording; however in a few instances 23-25 hours of recording is used due to inadequate recording and/or analysis. PrD mice and their controls were similarly recorded for 2 consecutive 24 hour periods at 1, 2, 3, 3.5, 4, 4.5, 5, and 5.5 m.p.i.. All prion-infected mice died between 5.5 and 6 m.p.i., on average 177 days (+/- 5.7 days, SD).

Estimation of the accuracy of HCS software

Numerous videos were hand scored and compared to HCS scoring. For final estimation of the accuracy of HCS presented in Supplementary Table I we reviewed approximately 100 instances of each behavior for a single C57Bl/6 mouse (as described in the Results), unless the behavior occurred fewer than 100 times during the 24 hour test video, giving an accuracy percentage for each behavior.

Data Analysis

Reported P-values were computed using the nonparametric Wilcoxon rank-sum tests (two-tailed), using the MATLAB function RANKSUM. We used a non-parametric test because the sample sizes were not large enough for us to confidently conclude that the data were normally distributed. However, unpaired two-tailed student's T tests gave very similar results. Reported P-values were not adjusted for multiple-hypothesis testing. However, as we tested for differences in 19 behaviors, at each time point fewer than one is expected to have a P-value less than 0.05 by chance. P-values for classification accuracy in Supplementary Table 2 are one-tailed, using the exact binomial test to compute the probability of making at least the observed number of correct predictions by chance.

References

(1993) A novel gene containing a trinucleotide repeat that is expanded and unstable on Huntington's disease chromosomes. The Huntington's Disease Collaborative Research Group. Cell 72:971-983.

Arndt SS, Surjo D (2001) Methods for the behavioural phenotyping of mouse mutants. How to keep the overview. Behav Brain Res 125:39-42.

Auwerx J, Avner P, Baldock R, Ballabio A, Balling R, Barbacid M, Berns A, Bradley A, Brown S, Carmeliet P, Chambon P, Cox R, Davidson D, Davies K, Duboule D, Forejt J, Granucci F, Hastie N, de Angelis MH, Jackson I, Kioussis D, Kollias G, Lathrop M, Lendahl U, Malumbres M, von Melchner H, Muller W, Partanen J, Ricciardi-Castagnoli P, Rigby P, Rosen B, Rosenthal N, Skarnes B, Stewart AF, Thornton J, Tocchini-Valentini G, Wagner E, Wahli W, Wurst W (2004) The European dimension for the mouse genome mutagenesis program. Nat Genet 36:925-927.

Brown SD, Chambon P, de Angelis MH (2005) EMPReSS: standardized phenotype screens for functional annotation of the mouse genome. Nat Genet 37:1155.

Carter RJ, Lione LA, Humby T, Mangiarini L, Mahal A, Bates GP, Dunnett SB, Morton AJ (1999) Characterization of progressive motor deficits in mice transgenic for the human Huntington's disease mutation. J Neurosci 19:3248-3257.

Chen D, Steele AD, Lindquist S, Guarente L (2005) Increase in activity during calorie restriction requires Sirt1. Science 310:1641.

Crabbe JC, Wahlsten D, Dudek BC (1999) Genetics of mouse behavior: interactions with laboratory environment. Science 284:1670-1672.

Cunningham C, Deacon RM, Chan K, Boche D, Rawlins JN, Perry VH (2005) Neuropathologically distinct prion strains give rise to similar temporal profiles of behavioral deficits. Neurobiol Dis 18:258-269.

Dell'Omo G, Vannoni E, Vyssotski AL, Di Bari MA, Nonno R, Agrimi U, Lipp HP (2002) Early behavioural changes in mice infected with BSE and scrapie: automated home cage monitoring reveals prion strain differences. Eur J Neurosci 16:735-742.

Hickey MA, Gallant K, Gross GG, Levine MS, Chesselet MF (2005) Early behavioral deficits in R6/2 mice suitable for use in preclinical drug testing. Neurobiol Dis 20:1-11.

Hockly E, Woodman B, Mahal A, Lewis CM, Bates G (2003) Standardization and statistical approaches to therapeutic trials in the R6/2 mouse. Brain Res Bull 61:469-479.

Hurlbert MS, Zhou W, Wasmeier C, Kaddis FG, Hutton JC, Freed CR (1999) Mice transgenic for an expanded CAG repeat in the Huntington's disease gene develop diabetes. Diabetes 48:649-651.

Kafkafi N, Benjamini Y, Sakov A, Elmer GI, Golani I (2005) Genotype-environment interactions in mouse behavior: a way out of the problem. Proc Natl Acad Sci U S A 102:4619-4624.

Kingsbury DT, Kasper KC, Stites DP, Watson JD, Hogan RN, Prusiner SB (1983) Genetic control of scrapie and Creutzfeldt-Jakob disease in mice. J Immunol 131:491-496.

Landolt HP, Glatzel M, Blattler T, Achermann P, Roth C, Mathis J, Weis J, Tobler I, Aguzzi A, Bassetti CL (2006) Sleep-wake disturbances in sporadic Creutzfeldt-Jakob disease. Neurology 66:1418-1424.

Lione LA, Carter RJ, Hunt MJ, Bates GP, Morton AJ, Dunnett SB (1999) Selective discrimination learning impairments in mice expressing the human Huntington's disease mutation. J Neurosci 19:10428-10437.

Mangiarini L, Sathasivam K, Seller M, Cozens B, Harper A, Hetherington C, Lawton M, Trottier Y, Lehrach H, Davies SW, Bates GP (1996) Exon 1 of the HD gene with an expanded CAG repeat is sufficient to cause a progressive neurological phenotype in transgenic mice. Cell 87:493-506.

Morton AJ, Wood NI, Hastings MH, Hurelbrink C, Barker RA, Maywood ES (2005) Disintegration of the sleep-wake cycle and circadian timing in Huntington's disease. J Neurosci 25:157-163.

Murphy KP, Carter RJ, Lione LA, Mangiarini L, Mahal A, Bates GP, Dunnett SB, Morton AJ (2000) Abnormal synaptic plasticity and impaired spatial cognition in mice transgenic for exon 1 of the human Huntington's disease mutation. J Neurosci 20:5115-5123.

Prusiner SB (1998) Prions. Proc Natl Acad Sci U S A 95:13363-13383.

Tibshirani R (1996) Regression shrinkage and selection via the lasso. Journal of the Royal Statistical Society 58:267-288.

Vonsattel JP, DiFiglia M (1998) Huntington disease. J Neuropathol Exp Neurol 57:369-384.

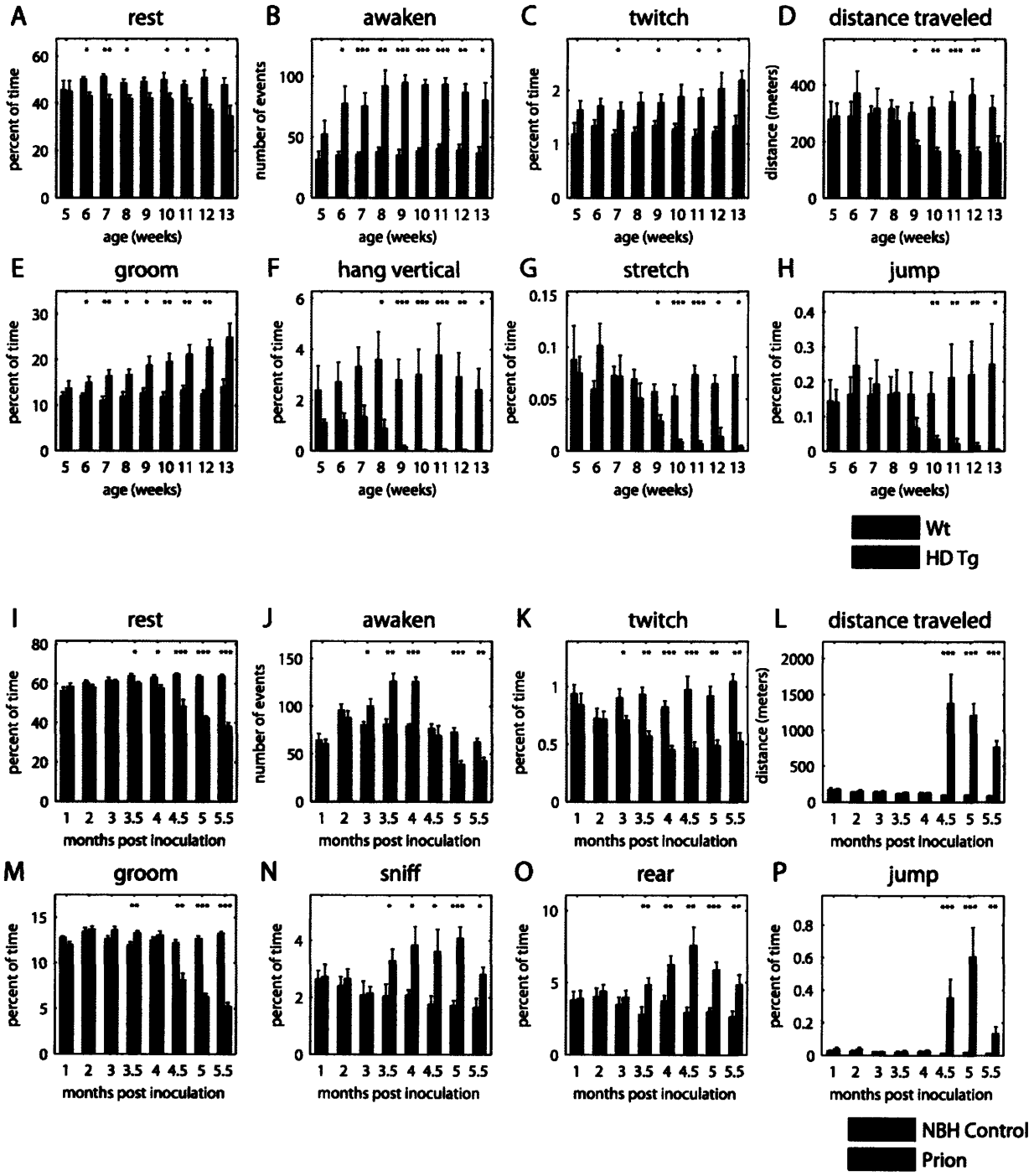

Figure 1 Behavioral alterations in Huntington's and Prion disease mice. Mean values (+/- SEM) for HD and controls are shown for rest (A), awaken (B), twitch (C), distance traveled (D), groom (E), hang vertical (F), stretch (G), jump (H). Mean values for PrD and controls are shown for rest (I), awaken (J), twitch (K), distance traveled (L), groom (M), sniff (N), rear (O), and jump (P). P-values were computed using a two-tailed Wilcoxon rank-sum test (nonparametric) and are indicated as follows * $P<0.05$, ** $P<0.01$, and *** $P<0.001$ (sample sizes for HD were n=5 HD Tg and WT control pairs for week 5 , n =7 for weeks 6-11, n=6 for week 12, and n=4 for week 13; for PrD, n=8 for every time point except for 5 m.p.i. where n=7 prion and n=8 controls).

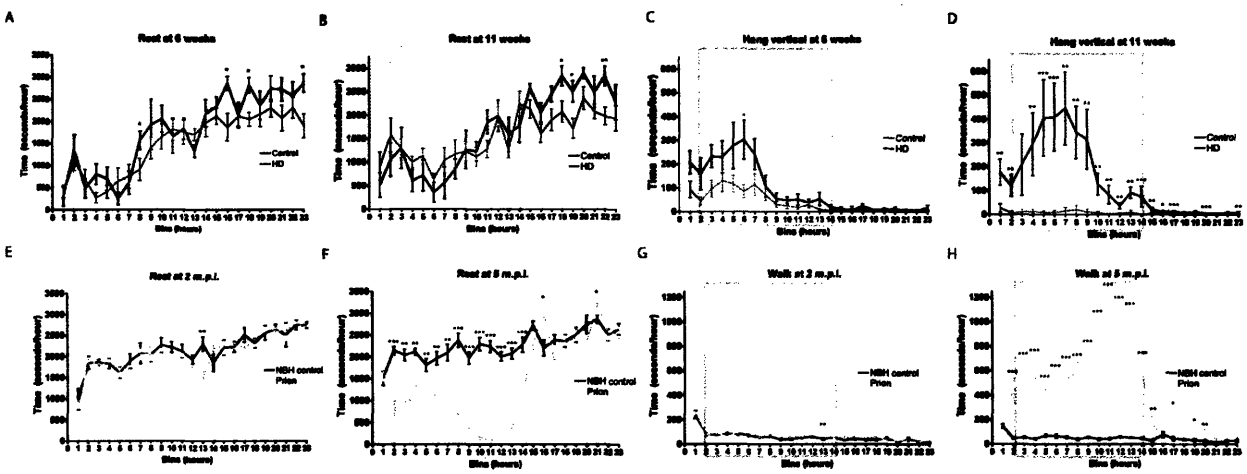

Figure 2 Behavioral alterations with respect to light and dark phases in HD and PrD mice. Resting at 6 weeks (A) and 11 weeks (B) and hanging vertical at 6 weeks (C) and 11 weeks (D) is displayed in 1 hour bins for HD mice (red line) and controls (black line). Resting at 2 m.p.i. (E) and at 5 m.p.i. (F) and walking at 2 m.p.i. (G) and 5 m.p.i. (H) is displayed in 1 hour bins for PrD mice (blue line) and controls (black line). Shaded boxes represent the dark cycle (19:00-7:00). P-values were computed using a two-tailed Mann-Whitney test (nonparametric) and are indicted as follows * $P<0.05$, ** $P<0.01$, and *** $P<0.001$ (sample sizes for each time point are n=7 HD Tg and n=7 Wt controls (A-D) and n= 8 prion and n=8 controls (E-H).

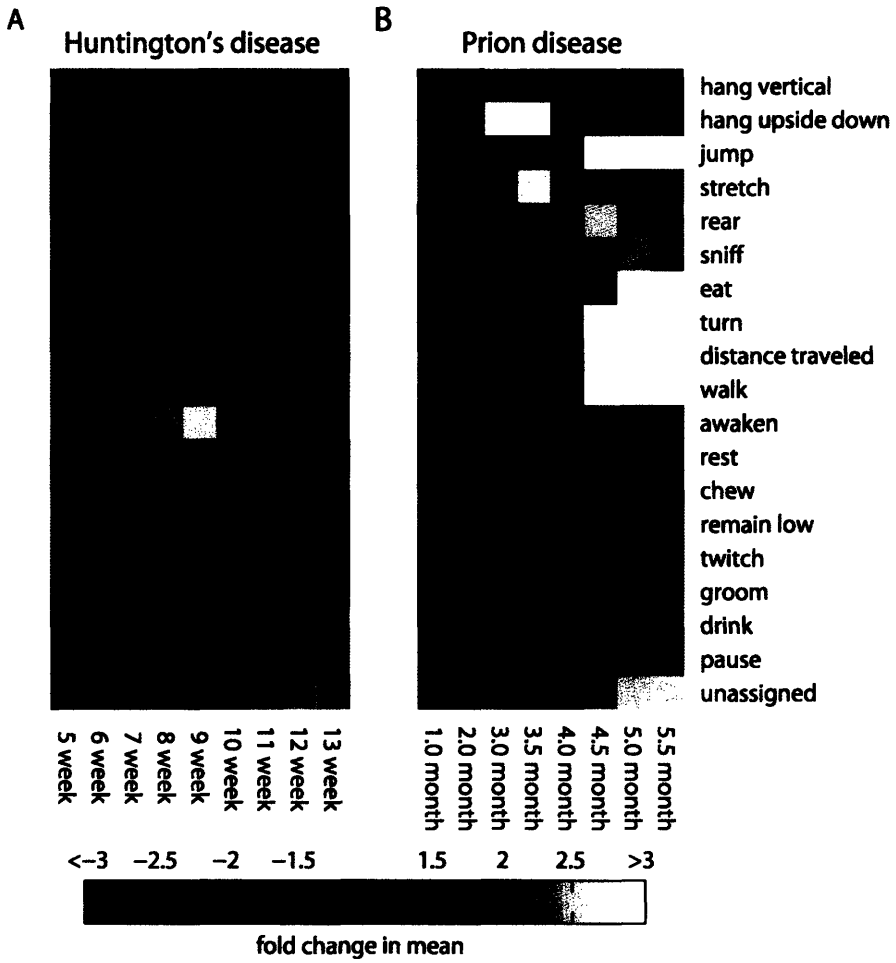

Figure 3 Phenotypic arrays of HD and PrD behaviors over time. Mean values for HD (A) or PrD (B) were divided by mean control values to give the fold increase or decrease in the behaviors listed. The fold increase or decrease is indicated in the figure as increasing intensity of blue for negative fold changes or yellow for positive fold changes.

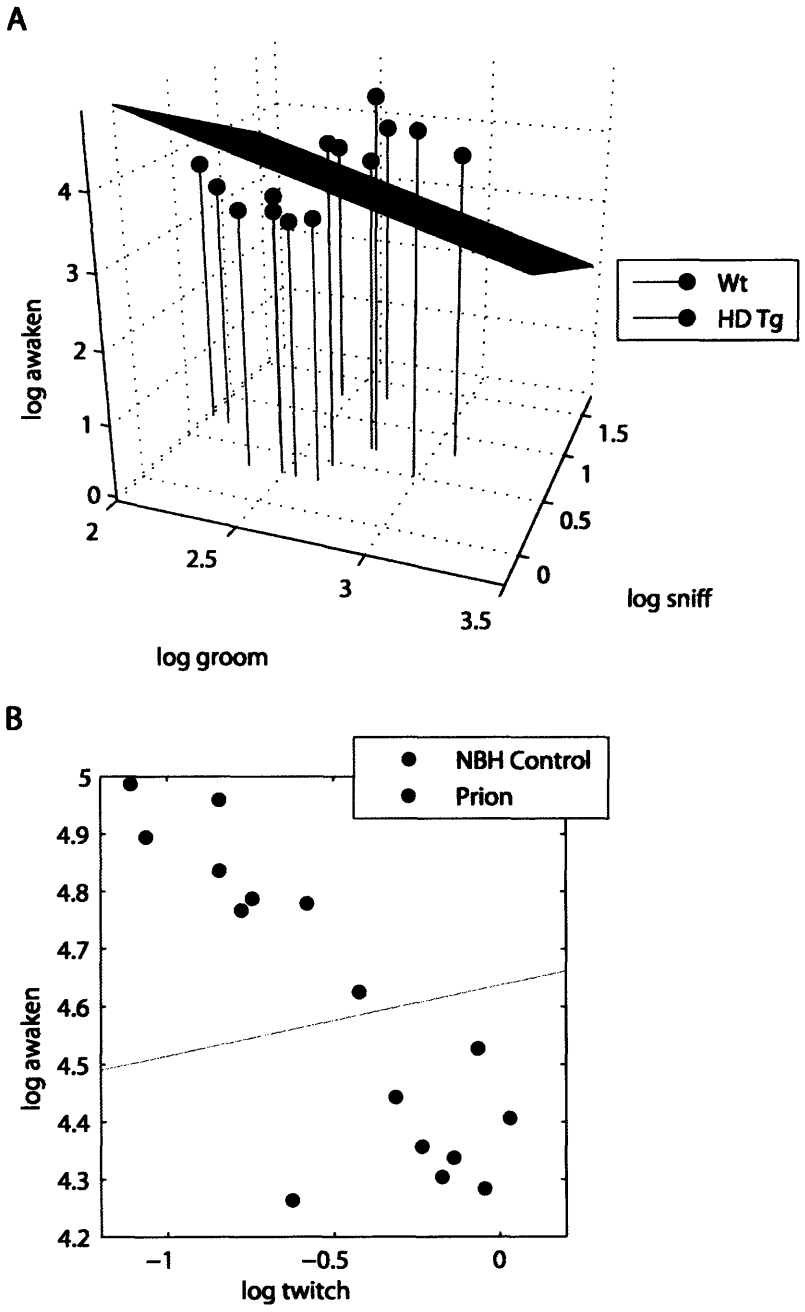

Figure 4 Multi-feature analyses to separate diseased from control mice. A three-dimensional plot of the log of awaken, groom, and sniff behaviors that discriminate HD from control mice at 7 weeks of age (A). A two-dimensional plot that separates PrD mice from controls at 4 m.p.i. using the log of awaken and twitch (B).

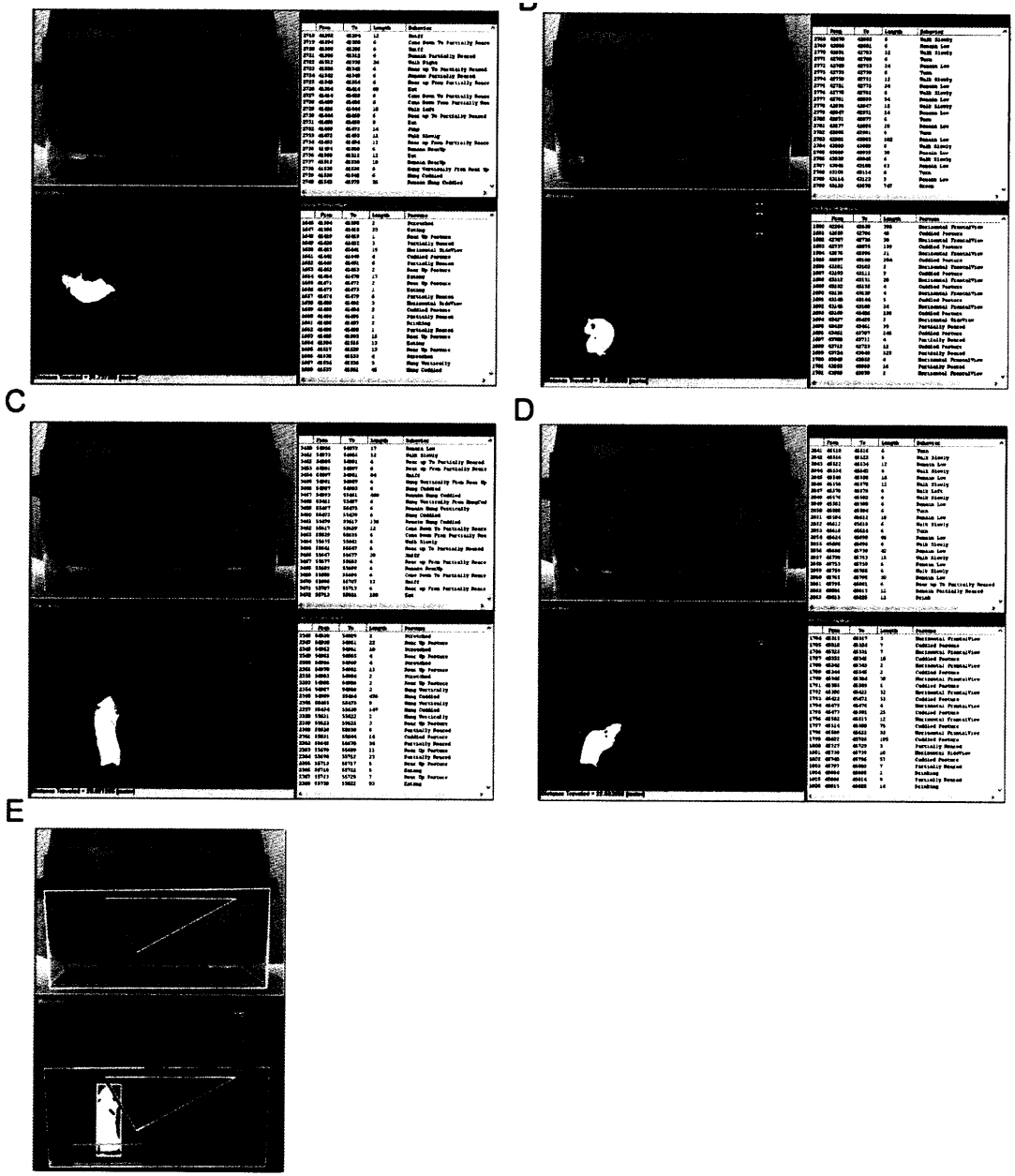

Figure 5 A picture of the video and HCS interface. Examples of hanging upside down (a), grooming (b), eating (c), and drinking (d) are shown. In (e) the line weight of the image in (c) is increased to make the cage demarcations more clear.

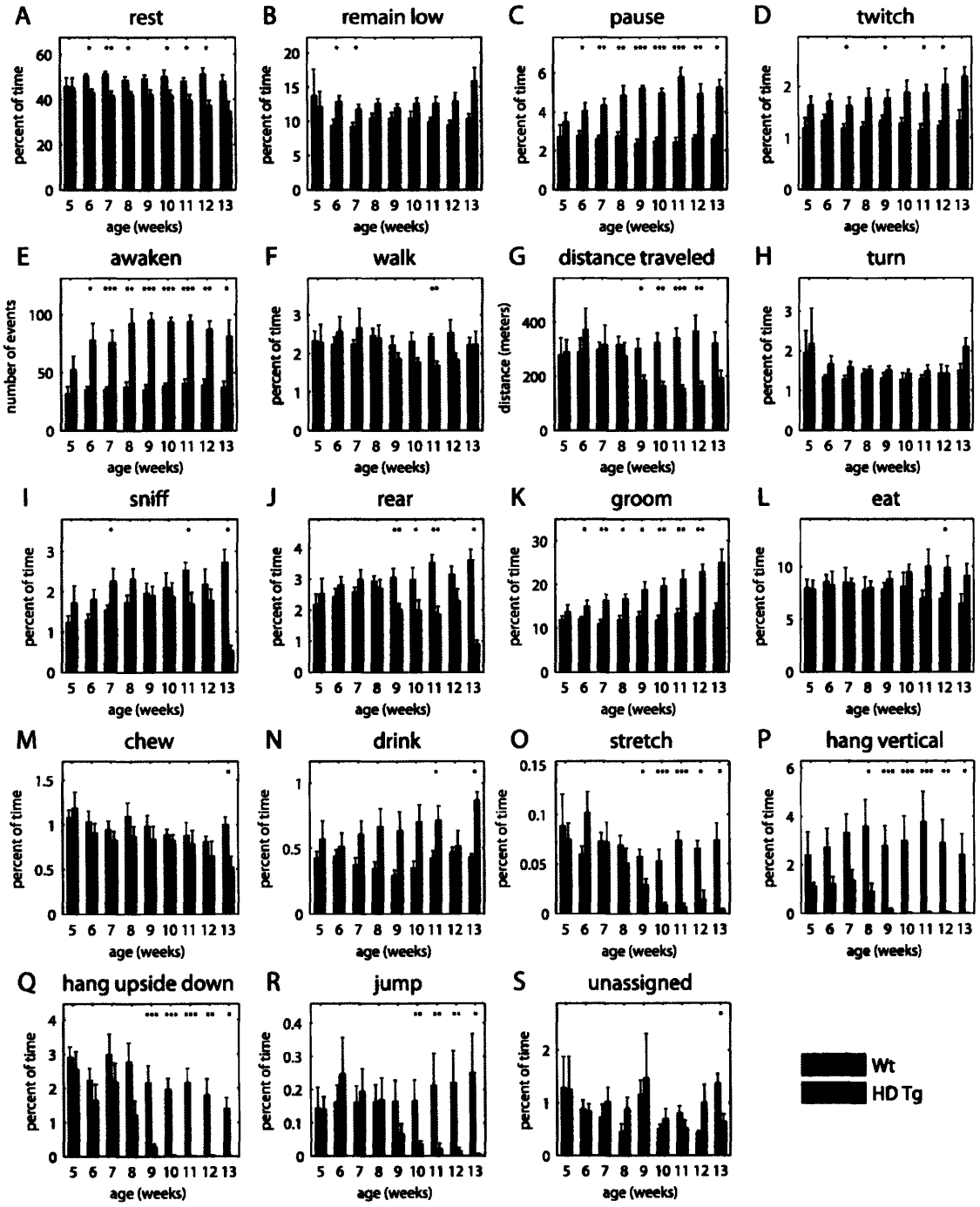

Figure 6 Behavioral alterations in Huntington's disease mice. Mean values (+/- SEM) are shown for rest (a), remain low (b), pause (c), twitch (d), awaken (e), walk (f), distance traveled (g), turn (h), sniff (i), rear (j), groom (k), eat (l), chew (m), drink (n), stretch (o), hang vertical (p), hang upside down (q), jump (r), and unassigned behavior (s). P-values were computed using a two-tailed Wilcoxon rank-sum test (nonparametric). P-values are indicated as follows * $P<0.05$, ** $P<0.01$, and *** $P<0.001$ (sample sizes for each time point are as follows (n=number of mice) week 5 n=5 HD Tg and WT control pairs, week 6 n=7, week 7 n=7, week 8 n=7, week 9 n=7, week 10 n=7, week 11 n=7, week 12 n=6, and week 13 n=4).

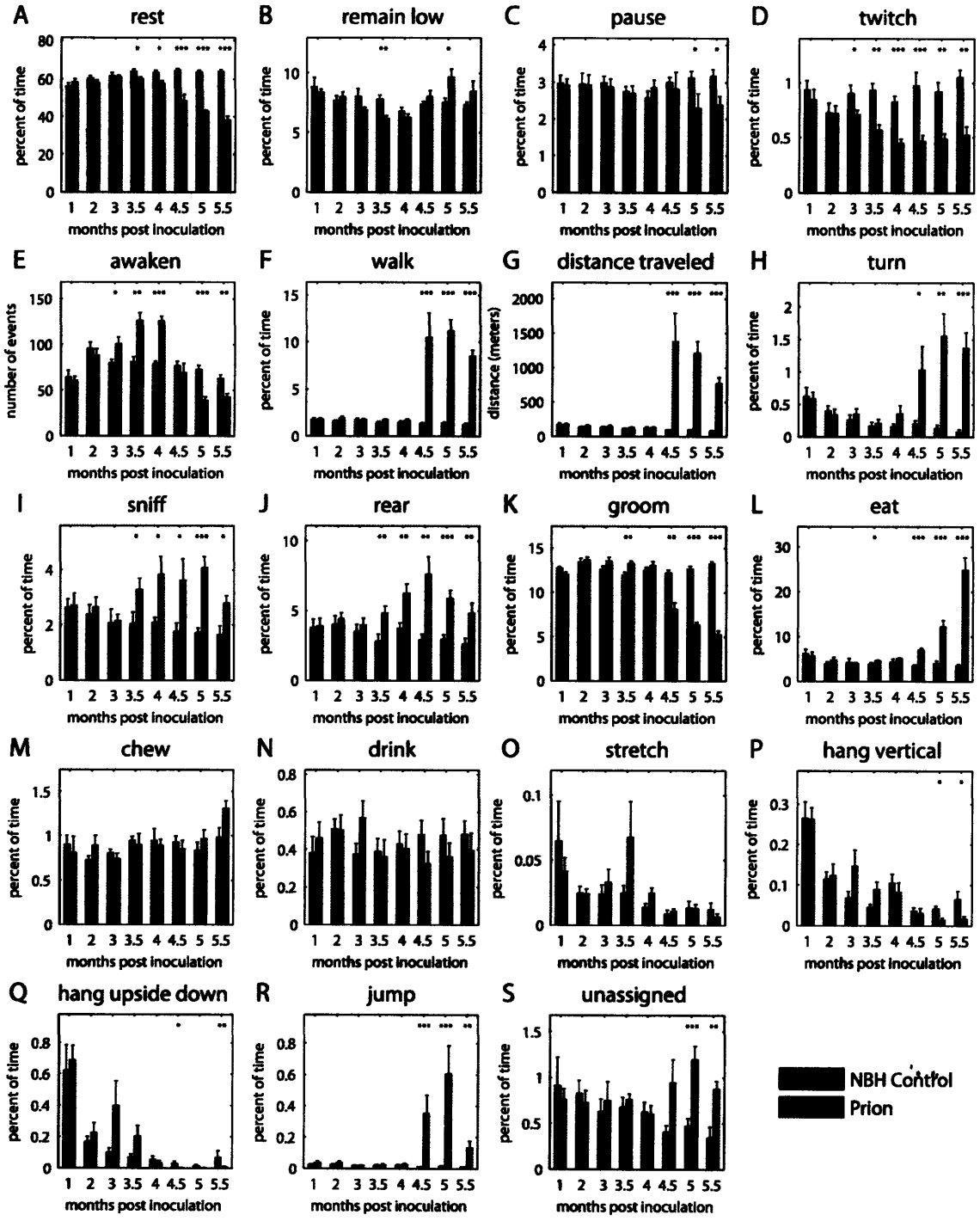

Figure 7 Behavioral alterations in prion disease mice. Mean values (+/- SEM) are shown for rest (a), remain low (b), pause (c), twitch (d), awaken (e), walk (f), distance traveled (g), turn (h), sniff (i), rear (j), groom (k), eat (l), chew (m), drink (n), stretch (o), hang vertical (p), hang upside down (q), jump (r), and unassigned behavior (s). P-values were computed using a two-tailed Wilcoxon rank-sum test (nonparametric). P-values are indicated as follows * $P<0.05$, ** $P<0.01$, and *** $P<0.001$ (sample sizes for each time point are n=8 prion and n=8 normal brain homogenate inoculated controls at all time points except for 5 m.p.i. with n=7 prion and n=8 normal brain homogenate inoculated controls).

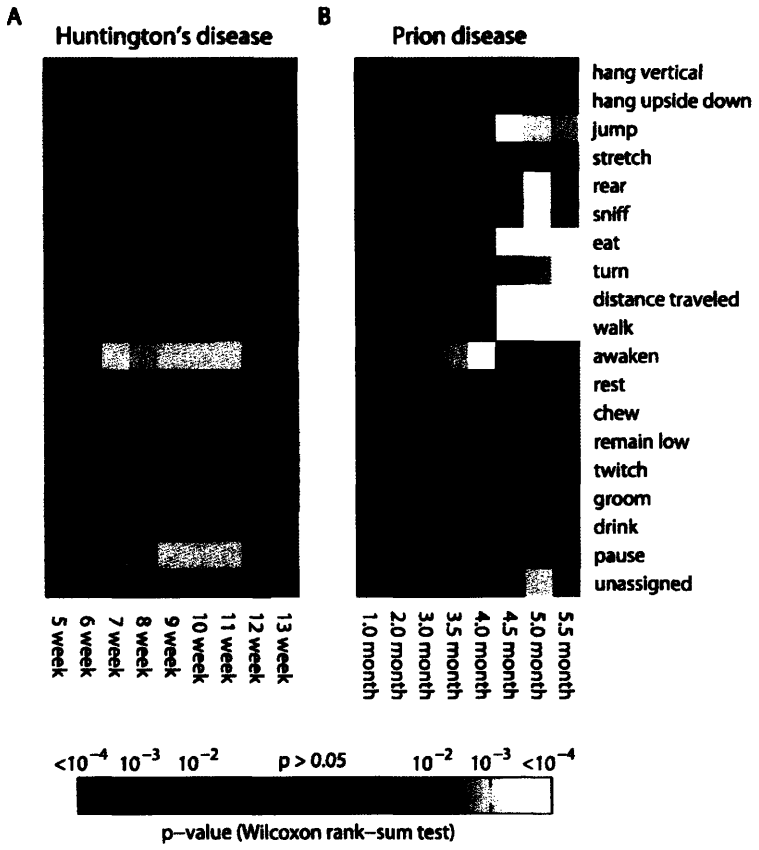

Figure 8 Figure 5 represented in terms of P-values (Wilcoxon rank-sum test).

Appendix

Supplemental Materials

Author contributions:

I designed and performed all experiments with input and occasional "hands on" assistance from Walker Jackson and intellectual input from Susan Lindquist. Walker Jackson introduced me to Clever Systems technology. Yiqing Liang and Vikant Kobla designed and worked out all the behavior recongintion software with end user input from me. Oliver King was responsible for the sophisticated aspects of the data analysis, such as multi-parameter behavioral comparisons and generation of the phenotypic arrays. Charles Yi assisted in manually rechecking HCS software scoring.

1	2	3	4	5	6	7
Behavior	#corr.	#Incorr.	Incorrect should be:	#HCS events	Spec.	Sens.
Rest	67	3	remain low (2), groom (1)	70	0.96	1.00
Turn	91	9	groom (4), remain low (3), walk (1), unknown (1)	5185	0.91	0.94
Twitch	87	13	turn (7), sniff (3), groom (2), stretch (1)	785	0.87	0.99
Walk	95	5	turn (2), unknown (3)	4487	0.95	0.95
Jump	22	9	rear (9)	39	0.71	0.94
Rear	71	29	groom (15), eat (5), remain low (5), drink (2), chew (1), walk (1)	7259	0.71	0.92
Remain low	88	12	groom (7), turn (2), rear (2), walk (1)	7698	0.88	0.92
Eat	90	10	groom (6), rear (4)	1028	0.90	0.66
Drink	80	8	rear (8)	103	0.91	0.39
Chew	50	50	eat (26), rear (14), groom (7), hang vert. (3)	435	0.50	0.46
Groom	92	8	remain low (6), walk (1), chew (1)	580	0.92	0.19
Hang upside down	100	0	n/a	320	1.00	0.99
Hang vertical	75	25	rear (25)	570	0.75	0.94
Sniff	62	38	groom (18), chew (11),	1527	0.62	0.97
Sniff	62	38	remain low (2) rear (2), unknown (5)	1527	0.62	0.97
Awaken	62	6	twitch (6)	69	0.91	1.00
Stretch	90	10	hang vert. (6), eat (2), chew (1), hang upside down (1)	200	0.90	0.95
Pause	83	17	groom (12), chew (3), remain low (2)	219	0.83	1.00
Unknown (Unassigned)	37	63	groom (21), walk (17), turn (8), rear (8), eat (3), sniff (3), remain low (1), stretch (1), jump (1)	183	0.37	0.20

Supplementary Table I. Accuracy assessment of scoring by HomeCageScan. The accuracy of HCS was assessed by inspecting approximately 100 instances of each behavior (according to HCS) in a 24 hour video of a single wild-type C57Bl/6 mouse. (For four behaviors, fewer than 100 total events were identified by HCS, so fewer than 100 were manually assessed.) The ratio of the number of the HCS instances that agreed with manual assessments (column 2) to the total number of scored instances (the sum of column 2 and column 3) gives the "specificity" of HCS for each behavior (column 6), i.e., the fraction of events that HCS classifies as a particular behavior that a human classifies as the same behavior. By weighting the incorrect classifications for each behavior (column 4) by the total number of HCS events for each behavior (column 5) we estimated of the "confusion matrix" that would be obtained if we had manually assessed all ~30000 HCS events. From this we computed an estimate of the "sensitivity" of HCS for each behavior (column 7), i.e., the fraction of events that a human would classify as a particular behavior that HCS correctly identifies. We estimated the overall accuracy to be ~83%, by taking the average of the specificities (column 6), weighted by the relative frequencies of the HCS events (column 5).

Huntington's Disease								
age (weeks)	true-pos	true-neg	false-pos	false-neg	correct	incorrect	total	binom p-val
5	2	3	2	3	5	5	10	0.62
6	5	6	1	2	11	3	14	0.029
7	6	7	0	1	13	1	14	0.00092
8	5	4	3	2	9	5	14	0.21
9	7	7	0	0	14	0	14	6.10E-05
10	7	7	0	0	14	0	14	6.10E-05
11	7	7	0	0	14	0	14	6.10E-05
12	5	6	0	1	11	1	12	0.0032
13	4	4	0	0	8	0	8	0.0039

Prion Disease								
age (m.p.i.)	true-pos	true-neg	false-pos	false-neg	correct	incorrect	total	binom p-val
1	5	5	3	3	10	6	16	0.23
2	2	4	4	6	6	10	16	0.89
3	4	4	4	4	8	8	16	0.60
3.5	6	6	2	2	12	4	16	0.038
4	7	8	0	1	15	1	16	0.00026
4.5	8	8	0	0	16	0	16	1.53E-05
5	7	7	0	0	14	0	14	6.10E-05
5.5	8	8	0	0	16	0	16	1.53E-05

Supplementary Table II. Cross-validation of predictions. We assessed the robustness of the diagnoses using cross-validation, holding out two mice at a time (a diseased mouse and its littermate paired control), training a diagnostic rule on the remaining mice using logistic regression with L_1 regularization (Tibshirani, 1996), and using this rule to predict (independently) whether each of the two removed mice were diseased or control. P-values were computed using the exact binomial test. Here true-positive refers to a correct classification of a diseased mouse, true-negative to a correct classification of a control mouse, false-positive to an incorrect classification of a control mouse, and false-negative to an incorrect classification of a diseased mouse.

Methods:

Behavioral Definitions

The software cannot recognize any action less than 6 frames (the recording speed used was 30 frames per second), so any behavior that is less than 6/30 of a second in duration is not scored as a separate behavior. Behaviors are scored based the on the posture of the mouse and the position of its body parts. Algorithms are proprietary. The behavioral definitions, some of which are merged in our data analysis, are listed below in alphabetical order:

Awaken: The end of a bout of rest (i.e. any activity that occurs after rest would be scored as an awaken event)

Chew: Mouse moves into a vertically huddled position with paws in front of face. When the mouse is eating food at the food bin then comes down to chew, the coming down and rearing back up are implied in the "chew" behavior and are not scored as "rearing".

Distance Traveled: Distance traveled measures only lateral movement (x-plane) in the cage (based on the center of mass of the mouse), and does not measure distance in the y- or z-planes. Thus it is an underestimate total distance traveled.

Drink: *Start of behavior:* mouth is level with drinking spout and then the drinking action proceeds. *End of behavior:* mouth withdrawn from drinking spout. Sniffing prior to drinking is labeled as drinking as long as the drinking action follows.

Eat: Mouse's snout is in the plane of the food bin, head and body movement is minimal. The speed of movement determines whether this is a "sniff" or "eat" behavior, with "sniff" as a faster movement than "eat". Moreover, if a mouse sniffs before eating, then this is considered part of eating behavior.

Groom: Mouse uses both front paws to clean himself and rubs them over body and face in a circular movement. This behavior can be detected by its repetitive movements.

Hang upside down: *Start of behavior*: both forelimbs and hindquarters are at or above the midpoint between the cage floor and with wire rack and limbs are in contact with wire rack. *End of behavior*: both paws up and hindquarters at or below midpoint of the cage.

Hang vertical: *Start of behavior*: both forelimbs up on wire rack (either the food bin or the top of the cage) AND both hindlimbs up or suspended. *End of behavior*: as soon as 1 paw touches the ground regardless of 1 or 2 paws are on the wire rack.

Jump: *Start of behavior*: nose points AND THEN body extends AND THEN at least one hindpaw leaves the ground. Body extension and forward propulsion may happen simultaneously. Jumps may be initiated from ground or reared up position. *End of behavior*: 1 OR both hindpaws on the ground.

Pause: Minimum of 3 seconds of "rest-like stillness" to be considered as 'pause' but not as long as 'rest' which is 30 seconds.

Remain low: Any prolonged inactivity that is neither 'rest' nor 'pause', or any other detectable behavior.

Rearing: Encompasses 8 behaviors measured separately by HCS. Rear Up – *start of behavior:* noise points up and then front paws leave the floor. *End of behavior*: mouse squatting on hind legs, back is curved and mouse is half way to the full stretch of rear up. Rear Up from Partially reared – *start of behavior:* mouse squatting on hind legs, back is curved and mouse is half way to the full stretch of rear up. *End of behavior*: mouse standing on hind legs only, behavior ends when nose reaches highest point. Rear Up to Partially reared – *start of behavior:* nose points up and then at least one paw leaves the floor. *End of behavior*: mouse squatting on hind legs, back is

curved and mouse is half way to the full stretch of rear up. Come Down – *start of behavior*: mouse is standing on hind legs, and nose begins to descend after highest point reached. *End of behavior*: at least one front paw is on the ground. Come down to partially reared – *start of behavior:* mouse is standing on hind legs, and nose begins to descend after highest point reached. *End of behavior*: mouse squatting on hind legs, back is curved and mouse is half way to the full stretch of rear up. Come Down from partially reared – *start of behavior:* mouse squatting on hind legs, back is curved and mouse is half way to the full stretch of rear up. *End of behavior*: at least one front paw is on the ground.

Rest: Mouse is in a non-reared non-hanging posture and not moving except for breathing, which is a sustained movement. A minimum of 30 seconds is required to be considered as 'rest'. Although 30 seconds appears a short threshold for 'rest' once mice remain inactive beyond 30 seconds they generally 'rest' for much longer periods of time. The average rest bout lasts for 590 seconds (from n=8 control mice at 2 m.p.i.).

Sniff: Body stationary but nose bobbing. This is a secondary behavior, only to be charted when mouse is not involved in other behaviors.

Stretch: Head extends, and or hind legs past normal position. The mouse extends its body to maximum length possible either horizontally or vertically and the back usually arches into a C shape especially when in vertical position. *Start of behavior*: head begins the extension forward. *End of behavior:* mouse returns to normal resting state.

Turn: *Start of behavior:* Nose changes direction, then body follows – must be at least a quarter turn to be counted. When mouse walks and turns at the same time turn takes priority.

Twitch: Any movement occurring during rest. Rest must occur immediately before and after the twitch.

Unassigned: A combination of 'unknown behavior' and 'no data'. For 'unknown behavior' a behavior is not recognized by HCS, typically these are very fast, erratic, or atypical movements. During periods of 'no data' the HCS software does not recognize the mouse, and therefore does not score behaviors. This typically occurs during light/dark cycle transitions when the video cameras have to readjust to changing lighting conditions and the image becomes blurry and the software loses track of the mouse.

Walk: At least 3 legs move and propel the mouse forward.

HCS software

HCS utilizes proprietary software algorithms to separate foreground objects (mice being recorded) from the background of the HC. It further identifies the animals' body parts (such as head, ears, mouth, fore- and hind-limbs, back and tail) and assigns postures to the animals, rather than reducing animals to points in space. Initially, as purchased, the system assigned behaviors to the mice based on defined sequences of identified postures and recorded those. To adapt the system for use in our disease models, we refined or modified some behavioral definitions. For example, what we term "rearing" is a sum of 8 separate behavioral classes defined by the HCS software, "rear up", "rear up from partially reared", "rear up to partially reared", "remain partially reared", "remain rear up", "come down", "come down to partially reared", "come down from partially reared". We also worked with CleverSys to improve the detection accuracy of some behaviors by increasing the signal-to-noise ratio. This often involved varying lighting and settings parameters (e.g., component size thresholds [the minimal and maximal pixel threshold values for a mouse]), to enable the software to better distinguish the mouse from the background. Initially the software could not perform analysis on videos longer than 2-3 hours, and by trouble-

shooting several software bugs, we were able to analyze 24 hour videos. We improved the accuracy of the software from less than 50% to nearly 90% on average across behaviors, with several behaviors approaching 99% accuracy.

To employ HCS over the entire diurnal cycle, we established successful conditions for light and dark phase video capture. The night recording capability was virtually untested and unused until we began our studies. In our longer, more behaviorally representative, recordings we found that mice burrowed into the bedding making it impossible for the software to recognize the animal after only a few minutes of recording in the dark. Thus we tested various light conditions and amounts of bedding to achieve a situation in which the mouse still had enough bedding for basic husbandry, but could also be observed by the camera over a period of hours during the night.

We also helped to test and identify hardware components required for high-throughput analysis. Initially the software was designed to operate in a "one cage-one camera" set up, limiting the throughput of the system to a level that was not useful for academic or industrial studies. We recognized the need to create a higher throughput system and successfully attempted a 4-cage 4-camera set up. To accomplish this we tested various video components (e.g., quads equipped for digital video, video cards capable of capturing large videos from the quads) and data collection parameters (e.g., the highest resolution video that we could get without bogging down the processors) in order to achieve reliable video analysis. Finally, we contributed to software development by identifying bugs and making suggestions for improving the user-friendliness of the software. As just one example, the software was initially mischaracterizing several unrelated behaviors as "eat" even though mice were clearly engaging in other completely unrelated behaviors, such as walk or jump. It was only after our modifications, achieved with

several reiterations of algorithms for scoring behavior that we identified important differences in eating behaviors between HD and control mice. Since we began beta testing HCS we have used more than 15 generations of the software, each of which was adapted based on our advice.

Multi-parameter behavioral analysis

Since the number of predictors (behaviors) exceeds the number of observations (mice), there was the danger of over-fitting the data, i.e., of finding rules that were tuned to random variations in the particular mice we observed; such rules may be accurate when applied to these mice but may not generalize well to other mice. We used L_1 regularization to control over-fitting during logistic regression. L_1 regularization tends to force the coefficients of redundant or less informative predictors to be exactly zero, so in effect automatically selects a subset of behaviors to use as predictors (Tibshirani, 1996). This makes the rules easier to interpret. This algorithm entails using maximum likelihood estimation to find the coefficients of the predictors, subject to the constraint that the sum of the absolute values of the coefficients (their L_1 norm) be less than some adjustable parameter t, after centering each predictor to have mean 0 and variance 1. The parameter t was chosen automatically according to the Bayesian information criterion (BIC), using the R package `glmpath`. Prior to computing logistic regressions with `glmpath`, raw behavior data (percent times for 17 behaviors, distance traveled, number of awaken events) were transformed via $f(x) = \log(x+0.01)$. This in most cases made the behavior-specific variances for diseased and control mice more nearly equal, and in most cases made the distribution of data for each class more nearly normal, based on maximum likelihood estimates of the mean and variance. (Adding 0.01 avoids taking the log of zero.) Default parameters for `glmpath` were used, except for max.arclength, which was set to 0.05 so that more points along the

regularization path would be computed exactly. Occasionally at early time points the regularization parameter t with the best BIC score gave a rule with no non-zero coefficients, so that predictions fell exactly on the decision boundary. To break the ties in these cases during cross-validation, we used the next-largest value of t along the regularization path.

We assessed the robustness of the diagnoses using cross-validation, holding out two mice at a time (a diseased mouse and its littermate paired control), training a diagnostic rule on the remaining mice using logistic regression with L_1 regularization (Tibshirani, 1996), and using this rule to predict (independently) whether each of the two removed mice were diseased or control. The number of correct predictions during cross-validation was significantly better than random for HD Tgs versus controls at week 6 and beyond, except for week 8, and for PrD mice vs. controls at 3.5 m.p.i and subsequent time points ($P<0.05$, exact binomial test, see supplementary table III). All predictions were correct for HD Tgs vs. controls beginning at 9 weeks, aside from a single misclassification at 12 weeks, and all predictions were correct for PrD mice vs. controls beginning at 4.5 m.p.i and beyond. Detailed results of cross-validation at all time points are given in Supplementary Table 2. For HD mice at week 7 only one misclassification was made during cross-validation, out of 14 mice total ($P=0.0009$), and for PrD mice at 4 m.p.i only one misclassification was made during cross-validation, out of 16 mice total ($P=0.0003$).

Chapter 4

Investigating Apoptotic Mechanisms of Cell Death in Infectious Prion Disease

The first section of this chapter relating to Caspase-12 was recently submitted for publication by Andrew Steele, Claudio Hetz, Caroline Yi, Walker S. Jackson, Andrew W. Borkowski, Junying Yuan, Robert Wollmann, and Susan Lindquist. The sections of the chapter relating to Bax and Bcl-2 were published by Andrew Steele, Oliver King, Walker Jackson, Claudio Hetz, Andrew Borkowski, Peter Thielen, Robert Wollmann, and Susan Lindquist in The Journal of Neuroscience *(2007)Vol. 27(47): 13022-13027*

Introduction

The pathological events observed in neurodegenerative disease culminate in a dramatic loss of neurons in the brain but the importance of cell death pathways in this process is controversial (Yuan et al., 2003; Shacka and Roth, 2006; Steele and Yi, 2006). Genetic manipulations of pro- or anti-apoptotic proteins have, in many cases, ameliorated pathological or clinical features in mouse models of neurodegenerative disease, including amyotrophic lateral sclerosis, ischemia, and axotomy (Dubois-Dauphin et al., 1994; Martinou et al., 1994; Kostic et al., 1997; Gould et al., 2006; Tsai et al., 2006; Li et al., 2007). However, in other studies modification of apoptosis has not altered the symptoms of neurodegeneration (Sagot et al., 1995; Selimi et al., 2000; Kang et al., 2003; Chiesa et al., 2005; Coulpier et al., 2006). Thus, apoptotic pathways have significant disease-modifying effects in a subset of neurodegenerative diseases.

While it is firmly established that the key pathogenic event in prion disease is the misfolding of the prion protein (PrP), the mechanism by which misfolded PrP causes neuronal dysfunction is poorly understood.(Aguzzi and Heikenwalder, 2006; Caughey and Baron, 2006; Steele, 2007). Different stress pathways implicated in prion toxicity include oxidative stress, mitochondrial dysfunction, calcium imbalance, and endoplasmic reticulum (ER) stress.(Hetz and Soto, 2006) Although ER stress is observed in different natural and experimental models of prion disease and other neurological disorders, genetic manipulation of this stress pathway is required to directly assess its requirement for disease progression.

Growing evidence suggests that the ER is potentially important not only for PrP maturation, but also for the formation of misfolded and cytotoxic, disease-associated forms of the protein.(Ivanova et al., 2001; Ma and Lindquist, 2001; Drisaldi et al., 2003) It was shown that alteration of ER homeostasis occurs in association with synapse loss and neuronal death

observed in infectious forms of prion disease.(Hetz et al., 2003; Hetz et al., 2005). Further, that stress inducible ER chaperones, such as Grp58 and Grp78/BiP, are upregulated in the brains of patients affected with Cruetzfeldt-Jacob disease. This also occurs in mouse models of prion disease, together with pro-apoptotic components associated with the ER stress pathway.(Hetz et al., 2003; Hetz et al., 2005). The processing of an ER resident caspase, caspases-12 (C12), was observed in prion-diseased brains from diverse species.(Hetz et al., 2003). C-12 has been implicated in numerous apoptotic paradigms and a range of neurodegenerative conditions.(Kalai et al., 2003; Shibata et al., 2003; Hitomi et al., 2004b; Hitomi et al., 2004a; Larner et al., 2004; Wootz et al., 2004; Aoyama et al., 2005). In addition to promoting ER stress induced cell death, C12 may function in the pro-inflammatory response.(Obeng and Boise, 2005; Saleh et al., 2006).

Prion infections cause characteristic lesions in the brain: spongiform vacuolation, aggregates of PrP, activation of microglia, proliferation of astrocytes, and ultimately loss of neurons (Aguzzi and Heikenwalder, 2006). The mechanism(s) of neuronal loss is unknown but various forms of neuronal death, including apoptosis, have been documented in diverse hosts with PrD (Liberski et al., 2004). Apoptosis has been described in the brains of patients affected by Creutzfeldt-Jakob disease and fatal familial insomnia and in prion-infected hamsters, mice, and sheep (Liberski et al., 2004; Hetz and Soto, 2006). Several studies (discussed below) have suggested important roles for Bax and Bcl-2 in the neurotoxic pathway caused by PrP mutants (Chiesa et al., 2005; Li et al., 2007; Nicolas et al., 2007).

Bax and Bcl-2 are at the core of the apoptotic pathway located at the mitochondria where multiple cell death signals converge to trigger apoptosis (Yuan et al., 2003). Downstream of apoptotic stimuli, Bax induces cell death by intramembranous homo-oligomerization and resultant permeabilization of the mitochondrial outer membrane, leading to release of

cytochrome c and activation of caspases (Danial and Korsmeyer, 2004). The Bcl-2 family is comprised of pro- and anti-apoptotic members, and is defined by the presence of up to four conserved domains within their primary structure (Reed, 2006). Pro-apoptotic members can be further subdivided into more fully conserved, "multidomain" members containing Bax homology (BH)1-3 or "BH3-only" members, such as Bim and Puma, which activate Bax.

To address directly the role of apoptosis in infectious PrD, we inoculated caspase 12 knockout (KO), Bax KO, and Bcl-2 neuronal overexpression transgenic (Tg) mice with the Rocky Mountain Laboratory (RML) strain of murine prions. To our surprise, Caspase-12 (C12) KO, Bax KO, and Bcl-2 overexpression Tg mice were not protected against prion toxicity. In fact, some features of PrD, such as behavioral alterations and survival, were made worse, while accumulation of proteinase-K resistant PrP and pathological changes were unaltered by diminishing apoptosis.

Results

ER stress and caspase-12 deletion in prion disease

We first confirmed that Rocky Mountain Laboratory (RML) prion strain infection of CD1 mice leads to the activation of C-12. Indeed as previously reported caspase activation was evident by its proteolytic processing at the later and end stage of disease, at 4.5 and 5 months post inoculation (m.p.i.) (Fig. 1). In addition, a progressive upregulation of the ER chaperone Grp58 was observed after prion infection (Fig. 1). This response was consistent with, but less robust, than that previously reported using a different prion strain, 139A.(Hetz et al., 2005) Moreover, phosphorylation of JNK, which is activated by ER stress(Urano et al., 2000) was induced in prion disease affected mice at 4.5 m.p.i. (Fig. 1, P-JNK). We also noted an increase in

aggregated PrP during the course of infection as indicated by a smear of SDS-resistant higher order oligomeric structures of PrP using the 6H4 antibody (Fig. 1).

To determine if C12 plays a significant role in the pathogenesis of infectious prion disease *in vivo*, we infected mice deficient for C12 with prions.(Nakagawa et al., 2000) This C12 knockout line has no known phenotypes other than resistance to ER-stress induced apoptosis. We inoculated C12 KO (n=13) and control mice (n=26) (which were C12+/+ and C12+/-) intracranially with RML strain of murine prions (6.5 log LD_{50}/dose) and assessed survival. To our surprise, there were no significant differences in the length of time required for the different C12 KO and WT groups to succumb to disease. Median survival was 171 d.p.i for C12 KO and 169 d.p.i. for C12 WT (P=0.13, log rank test) (Fig. 1).

We also determined the onset of behavioral symptoms using high resolution automated video-based behavior analysis of home cage activities, a recently developed technique that robustly distinguishes between mice inoculated with prions versus mock inoculated controls.(Steele et al., 2007) The symptoms of RML prion disease in C57BL/6 mice (the strain background used in this study) include decreased grooming and hanging (3a,b), as well as hyperactivity as measured by the percent of total time spent walking (Fig. 3c). We video recorded C12 WT and KO mice (n=6-9 per group) following prion inoculation. Their behaviors were indistinguishable, suggesting that deletion of C12 during prion disease does not alter the brain regions responsible for the behaviors examined.

In addition, we conducted detailed neuropathological analysis of C12 KO and control brains at 4.5 and 5 months post inoculation (m.p.i.). Their disease state was first assessed at the light miscroscopic level by hematoxin and eosin staining. Histological analysis of the brains sections revealed extensive but very similar cell damage and

vacuolation in C12 KO and WT prion infected brains compared to uninoculated control brains (Figure 1b). Based on the possible role of C12 in inflammatory responses, we determined GFAP immunoreactivity, a measure of inflammation in the brain expressed as GFAP synthesis in reactive astrocytes. GFAP staining increased during disease progression but was indistinguishable between C12 WT and KOs (Figure 1b).

Finally, we assessed the amount of prion replication in C12 KOs by western blotting as measured by the accumulation in the brain of proteinase K resistant PrP, the classic surrogate marker for prion infection. In terminally ill C12 KO and control brains (n=5 of each group), there were high levels of proteinase K resistant PrP in whole brain homogenates but no notable differences between C-12 KOs and controls (Fig. 1g)

Expression levels of Bcl-2 family members in prion disease

Given our negative results with respect to deleting caspase-12 in prion disease, we next focused our studies on 2 proteins that have been shown to have a central role in the execution of apoptosis, Bax and Bcl-2.

Alterations in the expression levels of pro- and anti-apoptotic proteins can be indicative of activation of particular cell death pathways. Therefore, we examined the expression levels of several key pro- and anti-apoptotic genes in the brains of RML infected CD1 mice that were sacrificed between 4 and 4.5 months after infection, which is approximately 3-4 weeks before the mice become moribund. By quantitative RT-PCR we observed a significant increase in the RNA levels of Puma and Bim, two potent activators of Bax-dependent apoptosis, when compared to control mice injected with normal brain homogenate ($P<0.05$, Student's T test, n=4 mice per group; Fig. 2A). In addition, a small but reproducible increase in the mRNA levels of Bcl-2 was

observed in prion infected mice, possibly reflecting a compensatory effect (Fig 1C). Similar changes in expression of Bcl-2 were observed in mice infected with another strain of prions, 139A (data not shown). We did not observe significant changes in the mRNA levels of Bax or Bcl-X_L in RML infected mice (Figure 1D and data not shown, respectively). Since similar changes in the expression of these upstream regulators, Bim and Puma, were observed in a mouse model of amyotrophic lateral sclerosis (Hetz et al., 2007) where Bax deletion significantly delayed cell loss and behavioral onset (Gould et al., 2006), our RT-PCR results suggested that prion infection may activate the main pro-apoptotic machinery.

Prion disease in Bax knockout mice

Since Bax is required for neuronal apoptosis in a variety of disease models (Chiesa et al., 2005; Gould et al., 2006; Heitz et al., 2007; Li et al., 2007) and its deletion delays disease symptoms in several models of neurodegeneration (Gould et al., 2006; Tsai et al., 2006; Li et al., 2007) we hypothesized that Bax KO mice would be protected against prion toxicity. To test this, we inoculated C57Bl/6 Bax KO and wild-type (WT) littermate controls with 5.5 $logLD_{50}$/30ul of RML prions intracranially (i.c.). We monitored their home cage behaviors using a high resolution automated system which presented robust diagnosis of PrD in mice in a previous study (Steele et al., 2007). Upon disease onset, RML infected mice show a striking increase in physical activity as manifested by increases in behaviors such as walking and jumping; other behaviors, such as grooming and hanging decrease during later stages of PrD. We video-recorded and analyzed prion-infected Bax KOs (n=13-16) and WT littermates (n=14-18) twice monthly beginning at 3 months post inoculation (m.p.i.), which is just prior to onset of symptoms in RML infected mice (Steele et al., 2007).

The overall profile of behavioral changes was similar in prion-infected Bax KO and control mice. However, several behavioral changes previously shown to be altered in RML PrD in C57Bl/6 mice were observed in the Bax KO mice before their WT littermate controls, suggesting that some PrD symptoms have an earlier onset in Bax KO mice. The prion-inoculated Bax KOs had a subtle increase in "walking" over controls at 3.0 and 3.5 m.p.i. (Fig. 3A), a subtle decrease in "resting" at 3.0 and 3.5 m.p.i. (Fig. 3B), no change in grooming (Fig. 3C), and a small decrease in "hang vertical" at 4.0 m.p.i. (Fig. 3D). Interestingly, later in disease progression two behaviors, "walk" and "rest", were also significantly altered between Bax KO and control mice. Importantly, the behavior of uninoculated Bax KO mice was indistinguishable from uninoculated WT controls with the exception of "eating", which was slightly elevated in Bax KO mice (data not shown).

Given that the behavioral onset in prion-infected Bax KOs was subtly enhanced, we next measured the survival and pathology of these mice after prion inoculation. We observed a seven day enhancement of disease in Bax KO mice in terms of median survival (median survival for Bax WT [n=23] was 181 d.p.i. and for Bax KO [n=13] was 174 d.p.i., P=0.041) (Figure 3E). This result suggests that deletion of Bax causes a very subtle enhancement of disease. Next we inspected brains from prion-infected Bax KO and control mice at 4.5 and 5 m.p.i., approximately 1-1.5 months before morbidity. Mock inoculated controls of both genotypes did not show any spongiform changes, nor was there any gliosis or evidence for neuronal loss (Fig. 3G i and iv). Brains from prion inoculated Bax KO and WT controls showed dramatic vacuolation visualized using a hematoxylin and eosin stain (Fig. 3G ii-iii). Widespread gliosis, a hallmark of neurodegeneration, was visualized with a stain for glial fibrillary acidic protein (GFAP) in the brains from prion-infected Bax KO and WT mice (Fig. 3G v-vi). There were no obvious

differences in pathology between Bax KO and controls in the hippocampus, thalamus, striatum, cortex, and cerebellum. To examine cell death in PrD brains, we performed TUNEL staining on samples taken at 4.5 and 5.0 m.p.i. The brains of Bax WT and Bax KO were almost completely devoid of TUNEL positive cells with the exception of the granular layer of the cerebellum, which showed an equivalent amount of TUNEL staining between both genotypes (and no staining in mock inoculated controls) (data not shown).

Finally, we assayed the formation of proteinase K resistant PrP, the classic surrogate marker for PrD, by treating brain homogenates from Bax KO and control mice (n=2 per group) at 4.5 and 5.0 m.p.i. with proteinase-K (PK). PK resistant PrP is the classic surrogate marker for the buildup of prion infectivity and the amount of aggregated PrP in the brain. Digestion with PK suggested that Bax KO (n=2) and WT controls (n=2) had similar amounts of prion deposition at the timepoints examined (Fig. 3F).

Prion disease in Bcl-2 neuronal overexpression transgenic mice

Since deleting Bax had a surprising and subtle enhancing effect on prion disease, we tested another mouse model with diminished apoptosis. Bcl-2 has a broad anti-apoptotic function and its over-expression protects neurons from damage and death in a variety of models (Dubois-Dauphin et al., 1994; Martinou et al., 1994; Chen et al., 1997; Kostic et al., 1997; Nicolas et al., 2007). We obtained mice (C57Bl/6, DBA/2 hybrids) that specifically overexpress human Bcl-2 in neurons under the neuronal enolase promote (Martinou et al., 1994). We inoculated Bcl-2 Tgs and WT littermate controls with 5.5 $\log LD_{50}$/30ul RML prions i.c. and analyzed their behavior twice monthly beginning at 3m.p.i. Similar to what we observed in the Bax KOs infected with prions, several known PrD-related behavioral alterations occurred earlier in the Bcl-2 Tg mice

compared to controls. For example, an increase in "walk" occurred earlier in Bcl-2 Tgs at 4.0 m.p.i (Fig. 4A), and "rest" (Fig. 4B), "groom" (Fig. 4C), and "hang vertical" (Fig. 4D) all showed decreases first in Bcl-2 Tgs at 4.0 m.p.i.

The Bcl-2 Tgs also succumbed to PrD slightly faster than the WT controls; the median survival of Bcl-2 Tgs was 11 days shorter than that of controls (the median survival for WT controls was 174 d.p.i. while for Bcl-2 Tgs the median survival was 163 d.p.i.; P=0.030, log rank test) (Figure 4E). Thus, in this model of PrD, too there is a subtle enhancement of incubation time, suggesting that Bcl-2 over-expression does not protect against prion toxicity and may even cause a very subtle enhancement of infectious PrD.

At the neuropathological level, brains from prion-infected Bcl-2 Tgs and control mice at 4.5 and 5 m.p.i. showed similar dramatic vacuolation (Figure 3G ii-iii) and gliosis in all regions examined (Figure 4G v-vi). There were no obvious differences in pathology in the hippocampus, thalamus, striatum, cortex, and cerebellum. We also assayed the amount of proteinase K resistant PrP by treating brain homogenates from Bcl-2 OE Tgs and controls at 4.5 and 5 m.p.i. with 50 ug/ml PK; no differences were noted (n=2 mice per group per time point, Figure 4F).

Discussion

By Western blotting we observed signs of ER stress and by RT-PCR we observed small alterations in the expression of pro- and anti-apoptotic genes prior to overt illness in prion inoculated brains, consistent with other reports (Park et al., 2000; Lyahyai et al., 2006). These results suggested that apoptotic pathways could be involved in mediating prion-induced neurodegeneration.

We first challenged the C12 KO mouse with RML prions, as this deletion causes resistance to ER stress induced cell death. Since we did not observe any alteration in the C12 KOs, we next challenged two well characterized mouse lines with demonstrated resistance to apoptosis with RML prions. Surprisingly both deletion of Bax and overexpression of Bcl-2 had subtle enhancing effects on PrD.

The role of apoptosis in genetic forms of PrD has been studied in several systems, both *in vitro* and *in vivo*. Apoptotic cell death has been observed in primary cultured neurons infected with prions (Cronier et al., 2004), treated with proteasome inhibitors (Ma et al., 2002), or both (Kristiansen et al., 2005). In a Tg mouse expressing a repeat expansion of PrP associated with disease in humans, deletion of Bax did not affect the behavioral phenotype but rescued the cerebellar granular neurons from death (Chiesa et al., 2005). The complexity of prion-induced death is underscored in a series of recent studies examining the roles of Bax and Bcl-2 in mediating mutant PrP toxicity *in vivo*. For example, Li and colleagues deleted Bax from two additional mutant PrP Tg models and observed that Bax deletion delayed cell loss in one deletion mutant line (PrPΔ32-134) while not affecting cell loss in another deletion mutant line (PrPΔ105-125) (Li et al., 2007). A recent study demonstrated a protective role of Bcl-2 overexpression in a mutant PrP Tg (PrPΔ32-134), as Bcl-2 overexpression delays neuronal loss and extends survival in these Tg mice (Nicolas et al., 2007). Finally, one group determined that the toxicity induced by ectopic expression of the PrP ortholog, doppel (Dpl), in the brain of mice lacking PrP is diminished by deletion of Bax (Heitz et al., 2007) while another group failed to detect a rescue upon deletion of Bax in a different model of Dpl toxicity (Dong et al., 2007). Thus, Bax dependent and independent pathways may mediate the toxicity of ectopic Dpl expression in the central nervous system.

One study of infectious bovine prions in Bax KO mice did not detect any differences between Bax KOs and controls in terms of survival or pathological changes (Coulpier et al., 2006). Our results are overall quite complementary to this study with the slight discrepancy that we see a small enhancement of disease in terms of the survival of Bax KOs inoculated with RML prions. This could be the result of using different prion strains or simply that the effect that we observed in the Bax KOs is subtle. Since we did not observe protection against cell death in prion-infected Bax KOs and neuronal Bcl-2 overexpression Tgs, the mechanism by which infectious PrP mediates toxicity must differ from that of mutant PrP and/or Dpl related toxicity, cases in which deletion of Bax and over-expression of Bcl-2 confer protection. The mechanism of cell death in infectious PrD may occur through Bax- and Bcl-2-independent pathways, non-apoptotic pathways or another possibility is that if apoptotic pathways are diminished (by deletion of Bax or overexpression of Bcl-2) then alternate pathways are rapidly induced. The fact that we observed subtle enhancements of some PrD symptoms may arise from altered brain structure/function in Bax KO and Bcl-2 mice, which both possess more neurons due to reduced developmental cell death or because some low level of neuronal apoptosis may be beneficial in prion-inoculated mice perhaps by reducing the production of infectious prions. Our results suggest that therapeutic targeting of Bax- and Bcl-2 dependent apoptotic pathways will not be a viable strategy for combating infectious PrD.

Our results unequivocally demonstrate that C12 and Bax are not necessary for RML prion pathogenesis and that Bcl-2 overexpression does not protect against prion pathogenesis. It is possible that compensatory pathways are activated in these mouse lines and that both apoptotic and non-apoptotic forms of cell death are activated in prion disease in a context dependent manner.

Materials and Methods

Mouse strains

All animal experiments were approved by the MIT committee on animal care. Food and water were provided *ad libitum* and mice were group housed (n=2-5 per cage) while being maintained on a 12:12 light-dark cycle. Mice were genotyped from isopropanol extracted DNA isolated from tail clips. Caspase-12 (C-12) knockout (KO) mice were previously described(Nakagawa et al., 2000) and subsequently backcrossed to C57Bl/6 for >10 generations. The primers for genotyping were "TN1" CCAATGAGCACTCTAAAATGATGAACT and "TN2" TTACAAAACTGATCACGTGGACAAAG for amplification of the WT allele and "PGKP-1" TTGGCGCTACCGGTGGATGTGGAATGTG and TN2 amplify the knockout allele. We noted that C-12 knockout females often died while giving birth, so we generated the mice used in this study by intercrossing mice heterozygous for the C-12 deletion allele. Bax KO mice (Knudson et al., 1995) were obtained from Jackson laboratories at N8 generations of backcross to C57Bl/6J, and were backcrossed one additional time. All mice used in our studies were generated by intercrossing Bax+/- x Bax+/- mice to generate littermate controls. Bcl-2 OE Tg mice (Dubois-Dauphin et al., 1994) were kindly provided by Nancy Forger (University of Massachusetts). This line was maintained on a mixed background composed of C57Bl/6 and DBA/2 and was crossed once to C57Bl/6 for ovarian transfer rederivation. For breeding we crossed Bcl-2 Tg+/- males to Tg-/- females.

Western Blotting

Brain homogenates were prepared in glass dounce homogenizers as 10% homogenates (weight/volume) of whole brain in PBS from sampels frozen at indicated timepoints. After sonication, large debris were pelleted by low speed centrifugation. Further dilutions were made

into RIPA buffer (20mM Tris pH 8.0, 150mM NaCl, 0.1% SDS, 0.5% DOC, 0.5% triton X-100) containing a protease inhibitor cocktail (Roche, Basel, Switzerland) or lysis buffer (PBS, 150mM NaCl, 1% Triton X-100, and 1% Tween 20) without protease inhibitor (for Figure 1G). The equivalent of 30–50ug of total protein was loaded onto 4-12% SDS-PAGE (Novex NuPage, Invitrogen), transferred to nitrocellulose membranes, and analysed by Western blotting as described previously (Steele et al., 2006). The following antibodies and dilutions were used: 6H4 anti-PrP 1:10,000 (Prionics), SAF83 anti-PrP 1:3000 (Cayman), anti-Caspase-12, 1:5,000 (Exalpha); anti-Grp58, 1:5,000 (StressGene), 1:1,000 anti-phospho JNK and anti-JNK (Cell Signaling Technology). For proteinase K treatment, 10% brain homogenates from terminally ill WT or Caspase-12 KOs were diluted to 1% in lysis buffer and treated with 50ug/ml proteinase K (Invitrogen) for 1 hour at 37C.

RNA extraction and quantitative RT-PCR

Total RNA was prepared brain homogenates using trizol (Invitrogen, Carlsbad, CA) and cDNA was synthesized with SuperScript III (Invitrogen, Carlsbad, CA) using random primers. Quantitative real-time PCR reactions employing SYBR green fluorescent reagent were performed in an ABI PRISM 7700 (Applied Biosystems, Foster City, CA). Relative amounts of mRNAs were calculated from the values of comparative threshold cycle by using beta actin as a control. Primer sequences were designed by Primer Express software (Applied Biosystems, Foster City, CA) and are identical to those reported in (Hetz et al., 2007).

Prion inoculations

For prion inoculations, brain homogenate was prepared as a 1% weight/volume suspension for C12 mice and 0.1% for Bax KO and Bcl-2 Tg mice from the brains of terminally ill Rocky Mountain Laboratory Chandler ("RML") strain infected mouse brain in PBS + 2%

FBS. Prions were inoculated directly into the brain using a $26^{3/8}$ gauge needle. The titer of prions was $6.5 \log LD_{50}$/30ul for C12 and $5.5 \log LD_{50}$/30ul for Bax KO and Bcl-2 Tg mice.

Behavioral analysis

Behavioral analysis was performed essentially as previously described (Steele et al., 2007). Briefly, mice were placed in new cages containing minimal bedding for a 24 hour video recording using dim red lighting during the dark cycle. Behavioral analysis of videos was performed using HomecageScan 2.0 (Clever Systems, Inc.) with definitions were previously described with the exception that "remain low" and "sleep" were merged under the title "rest" because the steel coat color in some of the Bax KO mice made it difficult to distinguish these two classes of inactivity.

Neuropathological analysis

Brains were immersion fixed in formalin, paraffin embedded, and sectioned coronally. Five micron sections were stained with hematoxylin and eosin. For GFAP immunostaining, sections were deparaffinized and then incubated in 98.6 degree waterbath at pH 6.0 for 40 minutes, after which the sections were stained using an automated stainer, using an rabbit anti-cow GFAP antibody at 1:400 dilution (Dako). A blinded analysis of vacuolation and gliosis in the hippocampus, thalamus, striatum, cortex, and cerebellum was conducted.

TUNEL staining was performed according to the manufacturer's protocol (Roche).

Statistical analysis

Statistical analysis was performed using GraphPad Prism. Student's T test was used for analysis of RT-PCR data, log rank test was used for survival data, and Wilcoxon rank sum test (non-parametric) was used for behavioral analysis.

References

Aguzzi A, Heikenwalder M (2006) Pathogenesis of prion diseases: current status and future outlook. Nat Rev Microbiol 4:765-775.

Aoyama K, Burns DM, Suh SW, Garnier P, Matsumori Y, Shiina H, Swanson RA (2005) Acidosis causes endoplasmic reticulum stress and caspase-12-mediated astrocyte death. J Cereb Blood Flow Metab 25:358-370.

Caughey B, Baron GS (2006) Prions and their partners in crime. Nature 443:803-810.

Chen DF, Schneider GE, Martinou JC, Tonegawa S (1997) Bcl-2 promotes regeneration of severed axons in mammalian CNS. Nature 385:434-439.

Chiesa R, Piccardo P, Dossena S, Nowoslawski L, Roth KA, Ghetti B, Harris DA (2005) Bax deletion prevents neuronal loss but not neurological symptoms in a transgenic model of inherited prion disease. Proc Natl Acad Sci U S A 102:238-243.

Coulpier M, Messiaen S, Hamel R, Fernandez de Marco M, Lilin T, Eloit M (2006) Bax deletion does not protect neurons from BSE-induced death. Neurobiol Dis 23:603-611.

Cronier S, Laude H, Peyrin JM (2004) Prions can infect primary cultured neurons and astrocytes and promote neuronal cell death. Proc Natl Acad Sci U S A 101:12271-12276.

Danial NN, Korsmeyer SJ (2004) Cell death: critical control points. Cell 116:205-219.

Dong J, Li A, Yamaguchi N, Sakaguchi S, Harris DA (2007) Doppel Induces Degeneration of Cerebellar Purkinje Cells Independently of Bax. Am J Pathol.

Drisaldi B, Stewart RS, Adles C, Stewart LR, Quaglio E, Biasini E, Fioriti L, Chiesa R, Harris DA (2003) Mutant PrP is delayed in its exit from the endoplasmic reticulum, but neither wild-type nor mutant PrP undergoes retrotranslocation prior to proteasomal degradation. J Biol Chem 278:21732-21743.

Dubois-Dauphin M, Frankowski H, Tsujimoto Y, Huarte J, Martinou JC (1994) Neonatal motoneurons overexpressing the bcl-2 protooncogene in transgenic mice are protected from axotomy-induced cell death. Proc Natl Acad Sci U S A 91:3309-3313.

Gould TW, Buss RR, Vinsant S, Prevette D, Sun W, Knudson CM, Milligan CE, Oppenheim RW (2006) Complete dissociation of motor neuron death from motor dysfunction by Bax deletion in a mouse model of ALS. J Neurosci 26:8774-8786.

Heitz S, Lutz Y, Rodeau JL, Zanjani H, Gautheron V, Bombarde G, Richard F, Fuchs JP, Vogel MW, Mariani J, Bailly Y (2007) BAX contributes to Doppel-induced apoptosis of prion-protein-deficient Purkinje cells. Dev Neurobiol 67:670-686.

Hetz C, Russelakis-Carneiro M, Maundrell K, Castilla J, Soto C (2003) Caspase-12 and endoplasmic reticulum stress mediate neurotoxicity of pathological prion protein. Embo J 22:5435-5445.

Hetz C, Thielen P, Fisher J, Pasinelli P, Brown RH, Korsmeyer S, Glimcher L (2007) The proapoptotic BCL-2 family member BIM mediates motoneuron loss in a model of amyotrophic lateral sclerosis. Cell Death Differ 14:1386-1389.

Hetz C, Russelakis-Carneiro M, Walchli S, Carboni S, Vial-Knecht E, Maundrell K, Castilla J, Soto C (2005) The disulfide isomerase Grp58 is a protective factor against prion neurotoxicity. J Neurosci 25:2793-2802.

Hetz CA, Soto C (2006) Stressing out the ER: a role of the unfolded protein response in prion-related disorders. Curr Mol Med 6:37-43.

Hitomi J, Katayama T, Taniguchi M, Honda A, Imaizumi K, Tohyama M (2004a) Apoptosis induced by endoplasmic reticulum stress depends on activation of caspase-3 via caspase-12. Neurosci Lett 357:127-130.

Hitomi J, Katayama T, Eguchi Y, Kudo T, Taniguchi M, Koyama Y, Manabe T, Yamagishi S, Bando Y, Imaizumi K, Tsujimoto Y, Tohyama M (2004b) Involvement of caspase-4 in endoplasmic reticulum stress-induced apoptosis and Abeta-induced cell death. J Cell Biol 165:347-356.

Ivanova L, Barmada S, Kummer T, Harris DA (2001) Mutant prion proteins are partially retained in the endoplasmic reticulum. J Biol Chem 276:42409-42421.

Kalai M, Lamkanfi M, Denecker G, Boogmans M, Lippens S, Meeus A, Declercq W, Vandenabeele P (2003) Regulation of the expression and processing of caspase-12. J Cell Biol 162:457-467.

Kang SJ, Sanchez I, Jing N, Yuan J (2003) Dissociation between neurodegeneration and caspase-11-mediated activation of caspase-1 and caspase-3 in a mouse model of amyotrophic lateral sclerosis. J Neurosci 23:5455-5460.

Knudson CM, Tung KS, Tourtellotte WG, Brown GA, Korsmeyer SJ (1995) Bax-deficient mice with lymphoid hyperplasia and male germ cell death. Science 270:96-99.

Kostic V, Jackson-Lewis V, de Bilbao F, Dubois-Dauphin M, Przedborski S (1997) Bcl-2: prolonging life in a transgenic mouse model of familial amyotrophic lateral sclerosis. Science 277:559-562.

Kristiansen M, Messenger MJ, Klohn PC, Brandner S, Wadsworth JD, Collinge J, Tabrizi SJ (2005) Disease-related prion protein forms aggresomes in neuronal cells leading to caspase activation and apoptosis. J Biol Chem 280:38851-38861.

Larner SF, Hayes RL, McKinsey DM, Pike BR, Wang KK (2004) Increased expression and processing of caspase-12 after traumatic brain injury in rats. J Neurochem 88:78-90.

Li A, Barmada SJ, Roth KA, Harris DA (2007) N-terminally deleted forms of the prion protein activate both Bax-dependent and Bax-independent neurotoxic pathways. J Neurosci 27:852-859.

Liberski PP, Sikorska B, Bratosiewicz-Wasik J, Gajdusek DC, Brown P (2004) Neuronal cell death in transmissible spongiform encephalopathies (prion diseases) revisited: from apoptosis to autophagy. Int J Biochem Cell Biol 36:2473-2490.

Lyahyai J, Bolea R, Serrano C, Monleon E, Moreno C, Osta R, Zaragoza P, Badiola JJ, Martin-Burriel I (2006) Correlation between Bax overexpression and prion deposition in medulla oblongata from natural scrapie without evidence of apoptosis. Acta Neuropathol (Berl) 112:451-460.

Ma J, Lindquist S (2001) Wild-type PrP and a mutant associated with prion disease are subject to retrograde transport and proteasome degradation. Proc Natl Acad Sci U S A 98:14955-14960.

Ma J, Wollmann R, Lindquist S (2002) Neurotoxicity and neurodegeneration when PrP accumulates in the cytosol. Science 298:1781-1785.

Martinou JC, Dubois-Dauphin M, Staple JK, Rodriguez I, Frankowski H, Missotten M, Albertini P, Talabot D, Catsicas S, Pietra C, et al. (1994) Overexpression of BCL-2 in transgenic mice protects neurons from naturally occurring cell death and experimental ischemia. Neuron 13:1017-1030.

Nakagawa T, Zhu H, Morishima N, Li E, Xu J, Yankner BA, Yuan J (2000) Caspase-12 mediates endoplasmic-reticulum-specific apoptosis and cytotoxicity by amyloid-beta. Nature 403:98-103.

Nicolas O, Gavin R, Braun N, Urena JM, Fontana X, Soriano E, Aguzzi A, Del Rio JA (2007) Bcl-2 overexpression delays caspase-3 activation and rescues cerebellar degeneration in prion-deficient mice that overexpress amino-terminally truncated prion. Faseb J.

Obeng EA, Boise LH (2005) Caspase-12 and caspase-4 are not required for caspase-dependent endoplasmic reticulum stress-induced apoptosis. J Biol Chem 280:29578-29587.

Park SK, Choi SI, Jin JK, Choi EK, Kim JI, Carp RI, Kim YS (2000) Differential expression of Bax and Bcl-2 in the brains of hamsters infected with 263K scrapie agent. Neuroreport 11:1677-1682.

Reed JC (2006) Proapoptotic multidomain Bcl-2/Bax-family proteins: mechanisms, physiological roles, and therapeutic opportunities. Cell Death Differ 13:1378-1386.

Sagot Y, Dubois-Dauphin M, Tan SA, de Bilbao F, Aebischer P, Martinou JC, Kato AC (1995) Bcl-2 overexpression prevents motoneuron cell body loss but not axonal degeneration in a mouse model of a neurodegenerative disease. J Neurosci 15:7727-7733.

Saleh M, Mathison JC, Wolinski MK, Bensinger SJ, Fitzgerald P, Droin N, Ulevitch RJ, Green DR, Nicholson DW (2006) Enhanced bacterial clearance and sepsis resistance in caspase-12-deficient mice. Nature 440:1064-1068.

Selimi F, Vogel MW, Mariani J (2000) Bax inactivation in lurcher mutants rescues cerebellar granule cells but not purkinje cells or inferior olivary neurons. J Neurosci 20:5339-5345.

Shacka JJ, Roth KA (2006) Bcl-2 family and the central nervous system: from rheostat to real complex. Cell Death Differ 13:1299-1304.

Shibata M, Hattori H, Sasaki T, Gotoh J, Hamada J, Fukuuchi Y (2003) Activation of caspase-12 by endoplasmic reticulum stress induced by transient middle cerebral artery occlusion in mice. Neuroscience 118:491-499.

Steele AD, Yi CH (2006) Neuromuscular denervation: Bax up against the wall in amyotrophic lateral sclerosis. J Neurosci 26:12849-12851.

Steele AD, Jackson WS, King OD, Lindquist S (2007) The power of automated high-resolution behavior analysis revealed by its application to mouse models of Huntington's and prion diseases. Proc Natl Acad Sci U S A 104:1983-1988.

Steele AD, Emsley JG, Ozdinler PH, Lindquist S, Macklis JD (2006) Prion protein (PrPc) positively regulates neural precursor proliferation during developmental and adult mammalian neurogenesis. Proc Natl Acad Sci U S A 103:3416-3421.

Steele AD, Lindquist, S., and Aguzzi, A. (2007) The prion protein knockout mouse: a phenotype under challenge. Prion 1.

Tsai MS, Chiu YT, Wang SH, Hsieh-Li HM, Lian WC, Li H (2006) Abolishing Bax-dependent apoptosis shows beneficial effects on spinal muscular atrophy model mice. Mol Ther 13:1149-1155.

Urano F, Wang X, Bertolotti A, Zhang Y, Chung P, Harding HP, Ron D (2000) Coupling of stress in the ER to activation of JNK protein kinases by transmembrane protein kinase IRE1. Science 287:664-666.

Wootz H, Hansson I, Korhonen L, Napankangas U, Lindholm D (2004) Caspase-12 cleavage and increased oxidative stress during motoneuron degeneration in transgenic mouse model of ALS. Biochem Biophys Res Commun 322:281-286.

Yuan J, Lipinski M, Degterev A (2003) Diversity in the mechanisms of neuronal cell death. Neuron 40:401-413.

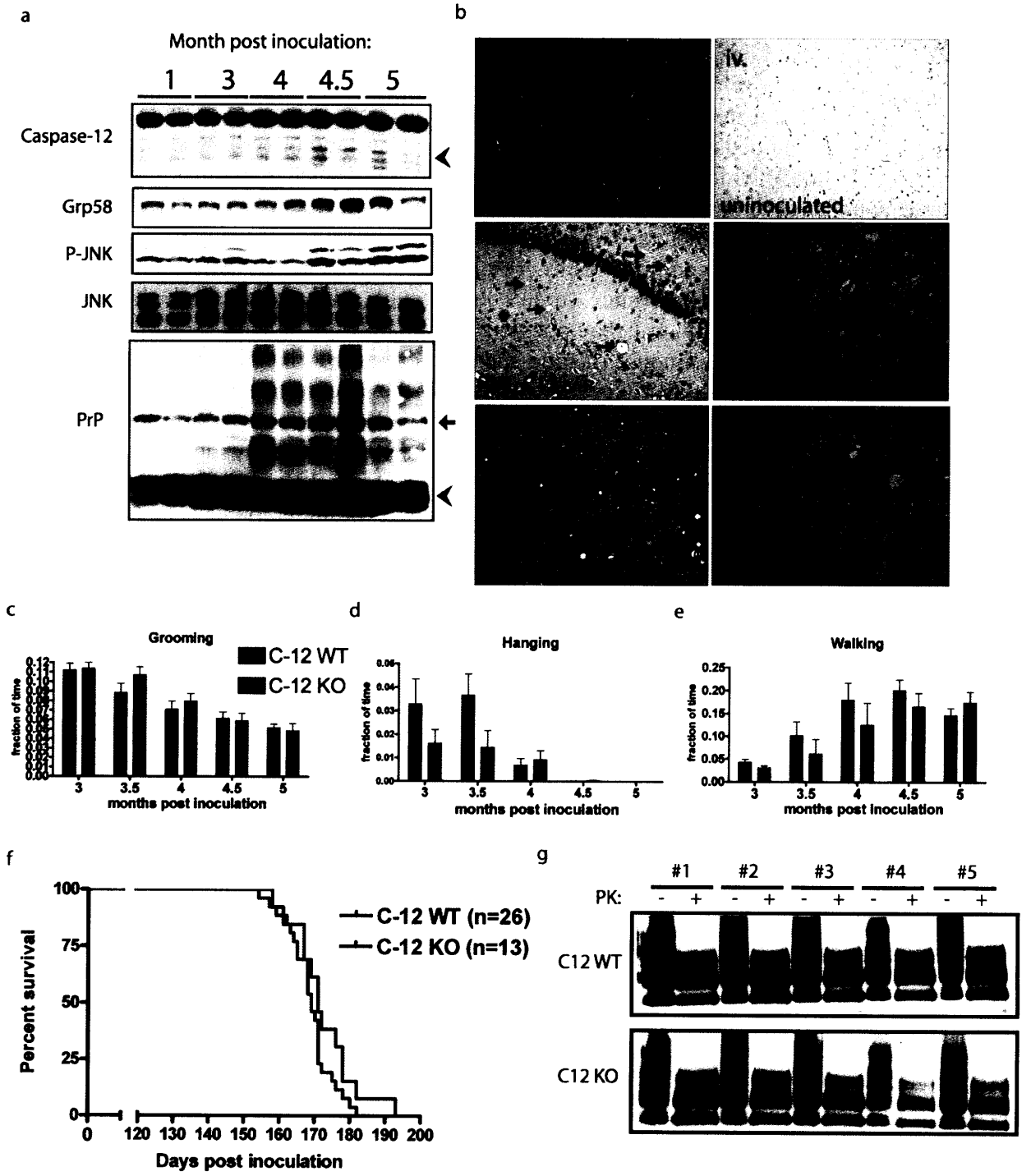

Figure 1 ER stress is activated in prion disease but caspase 12 (C12) is not required for pathologic changes associated with RML prion infection. (**a**) Upregulation of ER stress markers was determined in prion infected mice (n=2 per timepoint) after inoculation with 6.5logLD_{50} RML prions. Western blot analysis was performed to analyze the levels of C12, Grp58, JNK phosphorylation and total PrP. As a loading control, the total level of JNK was measured. Faint processing of C12 is visible at 4 months post inoculation (m.p.i.) but more clearly at 4.5 and 5 m.p.i. Phosphorylation of JNK (P-JNK) as well as induction of Grp58 was observed at 4.5 and 5

m.p.i. while higher order SDS-resistant PrP species were first visible at 4 m.p.i. (an arrow head marks the migration of monomeric PrP and an arrow denotes a non-specific band) (**b**) Analysis of spongiform changes in C12 WT and KO brain sections (**b**, i, ii, and iii) show a similar amount of vacuolation, indicated by arrows, in the hippocampus of prion inoculated mice but no vacuolation in uninoculated mice (WT is shown). The amount of gliosis was examined by staining for GFAP, which did not show staining in uninoculated samples (WT is shown) but showed abundant staining in prion inoculated samples from C12 WT and C12 KO (**b,** iv, v, and vi). For all of these parameters, blinded analysis did not reveal any differences between prion inoculated C12 KO and control brains. (**c-e**) Behavioral analysis was conducted on prion inoculated C12 WT and KO mice (n=6-9 per group). Mice were single housed and video recorded for 24 hours and their behaviors were quantitated by Homecagescan 2.0 software. (**c-d**) A similar decrease in the amount of time spent grooming and hanging was observed and (**e**) a similar dramatic increase in activity as measured by the percent of total time spent walking was observed in C12 WT and KO mice inoculated with prions. (**f**) The survival after prion inoculation of C12 WT (either +/+ or +/- for C12) and KO was nearly identical (median survival for C12 WT, 169 days, and median survival for C12 KO was 171 days, P=0.13). (**g**) The amount of proteinase K resistant PrP was assayed in whole brain homogenates taken from prion inoculated C12 WT (n=5) and C12 KO (n=5) mice (treated for 50ug/ml PK for 1 hour at 37C), which all showed ample PK resistant PrP by immunoblotting with SAF83.

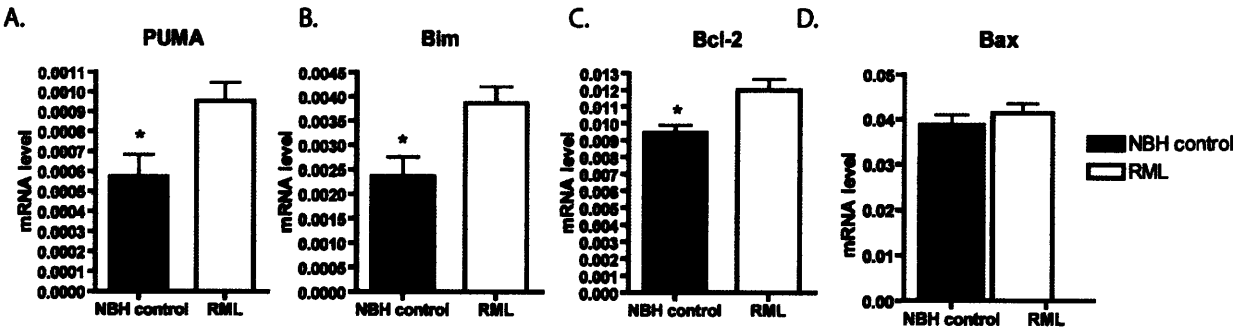

Figure 2. Alterations in the expression of pro- and anti-apoptotic genes in prion disease. RT-PCR was performed on trizol extracted brain samples from CD1 mice between 4 and 4.5 months after infection with prions or normal brain homogenate as a control. Levels of PUMA (A), Bim (B), Bcl-2 (C), and Bax (D) were examined (*$P<0.05$, Student's T test).

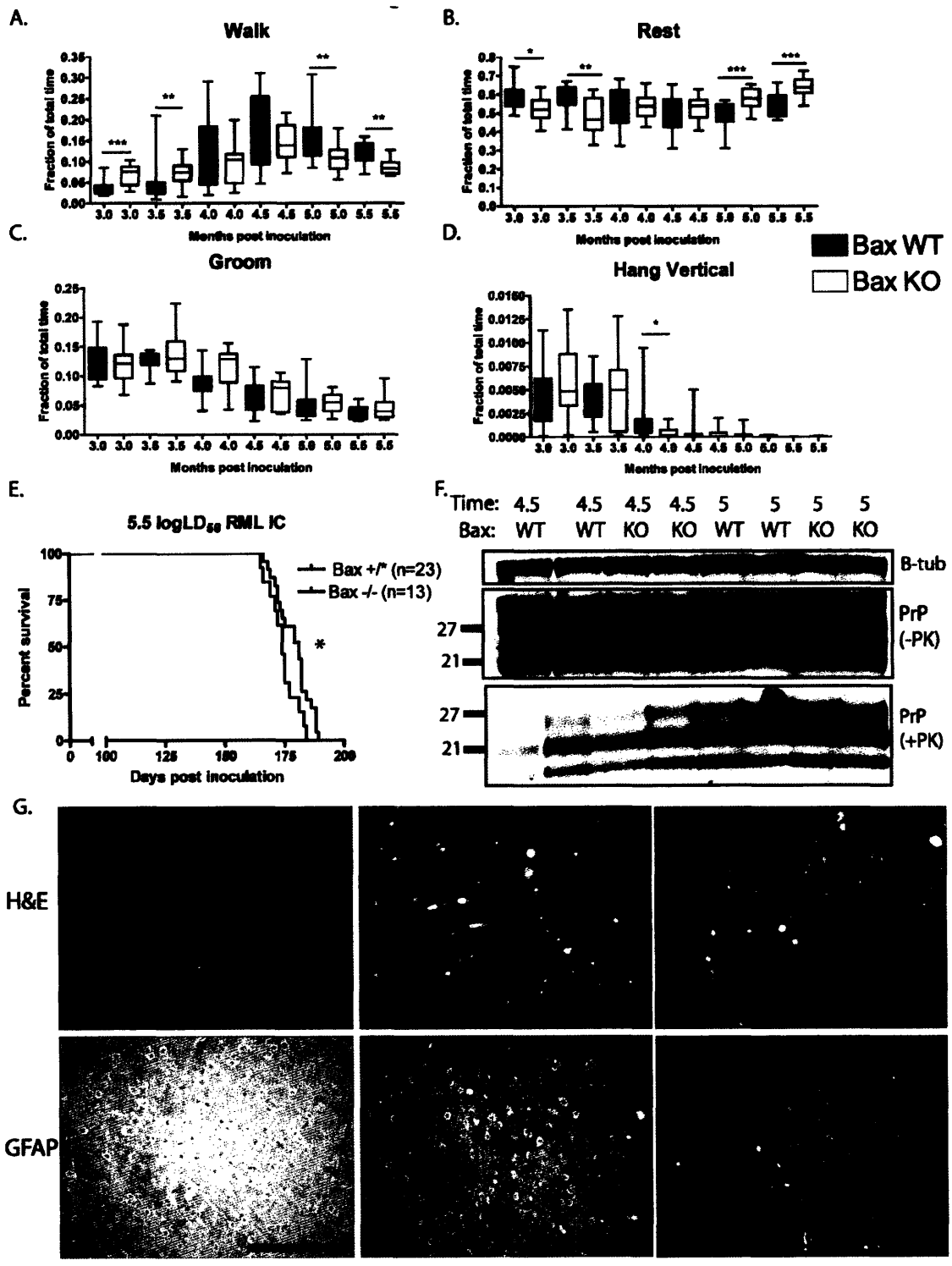

Figure 3 Deletion of Bax does not protect against prion disease. "Box and whisker" plots for behaviors known to be altered in prion disease such as walk (A), rest (B), groom (C), and hang vertical (D) are shown as for Bax knockout (gray bars) and controls (white bars). Sample sizes were n=13-16 at each time point for Bax KOs and n=14-18 for WT controls. Statistically significant results are denoted with asterics (* $P<0.05$, ** $P<0.01$, and *** $P<0.001$) and were computed using a Wilcoxon rank sum test. The upper and lower "whisker" represent the

maximum and minimum values for each timepoint while the "box" represents the 25^{th}-75^{th} percentiles, and the line represents the median value. Bax KO mice die faster from prion infection (P=0.041, log rank test)(F). Accumulation of proteinase K-resistant PrP was measured at 4.5 and 5.0 months post inoculation (m.p.i.) by western blotting n=2 mice per genotype per time point (G). The neuropathological changes were similar in prion-infected Bax KO and control mice, shown at 5 m.p.i., in terms of vacuolation in hematoxilin and eosin stained sections of uninoculated WT (Hi), prion-inoculated Bax WT (Hii) and Bax KO (Hiii). Gliosis measured by staining for GFAP was performed on sections from uninoculated WT mice which did not show any staining (Hiv) and on prion-inoculated Bax WT (Hv) and Bax KO (Hvi) samples (scale bar 100um).

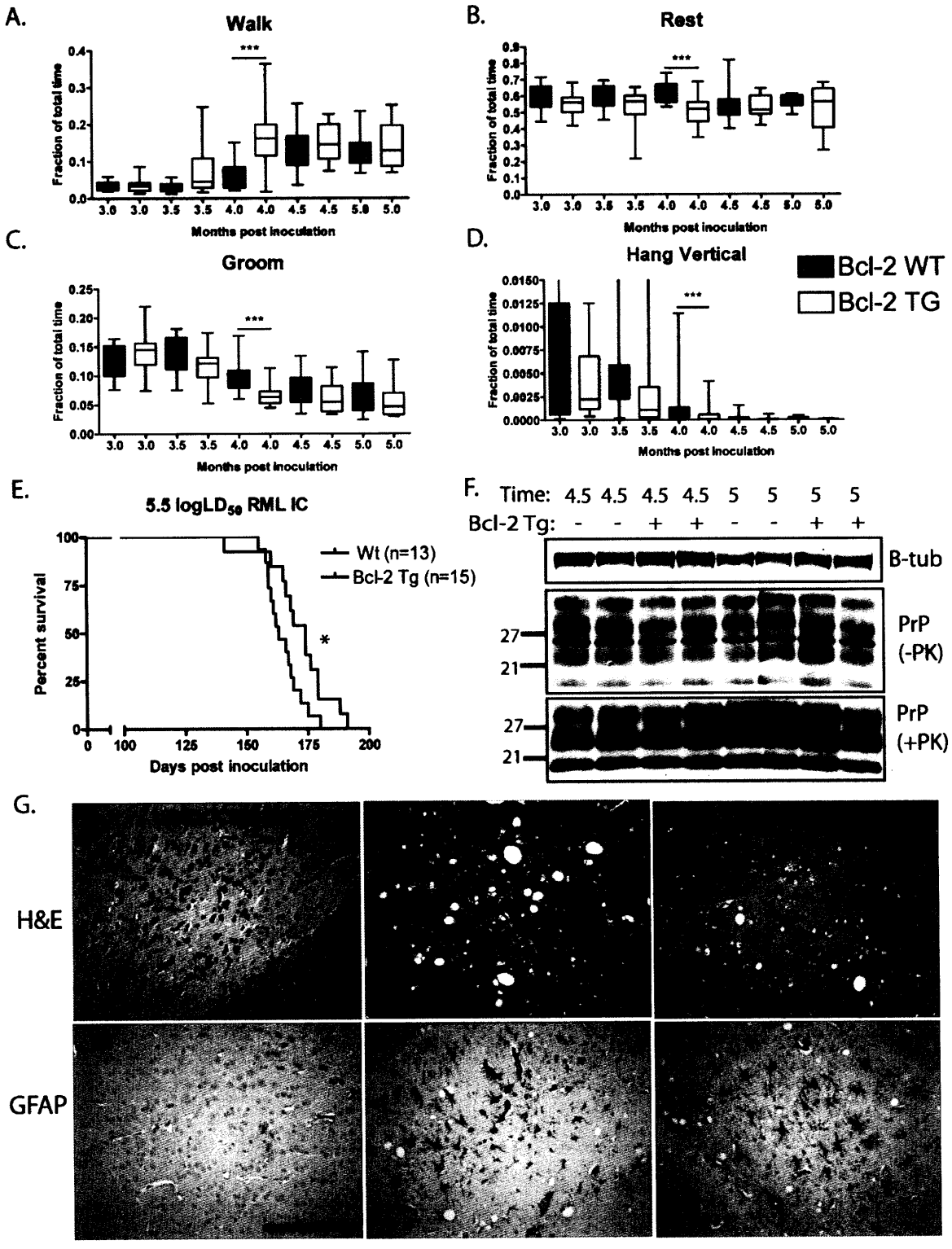

Figure 4 Overexpression of Bcl-2 in neurons does not protect against prion disease. "Box and whisker" plots for several behaviors known to be altered in prion disease such as walk (A), rest (B), groom (C), and hang vertical (D) are shown as for Bcl-2 TG (gray bars) and controls (white bars). Statistically significant results are denoted with asterics (* $P<0.05$, ** $P<0.01$, and *** $P<0.001$) and were computed using a Wilcoxon rank sum test. Bcl-2 TG mice die faster from

prion infection (P=0.03, log rank test)(F). Accumulation of proteinase K resistant PrP was measured at 4.5 and 5.0 months post inoculation (m.p.i.) by western blotting n=2 mice per genotype per time point (G). The neuropathological changes were similar in prion-infected Bcl-2 Tg and control mice, shown at 5 m.p.i., in terms of vacuolation in hematoxilin and eosin stained sections of uninoculated WT (Hi), prion-inoculated WT (Hii) and Bcl-2 Tg (Hiii). Gliosis measured by staining for GFAP was performed on sections from uninoculated WT mice which did not show any staining (Hiv) and on prion-inoculated WT (Hv) and Bcl-2 Tg (Hvi) samples (scale bar 100um).

Appendix

Supplemental Materials

Author contributions:

I designed and performed many of the experiments present in this chapter but I was part of a much larger collaborative research team. Claudio Hetz and Peter Thielen ran the RT-PCR reactions on samples that I prepared for them (Figure 2). Robert Wollmann conducted neuropathological analysis for Figures 1-3. Claudio Hetz performed Western blotting presented in Figure 1 on samples that I provided for him. Mouse husbandry, including tagging, tailing, and genotyping was performed almost completely by Artur Topolszki under my supervision. Walker Jackson assisted with many of the prion inoculations and Andrew Borkowski helped with the analysis of mouse behavior. Junying Yuan and Caroline Yi were instrumental in the early phases of this project, particularly with caspase-12 knockout mice.

Chapter 5

A Protective Role for Heat Shock Factor 1 in Prion Pathogenesis

This chapter will be submitted for publication by the following authors: Andrew Steele, Gregor Hutter, Walker Jackson, Frank Heppner, Oliver King, Andrew Borkowski, Gregory Raymond, Adriano Aguzzi, and Susan Lindquist.

Introduction

At present there are few treatments and little understanding of the pathogenic mechanisms at play in neurodegenerative diseases. Prion diseases are a special class of protein misfolding disorders, in that they can be transmitted within and between species as well as sporadic and inherited (Prusiner, 1998). In prion diseases the host encoded normally folded prion protein (termed PrP^{C}) is converted into a rogue self-perpetuating conformation (termed PrP^{Sc}) (Prusiner, 1998; Caughey and Baron, 2006). The ongoing conversion of PrP^{C} to PrP^{Sc} is an absolute requirement for neurotoxicity in prion disease (Mallucci et al., 2003; Aguzzi et al., 2007), yet beyond this basic observation we know little about the pathways mediating neurodegeneration.

The heat shock response is a highly conserved response to extreme changes in environmental temperatures and stresses (Lindquist and Craig, 1988; Mathew et al., 2000). Under normal conditions, the transcription factor named heat shock factor (Hsf) is sequestered in the cytosol in a complex with molecular chaperones (Shi et al., 1998; Zou et al., 1998). During conditions that perturb protein folding homeostasis, Hsf trimerizes and enters the nucleus(Sarge et al., 1993; Westwood and Wu, 1993), where it rapidly drives transcription of numerous genes involved both in protein refolding and degradation of misfolded proteins (Trinklein et al., 2004). In yeast and *C. Elegans* there is only one Hsf whereas in mammals there are three Hsfs (Hsf1, Hsf2, and Hsf4). Although interplay between Hsfs is complex (Homma et al., 2007) and not completely understood, a general picture has emerged where from gene targeting studies in mice, which defined Hsf1 as the critical responder to stress where as Hsf2 and Hsf4 have tissue restricted roles, such as in spermatogenesis and lens formation (McMillan et al., 2002; Wang et al., 2003; Fujimoto et al., 2004; Wang et al., 2004).

The relevance of the heat shock response and molecular chaperones to disease has been a topic of great interest (review). Since molecular chaperones, which refold and/or help to degrade damaged proteins (Lindquist and Craig, 1988), are induced during the heat shock response, particularly interest has emerged with respect to ameliorating protein misfolding diseases using small molecule inducers of the heat shock response (Westerheide and Morimoto, 2005). Indeed, several animal models of neurodegeneration have been treated with heat shock inducing compounds that delayed disease symptoms and pathology.(Kieran et al., 2004; Katsuno et al., 2005; Waza et al., 2005).

Since prion diseases are prototypic diseases of protein misfolding, we sought to determine if Hsf1 was a key regulator of prion pathogenesis. Indeed, a connection between Hsf1 and many neurodegenerative diseases has been suggested by several observations. In Cruetzfeldt-Jakob disease a prominent induction of heat shock proteins was noted in the Purkinje cells of the cerebellum (Kovacs et al., 2001). Also, upregulation of Hsf1 target genes such as polyubiquitins and Hsp70 genes was observed in a mouse model of infectious prion disease (Kenward et al., 1994). We observed that mice lacking Hsf1 are sensitized to prion toxicity in that they succumb to disease with faster kinetics than controls. Surprisingly, the phenotypic alterations associated with prion infection developed with similar kinetics in Hsf1 knoockouts (KO). In corroboration with the behavioral analysis, the pathological alterations in the brains of Hsf1 KOs and controls were nearly identical. Proteinase K-resistant PrP accumulated at a similar rate in Hsf1 KOs and controls, and prion infectivity as determined by bioassay was equal or slightly diminished at several timepoints in disease. We have uncovered a previously unappreciated protective role for Hsf1 in prion pathogenesis.

Results

Characterization of neurological parameters in Hsf1 knockouts

Hsf1 knockout (KO) mice were previously characterized in terms of 1) heat shock protein induction in response to thermal elevation, 2) systemic inflammation, 3) neonatal lethality, 4) cardiac ischemia...(Xiao et al., 1999) We first confirmed that PrP protein expression was not perturbed by deletion of Hsf1, since *Prnp* has heat shock elements in its promoter, which may promote its expression in response to elevated temperature (Shyu et al., 2000). Western blots of dilution series of whole brain homogenates from Hsf1 WT (n=2) and Hsf1 KO (n=2) show similar steady state levels of PrP using beta-tubulin was used as a loading control (Fig. 1A).

It was also reported that Hsf1 knockouts have abnormalities in their brains (Santos and Saraiva, 2004) and CNS disease (Homma et al., 2007). Santos and colleagues noted that their Hsf1 KOs had enlarged ventricles and astrogliosis, particularly in white matter regions (Santos and Saraiva, 2004). While Homma and colleagues also identified diminished myelination in Hsf1 KOs and motor deficiencies (Homma et al., 2007). Thus, we conducted detailed neuropathological analysis of the Hsf1 KOs from our colony (mixed 129SV x Balb/C hybrids) to determine whether these phenotypes were present in the Hsf1 KOs that were in our breeding colony. In Hsf1 WT and KO mice that were uninoculated or mock inoculated intracranially (IC) with 1% normal brain homogenate (a potential inflammatory insult) we did not detect any evidence of neurodegeneration. However, we did note a subtle white matter defect visualized with hematoxylin and eosin staining, which showed a variable amount of vacuolation and one representative samples is shown (Fig. 1Bi-ii) This phenotype was present in Hsf1 WT mice but at a much lower frequency (Bi). We next performed a Luxon-Nissl myelin stain, which had a slightly weaker reaction in the Hsf1 KO mice (Figure 1Biii-iv). GFAP staining, a measure of

reactive astrocytes, was present to a variable degree in this region of the cerebellum of Hsf1 KOs and not altogether absent from Hsf1 WT samples (Bv-vi). Staining for IBA1, a microglial marker, and CNPase, an enzyme expressed in myelinating cells, did not show a phenotypic difference in Hsf1 WT and KO samples (data not shown).

To determine the functional significance (if any) of this white matter defect, we conducted several control experiments. First, we assessed the survival of Hsf1 WT and KOs inoculated IC with a 1% normal brain homogenate (from hamster): 69% of Hsf1 WT mice (n=18) survived up to 469 days post inoculation when the study was terminated whereas 100% of Hsf1 KOs survived (n=8) (Fig. 1C) (tick marks indicate censored events, such as mice sacrificed due to extreme dermatitus). Motor performance was assessed on an accelerating treadmill (acceleration: 1cm/s/5 seconds) as conducted previously (Chen et al., 2005). The maximum speed at which mice could run was recorded at 4-6 month old (n=7 Hsf1 WT and n=6 Hsf1 KO) and 16-17 months old (n=8 Hsf1 WT and n=8 Hsf1 KO); there were no significant differences between Hsf1 WT and KO mice at either timepoint (Fig. 1D). Motor coordination was measured on the rotarod apparatus (Dunham and Miya, 1957) at 4-6 month old (n=7 Hsf1 WT and n=6 Hsf1 KO) and 16-17 months old (n=8 Hsf1 WT and n=8 Hsf1 KO). Hsf1 KOs showed a trend toward better performance on rotarod at 4-6 months old, remaining on rotarod for approximately 60 seconds longer than Hsf1 WT controls (P=0.082. Student's t test) (Fig 1E). At a late timepoint of 16-17 months of age, Hsf1 KOs outperformed outperformed Hsf1 WTs (n=8 Hsf1 WT and KO) (P=0.020, Student's T test). Since the rotarod tests cerebellar function and our other phenotypic testing did not show defects in Hsf1 KOs, we concluded that these mice do not suffer from neurodegeneration under basal conditions.

Survival of prion inoculated Hsf1 knockouts

We next inoculated Hsf1 WT and KO mice with Rocky Mountain Laboratory (RML) strain of murine prions. When injected directly into the brain, RML prions caused Hsf1 KOs to die ~18% faster than littermate Hsf1 WT controls. The median survival for Hsf1 KOs was 165 days post inoculation (dpi) (n=15) and Hsf1 WT was 200 dpi (n=18) ($P<0.0001$, log rank test) (Fig. 2a). We inoculated separate cohorts of mice with a range of doses of RML prions intracranically and saw a similar magnitude of enhancement at all doseses tested (Table I). We also delivered prions via an intraperitoneal route to test whether there was a peripheral prion replication or neuroinvasion phenotype in Hsf1 null aniamls. Hsf1 KOs (n=7) inoculated with 3.5logLD_{50} RML intraperitoneally succumbed to disease faster than Hsf1 WT controls (n=13) by 44 daysin terms of median survival (Figure 2B and Table I) ($P<0.0001$, log rank test). Since the difference between intraperitoneal and intracranial inoculations with 3.5logLD_{50} RML prions was quite similar (~16% enhancement of disease in IP inoculated Hsf1 KOs and an ~18% enhancement in IC inoculated Hsf1 KOs) we concluded that there is unlikely to be a peripheral prion replication or a neuroinvasion enhancement or defect in Hsf1 KO mice. We also noted that mice there were homozygous Hsf1+/+ or hemizygous for the deletion allele (Hsf1+/-) had identical kinetics of disease and were therefore call mice Hsf1 WT that have either one or two copies of the normal Hsf1 allele.

Onset of prion disease behavioral symptoms in Hsf1 knockouts

To better understand at what point in disease Hsf1 exerts its protective effect, we investigated the clinical symptoms of prion disease. We utilized video-based automated mouse behavioral analysis technology described in Chapter 3, which robustly discriminated between

mock inoculated control mice and RML prion infected mice in a prior study (Steele et al., 2007a) and was able to tease apart subtle difference in prion induced behavioral symptoms in a separate study (Steele et al., 2007b).

We followed the behavioral changes in RML inoculated Hsf1 WT (n=20) and Hsf1 KO (n=15) mice (from survival plot shown in Fig. 1) beginning at 1 month post inoculation (mpi) until these mice succumbed to disease. Given that the Hsf1 KOs died more than one month faster than controls; we expected to observe a commensurate enhancement in behavioral onset. Much to our surprise, the onset of behavioral symptoms was quite similar or only slightly accelerated in Hsf1 KOs compared to littermate Hsf1 WT controls (Fig. 2). One of the most obvious phenotypes that results from RML prion infection is a dramatic increase in activity, which is reflected in the lateral distance traveled in the home cage. The distance traveled in a 24 hour recording period began to increase in Hsf1 WT and KO mice at 4 mpi and became much more pronounced by 4.5 and 5 mpi (Fig, 2A). Although the Hsf1 KOs show a trend toward increasing distance traveled at 4 and 4.5 mpi, there are no significant differences from Hsf1 WT means. Another phenotype of prion disease, increased rearing, shows a similar increase in Hsf1 KO and control mice except for the last recording timepoint of Hsf1 KOs, 5 mpi, where the Hsf1 WT controls showing an increased rearing ($P<0.01$, Wilcoxon rank sum) (Fig. 2B). A decrease in hanging vertically or upsidedown from the wire food rack of the home cage, a complex motor behavior, is characteristic of RML prion disease. This decrease in hanging showed a similar progressive decline in both Hsf1 WT and KO mice. At one early timepoint, 2.5 mpi, Hsf1 KOs had a significant increase in hanging ($P<0.05$, Wilcoxon rank sum test) and at the last recording of Hsf1 KOs, 5 mpi, there the was a significant decrease in the hanging behavior of Hsf1 KOs ($P<0.05$, Wilcoxon rank sum) (Fig. 2C). Decreased grooming is another feature of RML prion

infection (Steele et al., 2007a). This progressive decline in grooming behavior was slightly more severe in Hsf1 KOs than in Hsf1 WT controls ($P<0.05$ at 4.5 and $P<0.01$ at 5m.p.i., Wilcoxon rank sum test) (Fig. 2D).

Analysis of several other behaviors of Hsf1 WT and KO mice, including jumping, resting, rearing, and drinking were indistinguishable with the exception of eating was significantly decreased at many timepoints in Hsf1 KOs (data not shown). Thus, our analysis suggests that the onset of RML prion induced behavioral symptoms occurs at a similar or slightly earlier timepoint (~4-4.5 mpi) in Hsf1 KOs compared to controls. However, the clinical course, that is the amount of time from the onset of disease phenotypes until death, is drastically reduced in Hsf1 KOs compared to Hsf1 WT controls.

Pathological features of prion disease in Hsf1 knockouts

Next we conducted neuropathological analysis of brain samples taken from IC prion inoculated Hsf1 KO and control mice at several timepoints; 3.5, 4, 4.5 mpi and endpoint. We examined hematotoxylin and eosin stained sections to assess the amount of spongiform changes in the prion inoculated samples. At 3.5 mpi there was little to no spongiosis and then by 4 and 4.5 mpi as well as terminal samples vacuolation was evident in prion inoculated Hsf1 WT and KO samples (Fig. 4). The kinetics, extent, or regional distribution of vacuolation did not differ between Hsf1 WT and KO samples.

We also assessed gliosis by measuring the accumulation of reactive astrocytes by staining sections with the astrocyte antigen, glial fibrillary acidic protein (GFAP). GFAP staining was evident in prion inoculated samples by 4 to 4.5 mpi and similar to hmatotoxylin and eosin staining, we did not observe any differences in the regional distribution, strength, or kinetics of

the glial response (Fig. 4). We stained for PrP aggregates by formic acid treating brain samples to destroy endogenous PrP, leaving only PrP deposits. We did not observe any differences in PrP aggregate accumulation in the brains of Hsf1 KO and controls (Fig. 4).

Accumulation of proteinase K-resistant PrP and prion infectivity in Hsf1 knockouts

Since immunohistochemical staining for PrP aggregation is not quantitative, we utilized proteinase K (PK) digestion to better assay the aggregation state of PrP. We measured the amount of PK-resistant PrP in whole brain homogenates from prion inoculated Hsf1 WT (n=6) and Hsf1 KO (n=6) mice sacrificed at 3.5 mpi and also in samples taken from terminally ill mice (n=6 per genotype). At 3.5 mpi, PK treatment (50ug/ml for 1 hour at 37C) digested away almost all of PrP, but a faint amount of PK-resistant PrP was samples, irrespective of the Hsf1 genotype. In terminal samples there was a large amount of accumulated PK-resistant PrP in all Hsf1 WT and Hsf1 KO samples.

Since PK resistance does not always predict prion infectivity (Lasmezas et al., 1997; Piccardo et al., 2007) we next determined prion titers using a bioassay. The titer of prion infectivity was bioassayed in *Tga*20 transgenic PrP overexpression mice by pooling n=2 Hsf1 WT and n=2 Hsf1 KO brains at 2, 3, 4, and 5 mpi and the terminal samples were bioassayed in CD1 mice with brain samples pooled from n=4 Hsf1 WT and n=4 Hsf1 KO. Contrary to our expectation that prion infectivity would build up faster in Hsf1 KOs, we observed a similar or diminshed development of prion infectivity in Hsf1 KOs (Figure 5B, Table II). At 2 mpi, there was a statistically significant decrease in titer (P=0.019, boot strapped P values) and in terminal samples there was also a significant decrease in prion titer (P=0.016, boot strapped P values)

(Table II). At the other timepoints tested, 3, 4, and 5 mpi, there were no statistically significant differnces (Table II) in prion titers between Hsf1 WTs and KOs.

Discussion

We have demonstrated that deletion of Hsf1 accelerates prion disease in terms of survival. Interestingly, the other major features of prion disease—behavioral symptoms, neuropathological changes, and aggregation of PrP—show normal kinetics. The disease symptoms of RML prion inoculation occured around 4 mpi in both the Hsf1 WT and KO mice, with some changes, such as decreased grooming, occur slightly earlier in the Hsf1 KOs. The accumulation of proteinase K-resistant PrP was fist seen at 3.5 mpi in both the Hsf1 WT and KO samples and prion titer showed a similar increase over the course of disease. Taken together, these results suggest that the Hsf1 KOs have a much shorter clinical phase of prion disease, defining Hsf1's critical protective activity to the time after disease phenotypes arise.

How does Hsf1 function to prolong the survival of prion infected mice? There are numerous target genes (~300) that are up-regulated by Hsf1 in response to thermal elevation, as identified using transcriptional profiling of cultured Hsf1 KO fibroblasts (Trinklein et al., 2004). Adding an additional layer of complexity to this question, Hsf1 can also function as a transcriptional repressor and some studies directly link Hsf1's repressor activity to apoptosis (Xie et al., 2002; Xie et al., 2003). However, at present there is conflicting evidence on the importance of apoptotic pathways in prion diseases (as discussed in Chapter 4). Indeed, we tested on attractive Hsf1 target protein, Hsp70, which has diverse protective properties and has been shown to refold damaged proteins in several neurodegenerative disease models. We inoculated mice overexpressing the inducible isoform of Hsp70 or deleted for both isoforms of Hsp70i,

which is encoded by two genes. However, both of these transgenic lines had a disease profile identical to that of controls in terms of survival after inoculation IC with RML prions (Supplemental figures 1 and 2). Since Hsf1 is likely to respond differently to thermal elevation than to insults of prion protein misfolding, a worthwhile experiment would be to conduct transcriptional profiling experiments from microdissectd brain tissue to determine which genes are up- or down-regulated in Hsf1 KOs and controls during different phases of prion disease.

Another key unanswered question about prion disease is whether the conformational conversion of PrP influenced by molecular chaperones. Indeed in the yeast system molecular chaperones are required for the maintenance of all known yeast prions (Shorter and Lindquist, 2005). Associations between molecular chaperones and PrP have been described for the ER chaperone BiP, an Hsp70 family member, associating with mutant PrP (Jin et al., 2000). In a cell free conversion reaction, the conformation conversion of PrP was assisted by by the bacterial chaperone GroEL and the yeast protein remodeling facotor Hsp104 (DebBurman, 1997 #186;Shorter, 2005 #194;Schirmer, 1997 #185). However, the mamallian counterparts of these proteins remain unidentified. Also, transgenic expression of Hsp104 does not protect against prion replication (Dandoy-Dron et al., 2006). Thus, the evidence for chaperoning of the conformational conversion of PrP^{C} to PrP^{Sc} is only by analogy to the yeast system.

Our results are of importance because they provide clearcut evidence that Hsf1 is causally involved in protection against neurodegeneration. The link between Hsf1 and its target proteins in the causality of neurodegenerative disease has been largely circumstantial. Numerous reports have noted upregulation of particular chaperones that correlates with neuroprotection (Auluck and Bonini, 2002; Auluck et al., 2002; Tagawa et al., 2007), but by taking a genetic approach we were able to demonstrate that Hsf1 is required for maintaining viability during the

clinical phase of prion infection. Indeed, it could be that boosting the heat shock response during prion disease would be an effective therapeutic strategy. At least a decade ago it was demonstrated that prion infected neuroblastoma cells present a defective heat shock response (Tatzelt et al., 1995). Although the mechanism of this effect remains unclear, it was later shown that gendanamycin, a potent heat shock inducing drug, restores this defective heat shock response in cultured cells infected with prions (Tatzelt, 1998 #223). As recently described for a constitutively active Hsf1 mutant in Huntington's disease (Fujimoto et al., 2005), perhaps a therapeutic strategy involving targeted activation of Hsf1 could ameliorate prion or other protein misfolding diseases,

Materials and Methods

Mouse strains and genotyping

All mouse experiments were approved by the MIT Committee on Animal Care. Food and water were provided *ad libitum* and mice were singly housed for the duration of the study while being maintained on a 12:12 light-dark cycle. The construction of the Hsf1 deletion (McMillan et al., 1998) and characterization of the knockout mice (Xiao et al., 1999) were previously described. Mice were obtained on a mixed 129xx x Balb/C strain background and maintained by intercrossing mice hemizygous for the Hsf1 deletion allele.

Prion inoculations and titer calculation

For prion injections, mice were injected intracranially with 30ul of RML strain murine prions, which had been previously titered. Normal brain homogenate controls were included in several experiments, such as pathological analysis and for analysis of the survival of uninfected mice. For pathology, we found that normal brain homogenate injected samples were

indistinguishable from uninjected samples. The titering of samples taken at 2, 3, 4, and 5 mpi utilized *Tga*20 mice that had been backcrossed to C57Bl/6J for 5-6 generations and bred onto a WT PrP genome (Steele et al., 2006). For tittering the terminal brain samples

Statistical Analysis

First, examining only a single population of mice at a time, we drew 10,000 bootstrap samples from the population. For example, if there were N mice in the population, we randomly selected N mice from the population, but with replacement, and this was done 10,000 times. Then the titer was computed for each of these 10,000 randomly resampled populations, and these values were used to estimate 95% confidence intervals for the titer, by eliminating the 2.5% of extreme values from each end of the distribution of titers. The two populations, Hsf1 WT and Hsf1 KO, were separately simulated and bootstrap confidence intervals were computed for each of them.

To compute P-values for differences between populations, one N mice and the other of M mice, we first computed the titers for each population separately. We then pooled all the mice together into a population of size N+M. Then, 10000 times, we resampled (again with replacement) one group of N mice and one group of M mice from this pooled population, and computed the difference in titers for these two populations. The fraction of times for which this difference was bigger than the difference between the two original non-resampled titers gives the empirical P-value.

Other statistical calculations were performed using Graphpad Instat (Wilcoxon rank sum) for behavioral data or Graphpad Prism (log rank test) for survival data.

Western Blotting

Brain homogenates were prepared in glass dounce homogenizers as 10% homogenates (weight/volume) of whole brain in PBS from sampels frozen at indicated timepoints. After sonication, large debris were pelleted by low speed centrifugation. Further dilutions were made into lysis buffer containing (PBS + 1% Tween 20 + 1% Triton X 100 and 150mM NaCl). The equivalent of 30–50ug of total protein was loaded onto 10% Bis-Tris gels (Invitrogen, transferred to nitrocellulose membranes, and analysed by Western blotting using the monoclonal antibody SAF83 (Cayman Chemical). Using infrared conjugated secondary antibodies, protein was visualized using the Licor Odyssey scanner.

Behavioral analysis

Video based software analysis of behavior was conducted similarly to what was described in our prior study (Steele et al., 2007a). Briefly, mice which were normally group housed (n=2-5) were singly caged and video recorded for 24 hours, a complete light-dark cycle (dim red lights were used for recording in the dark phase). The videos were analyzed using the definitions and settings described in (Steele et al., 2007a) using HomecageScan 2.0 software (Clever Systems, Inc, Reston, VA)

Neuropathological analysis

Brains were immersion fixed in formalin and treated with 98% formic acid for 1 hour then fixed for >24 hours prior to paraffin embedding. 2 micron thick sections were cut onto positively charged glass slides and stained with hematoxylin and eosin, or immunostained. For prion aggregate staining, sections were deparaffinized and incubated for 6 minutes in 98% formic acid then washed in distilled water for 5 min. Sections were heated to 100°C in a pressure cooker in citrate buffer (pH 6.0), cooled for 3 minutes, then washed in distilled water for 5 minutes. Immunohistochemical stains were performed on an automated Nexus staining apparatus

(Ventana Medical Systems) using an IVIEW DAB Detection Kit (Ventana). After incubation with protease 1 (Ventana) for 16 min, sections were incubated with anti-PrP SAF-84 (SPI bio; 1:200) for 32 min. Sections were counterstained with hematoxylin. GFAP (1:1000 for 24 min.; DAKO) immunohistochemistry for astrocytes and Iba1 (1:2500 for 32 min.; Wako Chemicals) for microglia was performed similarly, however with antigen retrieval by heating to 100°C in EDTA buffer (pH8.0) within a steamer. A blinded analysis of vacuolation and gliosis in the hippocampus, thalamus, striatum, cortex, and cerebellum was conducted.

References

Aguzzi A, Heikenwalder M, Polymenidou M (2007) Insights into prion strains and neurotoxicity. Nat Rev Mol Cell Biol 8:552-561.

Auluck PK, Bonini NM (2002) Pharmacological prevention of Parkinson disease in Drosophila. Nat Med 8:1185-1186.

Auluck PK, Chan HY, Trojanowski JQ, Lee VM, Bonini NM (2002) Chaperone suppression of alpha-synuclein toxicity in a Drosophila model for Parkinson's disease. Science 295:865-868.

Caughey B, Baron GS (2006) Prions and their partners in crime. Nature 443:803-810.

Chen D, Steele AD, Lindquist S, Guarente L (2005) Increase in activity during calorie restriction requires Sirt1. Science 310:1641.

Dandoy-Dron F, Bogdanova A, Beringue V, Bailly Y, Tovey MG, Laude H, Dron M (2006) Infection by ME7 prion is not modified in transgenic mice expressing the yeast chaperone Hsp104 in neurons. Neurosci Lett 405:181-185.

Dunham NW, Miya TS (1957) A note on a simple apparatus for detecting neurological deficit in rats and mice. J Am Pharm Assoc Am Pharm Assoc (Baltim) 46:208-209.

Fujimoto M, Takaki E, Hayashi T, Kitaura Y, Tanaka Y, Inouye S, Nakai A (2005) Active HSF1 significantly suppresses polyglutamine aggregate formation in cellular and mouse models. J Biol Chem 280:34908-34916.

Fujimoto M, Izu H, Seki K, Fukuda K, Nishida T, Yamada S, Kato K, Yonemura S, Inouye S, Nakai A (2004) HSF4 is required for normal cell growth and differentiation during mouse lens development. Embo J 23:4297-4306.

Homma S, Jin X, Wang G, Tu N, Min J, Yanasak N, Mivechi NF (2007) Demyelination, astrogliosis, and accumulation of ubiquitinated proteins, hallmarks of CNS disease in hsf1-deficient mice. J Neurosci 27:7974-7986.

Jin T, Gu Y, Zanusso G, Sy M, Kumar A, Cohen M, Gambetti P, Singh N (2000) The chaperone protein BiP binds to a mutant prion protein and mediates its degradation by the proteasome. J Biol Chem 275:38699-38704.

Katsuno M, Sang C, Adachi H, Minamiyama M, Waza M, Tanaka F, Doyu M, Sobue G (2005) Pharmacological induction of heat-shock proteins alleviates polyglutamine-mediated motor neuron disease. Proc Natl Acad Sci U S A 102:16801-16806.

Kenward N, Hope J, Landon M, Mayer RJ (1994) Expression of polyubiquitin and heat-shock protein 70 genes increases in the later stages of disease progression in scrapie-infected mouse brain. J Neurochem 62:1870-1877.

Kieran D, Kalmar B, Dick JR, Riddoch-Contreras J, Burnstock G, Greensmith L (2004) Treatment with arimoclomol, a coinducer of heat shock proteins, delays disease progression in ALS mice. Nat Med 10:402-405.

Kovacs GG, Kurucz I, Budka H, Adori C, Muller F, Acs P, Kloppel S, Schatzl HM, Mayer RJ, Laszlo L (2001) Prominent stress response of Purkinje cells in Creutzfeldt-Jakob disease. Neurobiol Dis 8:881-889.

Lasmezas CI, Deslys JP, Robain O, Jaegly A, Beringue V, Peyrin JM, Fournier JG, Hauw JJ, Rossier J, Dormont D (1997) Transmission of the BSE agent to mice in the absence of detectable abnormal prion protein. Science 275:402-405.

Lindquist S, Craig EA (1988) The heat-shock proteins. Annu Rev Genet 22:631-677.

Mallucci G, Dickinson A, Linehan J, Klohn PC, Brandner S, Collinge J (2003) Depleting neuronal PrP in prion infection prevents disease and reverses spongiosis. Science 302:871-874.

Mathew A, Shi Y, Jolly C, Morimoto RI (2000) Analysis of the mammalian heat-shock response. Inducible gene expression and heat-shock factor activity. Methods Mol Biol 99:217-255.

McMillan DR, Xiao X, Shao L, Graves K, Benjamin IJ (1998) Targeted disruption of heat shock transcription factor 1 abolishes thermotolerance and protection against heat-inducible apoptosis. J Biol Chem 273:7523-7528.

McMillan DR, Christians E, Forster M, Xiao X, Connell P, Plumier JC, Zuo X, Richardson J, Morgan S, Benjamin IJ (2002) Heat shock transcription factor 2 is not essential for embryonic development, fertility, or adult cognitive and psychomotor function in mice. Mol Cell Biol 22:8005-8014.

Piccardo P, Manson JC, King D, Ghetti B, Barron RM (2007) Accumulation of prion protein in the brain that is not associated with transmissible disease. Proc Natl Acad Sci U S A 104:4712-4717.

Prusiner SB (1998) Prions. Proc Natl Acad Sci U S A 95:13363-13383.

Santos SD, Saraiva MJ (2004) Enlarged ventricles, astrogliosis and neurodegeneration in heat shock factor 1 null mouse brain. Neuroscience 126:657-663.

Sarge KD, Murphy SP, Morimoto RI (1993) Activation of heat shock gene transcription by heat shock factor 1 involves oligomerization, acquisition of DNA-binding activity, and nuclear localization and can occur in the absence of stress. Mol Cell Biol 13:1392-1407.

Shi Y, Mosser DD, Morimoto RI (1998) Molecular chaperones as HSF1-specific transcriptional repressors. Genes Dev 12:654-666.

Shorter J, Lindquist S (2005) Prions as adaptive conduits of memory and inheritance. Nat Rev Genet 6:435-450.

Shyu WC, Kao MC, Chou WY, Hsu YD, Soong BW (2000) Heat shock modulates prion protein expression in human NT-2 cells. Neuroreport 11:771-774.

Steele AD, Jackson WS, King OD, Lindquist S (2007a) The power of automated high-resolution behavior analysis revealed by its application to mouse models of Huntington's and prion diseases. Proc Natl Acad Sci U S A 104:1983-1988.

Steele AD, Emsley JG, Ozdinler PH, Lindquist S, Macklis JD (2006) Prion protein (PrPc) positively regulates neural precursor proliferation during developmental and adult mammalian neurogenesis. Proc Natl Acad Sci U S A 103:3416-3421.

Steele AD, King OD, Jackson WS, Hetz CA, Borkowski AW, Thielen P, Wollmann R, Lindquist S (2007b) Diminishing Apoptosis by Deletion of Bax or Overexpression of Bcl-2 Does Not Protect against Infectious Prion Toxicity In Vivo. J Neurosci 27:13022-13027.

Tagawa K, Marubuchi S, Qi ML, Enokido Y, Tamura T, Inagaki R, Murata M, Kanazawa I, Wanker EE, Okazawa H (2007) The induction levels of heat shock protein 70 differentiate the vulnerabilities to mutant huntingtin among neuronal subtypes. J Neurosci 27:868-880.

Tatzelt J, Zuo J, Voellmy R, Scott M, Hartl U, Prusiner SB, Welch WJ (1995) Scrapie prions selectively modify the stress response in neuroblastoma cells. Proc Natl Acad Sci U S A 92:2944-2948.

Trinklein ND, Murray JI, Hartman SJ, Botstein D, Myers RM (2004) The role of heat shock transcription factor 1 in the genome-wide regulation of the mammalian heat shock response. Mol Biol Cell 15:1254-1261.

Wang G, Zhang J, Moskophidis D, Mivechi NF (2003) Targeted disruption of the heat shock transcription factor (hsf)-2 gene results in increased embryonic lethality, neuronal defects, and reduced spermatogenesis. Genesis 36:48-61.

Wang G, Ying Z, Jin X, Tu N, Zhang Y, Phillips M, Moskophidis D, Mivechi NF (2004) Essential requirement for both hsf1 and hsf2 transcriptional activity in spermatogenesis and male fertility. Genesis 38:66-80.

Waza M, Adachi H, Katsuno M, Minamiyama M, Sang C, Tanaka F, Inukai A, Doyu M, Sobue G (2005) 17-AAG, an Hsp90 inhibitor, ameliorates polyglutamine-mediated motor neuron degeneration. Nat Med 11:1088-1095.

Westerheide SD, Morimoto RI (2005) Heat shock response modulators as therapeutic tools for diseases of protein conformation. J Biol Chem 280:33097-33100.

Westwood JT, Wu C (1993) Activation of Drosophila heat shock factor: conformational change associated with a monomer-to-trimer transition. Mol Cell Biol 13:3481-3486.

Xiao X, Zuo X, Davis AA, McMillan DR, Curry BB, Richardson JA, Benjamin IJ (1999) HSF1 is required for extra-embryonic development, postnatal growth and protection during inflammatory responses in mice. Embo J 18:5943-5952.

Xie Y, Zhong R, Chen C, Calderwood SK (2003) Heat shock factor 1 contains two functional domains that mediate transcriptional repression of the c-fos and c-fms genes. J Biol Chem 278:4687-4698.

Xie Y, Chen C, Stevenson MA, Auron PE, Calderwood SK (2002) Heat shock factor 1 represses transcription of the IL-1beta gene through physical interaction with the nuclear factor of interleukin 6. J Biol Chem 277:11802-11810.

Zou J, Guo Y, Guettouche T, Smith DF, Voellmy R (1998) Repression of heat shock transcription factor HSF1 activation by HSP90 (HSP90 complex) that forms a stress-sensitive complex with HSF1. Cell 94:471-480.

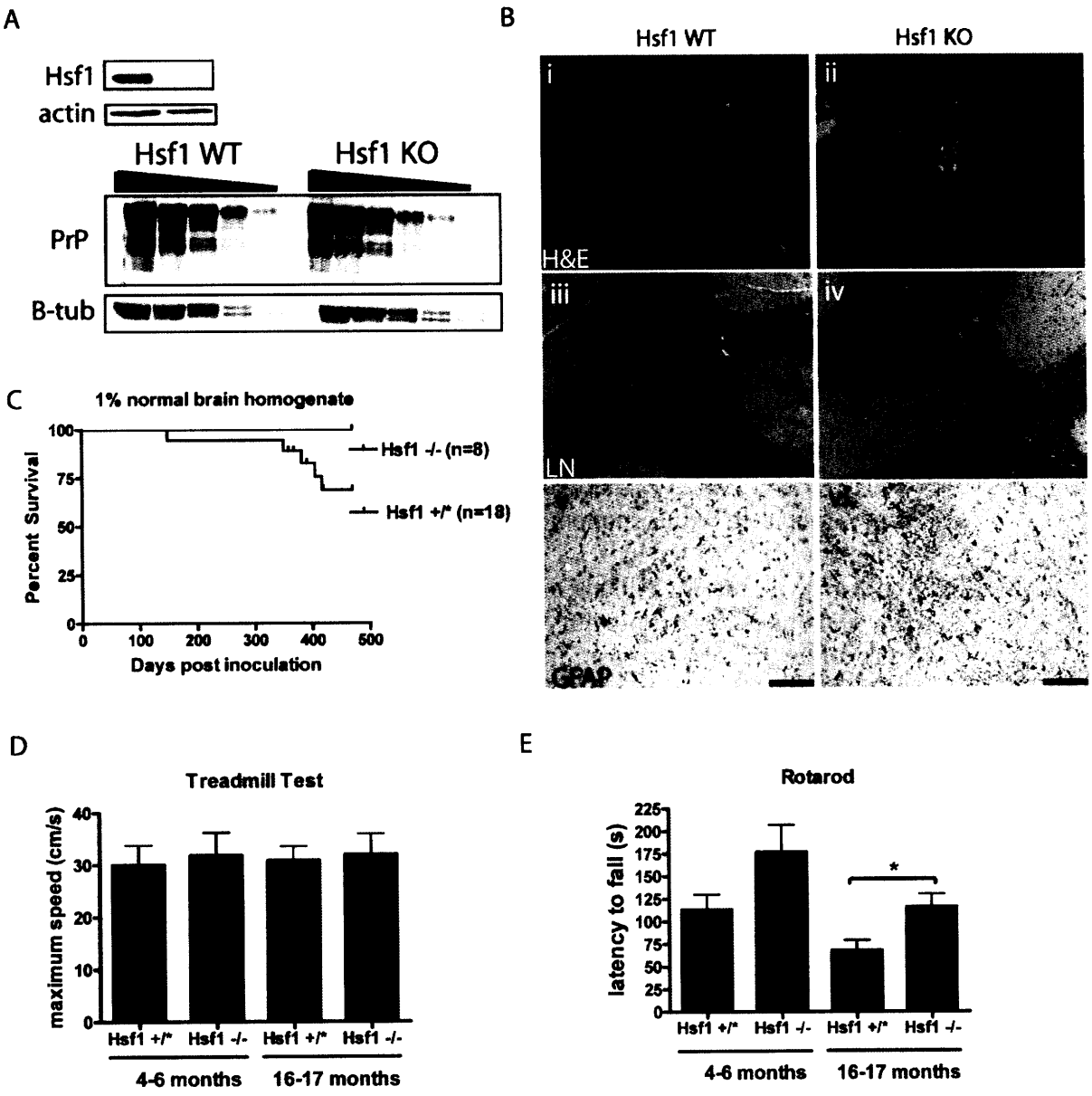

Figure 1 Characterization of neurologic parameters in Hsf1 KO mice. Western blots of dilution series of whole brain homogenates from Hsf1 WT (n=2) and Hsf1 KO (n=2) show similar steady state levels of PrP. Beta-tubulin was used as a loading control (A). Histological characterization of Hsf1 KOs suggests a subtle myelination defect in the cerebellum. Hematotoxylin and eosin staining showed a variable amount of vacuolation and one representative samples is shown (scale bar 200um)(Bii). This phenotype was present in Hsf1 WT mice but at a much lower frequency (Bi). Luxon-Nissl myelin stain is weaker in the cerebellum of Hsf1 KO mice (scale bar 100um)(Biii-iv). Gliosis measured with GFAP staining showed a subtle increase over Hsf1 WTs in this region of the cerebellum of Hsf1 KOs (Bv-vi). Assessment of survival in Hsf1 WT and KOs inoculated with a 1% normal brain homogenate (from hamster): 69% of Hsf1 WT mice (n=18) survived up to 469 days post inoculation when the study was terminated whereas 100% of Hsf1 KOs survived (n=8) (C) (tick marks indicate censored events, such as mice sacrificed

due to extreme dermatitus). Motor performance was assessed on an accelerating treadmill (acceleration: 1cm/s/5 seconds). The maximum speed at which mice could run was recorded at 4-6 month old (n=7 WT and n=6 Hsf1 KO) and 16-17 months old (n=8 for each group); there were no significant differences between Hsf1 WT and KO mice at either timepoint (D). Motor coordination was measured on the rotarod apparatus for Hsf1 WT (n=7) and Hsf1 KO (n=6) at 4-6 months of age and at 16-17 months of age (n=8 for both Hsf1 WT and KO). Hsf1 KOs outperformed Hsf1 WTs (n=8 for Hsf1 WT and for KO) at the later timepoint ($P<0.05$, Student's T test).

A

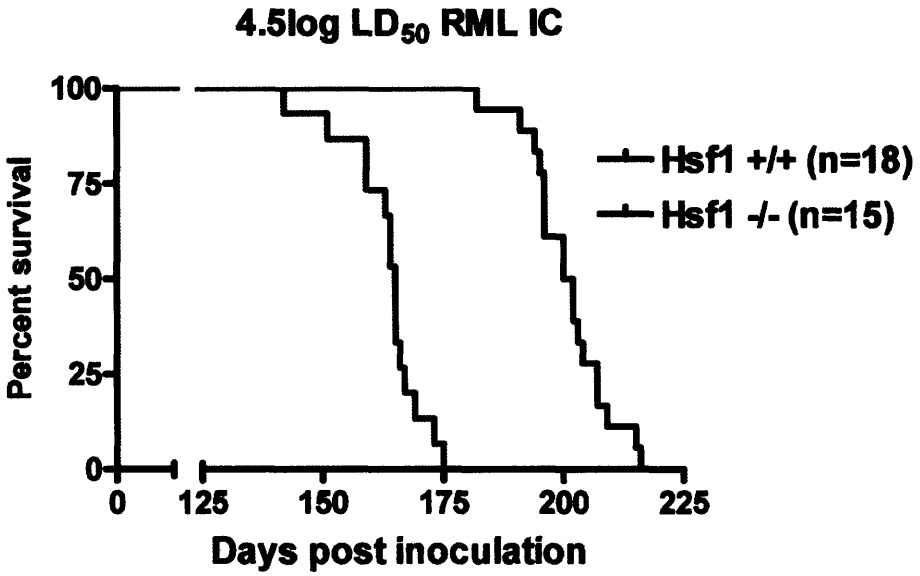

B

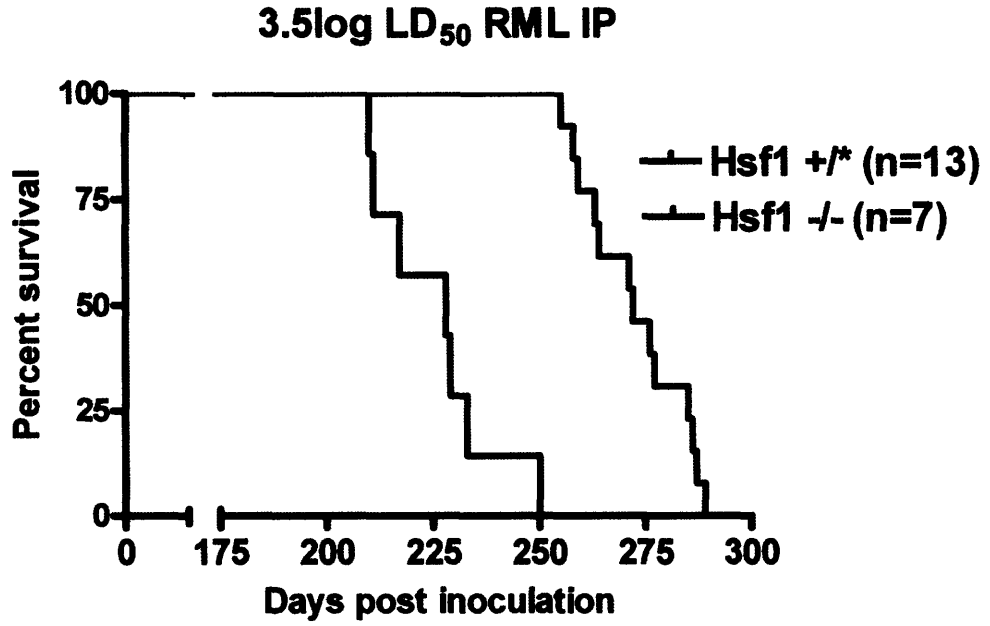

Figure 2 Hsf1 knockouts succumb to disease with accelerated kinetics. Survival of Hsf1 WT (n=18) and KOs (n=15) inoculated intracranially with 4.5logLD_{50} RML prions ($P<0.0001$, log rank test) (A) (note: x-axis is broken to begin at 125 days post inoculation). Intraperitoneal infection of Hsf1 WT (n=13) and KOs (n=7) with 3.5logLD_{50} RML prions ($P<0.0001$, log rank test) (B) (note: x-axis is broken to begin at 175 days post inoculation).

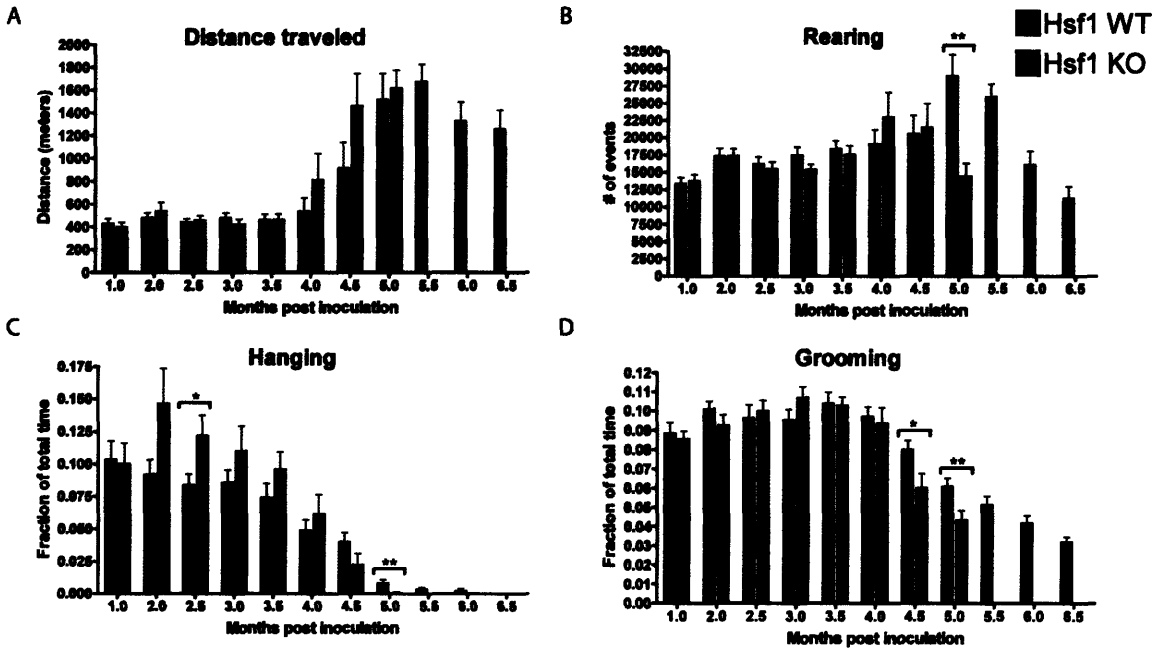

Figure 3 Prion induced behavioral alterations in home cage behaviors occur with similar kinetics in Hsf1 WT and KO mice (for Hsf1 WT n=20 at all timepoints except at 6.5 months post inoculation where n=19 and for Hsf1 KO n=15 at all timepoints except at 5 months post inoculation where n=14). The increase in distance traveled, which measures lateral movement (meters), shows a similar onset in Hsf1 WT and KO mice infected with RML prions (**A**). Another phenotype of prion disease, increased rearing, shows a similar increase in Hsf1 KO and control mice except for the last recording timepoint of Hsf1 KOs, 5 mpi, where the Hsf1 WT controls showing an increased rearing ($P<0.01$, Wilcoxon rank sum) (**B**). The decrease in hanging from the wire food rack was similar between Hsf1 WT and KO mice (at one early timepoint, 2.5 mpi, Hsf1 KOs had a significant increase in hanging $P<0.05$, Wilcoxon rank sum test) and at the last recording of Hsf1 KOs, 5 mpi, there the was a significant decrease in the hanging behavior of Hsf1 KOs ($P<0.05$, Wilcoxon rank sum) (**C**). The decrease in grooming behavior was slightly more severe in Hsf1 KOs, which showed less grooming at 4.5 ($P<0.05$) and 5 mpi ($P<0.01$, Wilcoxon rank sum test) (**D**).

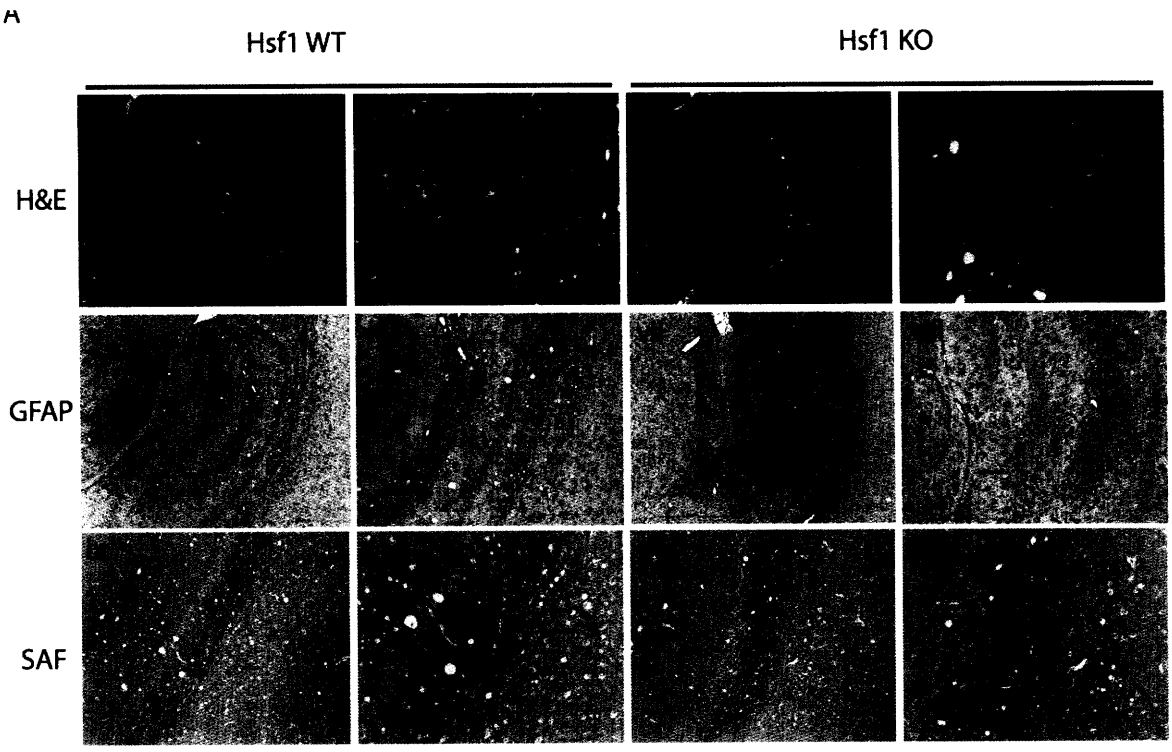

Figure 4 Similar neuropathological changes in Hsf1 KO and control brains. Spongiform changes were visualized with a hematoxylin and eosin staining. Representative images of hippocampi from RML prion inoculated Hsf1 WT and KO are shown (A) at low magnificaiton in **i** and **iii** and at higher power in **ii** and **iv**. The glial response was assessed by staining against the astrocyte antigen GFAP. Dramatic astrocytosis was observed in hiccocampi from both Hsf1 WT and KO samples shown at low magnificaiton in **v** and **vi** and at higher power in **vii** and **viii**. Immunohistochemistry specifically against disease associated PrP showed equivalent staining in Hsf1 WT and KO samples shown shown at low magnificaiton in **ix** and **x** and at higher power in **xi** and **xii** (scale bars correspond to 500um)

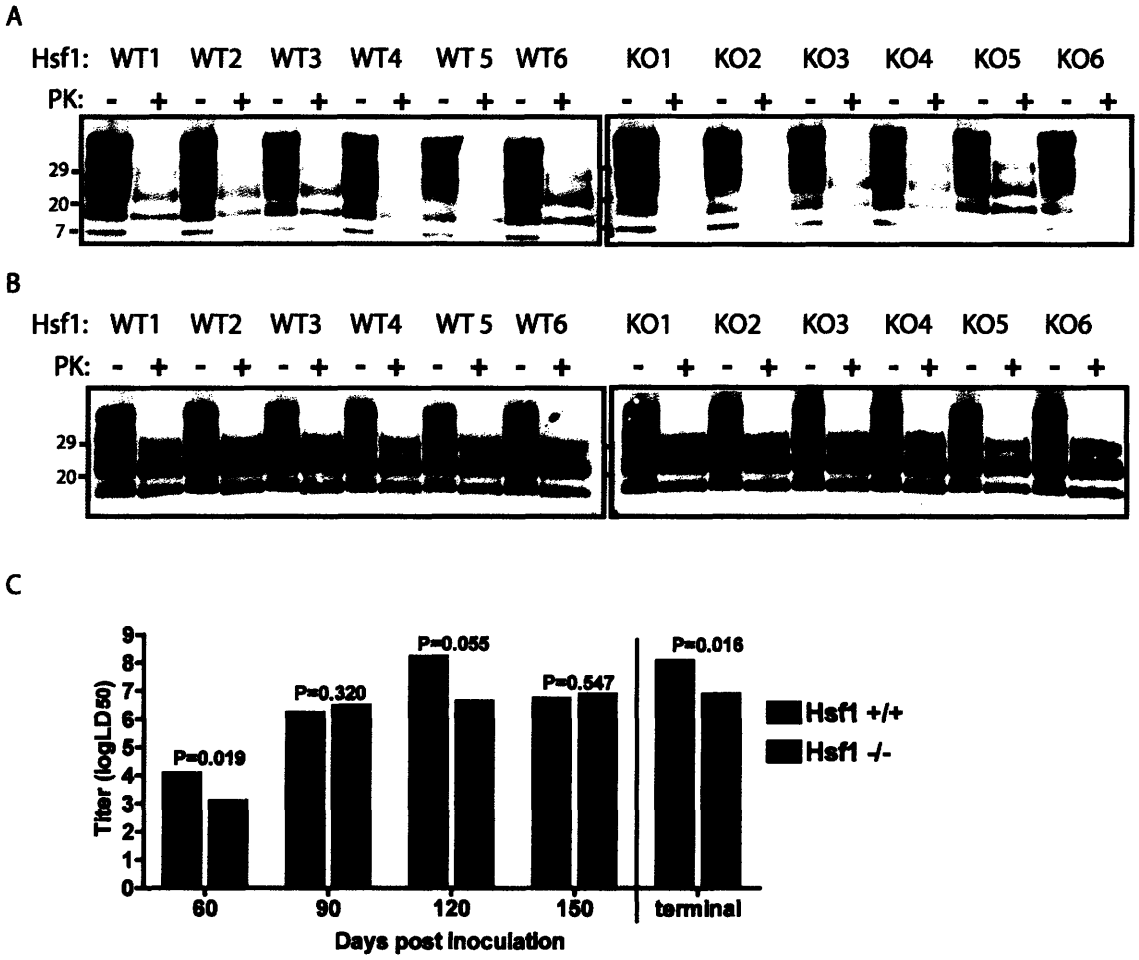

Figure 5 Measurement of proteinase K (PK)-resistant PrP and prion titers. The amount of PK-resistant PrP was measured by immunoblotting PK treated brain homogenates (50ug/ml PK for 1 hour at 37C) at 3.5 months post inoculation and in terminal samples (A). The titer of prion infectivity was bioassayed in *Tga*20 transgenic PrP overexpression mice by pooling Hsf1 WT (n=2) and Hsf1 KO (n=2) brains at 60, 90, 120, and 150 and the terminal samples were bioassayed in CD1 mice with brain samples pooled from Hsf1 WT (n=4) and Hsf1 KO (n=4). Bootstrapped P values are shown above each set of bars for within timepoint comparisons of titer.

Table I. Summary of RML prion inoculations in Hsf1 knockout and control mice

RML inoculum dose/route	Median survival (days) and # of animals	Difference in median survival (WT-KO) (days)	P value (log rank test)
6.5 $logLD_{50}$ IC	WT (n=18) 177 KO (n=12) 144	-33	<0.0001
5.5 $logLD_{50}$ IC	WT (n=16) 184 KO (n=16) 146	-38	<0.0001
4.5 $logLD_{50}$ IC	WT (n=18) 201 KO (n=15) 165	-36	<0.0001
3.5 $logLD_{50}$ IC	WT (n=38) 202 KO (n=12) 181	-22	<0.0001
2.5 $logLD_{50}$ IC	WT (n=) 225 KO (n=) 186	-39	0.0003
5.5 $logLD_{50}$ IP	WT (n=19) 254 KO (n=8) 201	-53	<0.0001
3.5 $logLD_{50}$ IP	WT (n=13) 272 KO (n=7) 228	-44	<0.0001

Abbreviations: RML, Rocky Mountain Laboratory; IC, intracranial; IP, intraperitoneal

Table II. Summary of titration experiments from Hsf1 knockout and control brains

Timepoint	Dilution	Survival of recipients (days post inoculation)	Titer ($logLD_{50}$/ 30ul)	Bootstrapped P values
Hsf1 WT 2 MPI (n=2)	10^{-2}	72, 73, 74, 75, 76	4.1	0.019
	10^{-3}	94, 94, 96, 98, 99		
	10^{-4}	112, >202, >202, >202, >202		
	10^{-5}	123, 129, >202, >202, >202		
	10^{-6}	>202, >202, >202, >202, >202		
	10^{-7}	>202, >202, >202, >202, >202, >202		
Hsf1 KO 2 MPI (n=2)	10^{-2}	79, 93, 94, 96	3.1	
	10^{-3}	104, 109, 129, >202, >202		
	10^{-4}	>202, >202, >202, >202, >202, >202		
	10^{-5}	>202, >202, >202, >202, >202, >202		
	10^{-6}	>202, >202, >202, >202, >202, >202		
	10^{-7}	>202, >202, >202, >202, >202, >202		
Hsf1 WT 3 MPI (n=2)	10^{-2}	62, 66, 74, 75		
	10^{-3}	75, 75, 76, 77	6.25	0.320
	10^{-4}	73, 81, 83, 84		
	10^{-5}	89, 99, 100, 101		
	10^{-6}	90, 98, >201, >201		
	10^{-7}	105, >201, >201, >201		
	10^{-8}	>201, >201, >201, >201		
Hsf1 KO 3 MPI (n=2)	10^{-2}	66, 68, 69, 72	6.5	
	10^{-3}	63, 76, 78, 79		
	10^{-4}	85, 87, 90, 97		
	10^{-5}	94, 94, 104, 107		
	10^{-6}	120, 124, 139, 144		
	10^{-7}	>201, >201, >201, >201		
	10^{-8}	>201, >201, >201, >201		
Hsf1 WT 4 MPI (n=2)	10^{-3}	74, 74, 75, 75, 76	8.25	0.055
	10^{-4}	74, 74, 83, 83		
	10^{-5}	84, 89, 90, 91		
	10^{-6}	90, 105, 124, 133		
	10^{-7}	91, 124, 131, >200		
	10^{-8}	125, 133, >200, >200		
	10^{-9}	105, 179, >200, >200		
Hsf1 KO 4 MPI (n=2)	10^{-3}	70, 70, 71, 74	6.65	

Table II (continued)

	10^{-4}	83, 84, 87, 90		
	10^{-5}	84, 90, 93, 96		
	10^{-6}	93, 131, >200, >200		
	10^{-7}	131, >200, >200, >200, >200		
	10^{-8}	124, >200, >200, >200, >200		
	10^{-9}	106, >200, >200, >200		
Hsf1 WT 5 MPI (n=2)	10^{-4}	70, 82, 83, 85	6.75	0.547
	10^{-5}	82, 83, 83, 84, 85		
	10^{-6}	96, 97, 103, 111		
	10^{-7}	113, >200, >200, >200		
	10^{-8}	>200, >200, >200, >200		
	10^{-9}	>200, >200, >200, >200		
	10^{-10}	>200, >200, >200, >200		
Hsf1 KO 5 MPI (n=2)	10^{-4}	75, 76, 81, 81	6.9	
	10^{-5}	87, 92, 98, 109		
	10^{-6}	109, 130, 188		
	10^{-7}	119, 122, >200, >200, >200		
	10^{-8}	>200, >200, >200, >200, >200		
	10^{-9}	>200, >200, >200, >200		
	10^{-10}	>200, >200, >200, >200		
Hsf1 WT* terminal (n=4)	10^{-3}	160, 163, 166, 166	8.1	0.016
	10^{-4}	153, 164, 170, 170, 176		
	10^{-5}	166, 174, 174, 174, 174		
	10^{-6}	174, 182, 182, 188, 188		
	10^{-7}	192, 195, 210, 226, 226		
	10^{-8}	239, 266, >300, >300, >300		
	10^{-9}	239, >300, >300, >300, >300		
Hsf1 KO* terminal (n=4)	10^{-3}	153, 153, 160, 161, 161	6.9	
	10^{-4}	170, 170, 172, 175, 177		
	10^{-5}	160, 175, 179, 182, 184		
	10^{-6}	180, 182, 196, 198, >300		
	10^{-7}	182, 205, 223, >300, >300		
	10^{-8}	>300, >300, >300, >300		
	10^{-9}	>300, >300, >300, >300		

Abbreviations: mpi, months post inoculation:
*CD1 recipient mice were used for determining these titers whereas *Tg*20 mice were used for all other titrations

Appendix

Supplemental Material

Author contributions:

I designed, performed, and coordinated many of the experiments present in this chapter but I was part of a much larger collaborative research team. Frank Heppner taught me almost everything that I know about neuropathology during my brief visit to Adriano Aguzzi's laboratory in the summer of 2005. Gregor Hutter, a student in Aguzzi lab, continued our collaboration providing key contributions to the neuropathological analysis of the uninoculated Hsf1 KOs and the prion inoculated mice. Walker Jackson assisted with numerous prion inoculations and had a large role in shaping this project. Artur Topolszki assisted with numerous prion inoculations and oversaw an enormous breeding colony to generate the many mice used in this study. Andrew Borkowski contributed to the behavioral analysis. Oliver King assisted with analysis of the behavioral data and bootstrapped P-values for the prion tittering experiments. Gregory Raymond was extremely helpful to me when I was setting up our laboratory for prion work, and he provided us with numerous prion strains and advice.

Hsp70i and prion disease

We also studied the effects of the inducible isoform of Hsp70 ("Hsp70i" on prion pathogenesis. We obtained mice that transgenically express Hsp70i from rat (Cummings et al., 2001). These mice show resistance to several toxic insults, including overexpression of a protein associated with neurodegeneration (Cummings et al., 2001). We also obtained mice that are deleted for the two inducible isoforms of Hsp70i (Hsp70.1 and Hsp70.3) (Hunt et al., 2004). Importantly, these mice show enhanced susceptibility to Huntington's disease (Jennifer Wacker and Paul Muchowski, personal communication), confirming the importance of these genes in protecting against neurodegeneration. We did not observe any protection against disease in the Hsp70i overexpression transgenic or any enhancement of disease in the Hsp70i dKO in terms of survival. Several prion inoculation experiments are described in the figures below.

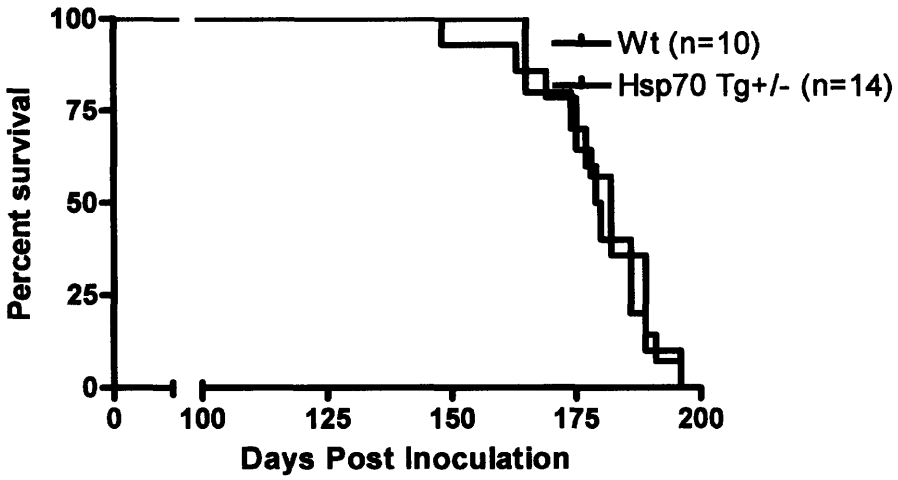

Supplemental Figure 1 Transgenic overexpression of Hsp70i does not alter the survival of mice inoculated intracranially with RML prions ($5.5 \log LD_{50}$). (P=0.77, log rank test).

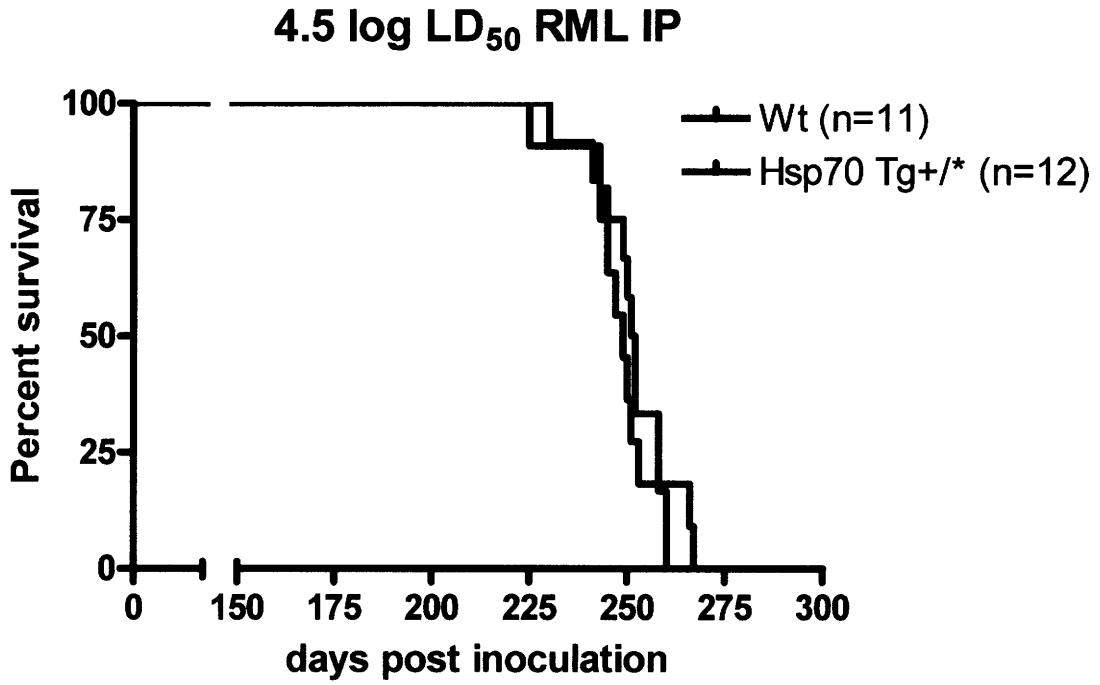

Supplemental Figure 2 Transgenic overexpression of Hsp70i does not alter the survival of intraperitoneally inoculated mice (4.5logLD_{50}) (P=0.96, log rank test).

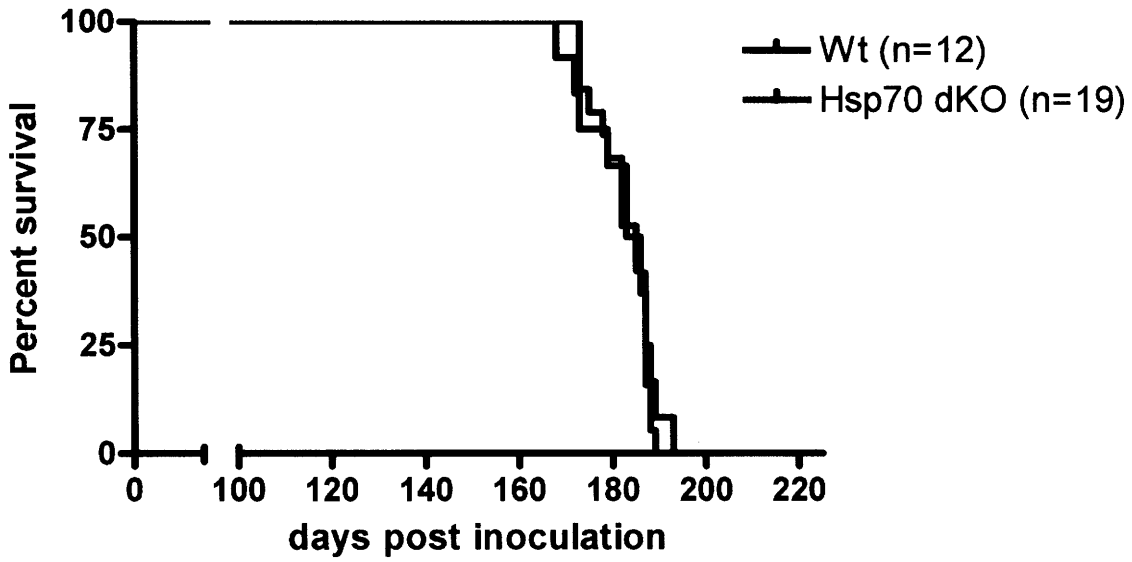

Supplemental Figure 3 Deletion of the inducible isoforms of Hsp70i (Hsp70.1 and Hsp70.3 double knockout) does not alter survival after intracranial inoculation with 3.5logLD50 RML prions (P=0.49, log rank test)

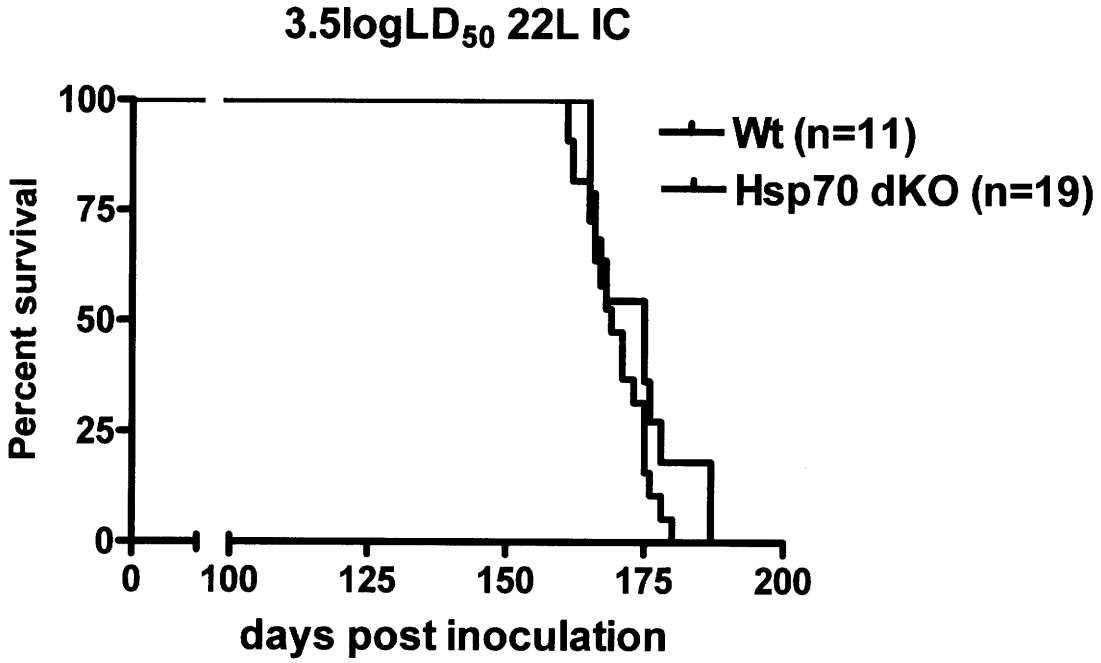

Supplemental Figure 4 Deletion of the inducible isoforms of Hsp70i (Hsp70.1 and Hsp70.3 double knockout) does not alter survival after intracranial inoculation with 3.5logLD50 22L prions (P=0.21, log rank test)

Methods

Mice were injected intracranially with RML or 22L strain of murine prions corresponding at the doses indicated in the figure legends. Mice were monitored daily for typical prion symptoms, such as imbalance, priapism (males), and weight loss, and were sacrificed when they became moribund, or unable to gain access to the food bin or water spout.

References

Cummings CJ, Sun Y, Opal P, Antalffy B, Mestril R, Orr HT, Dillmann WH, Zoghbi HY (2001) Over-expression of inducible HSP70 chaperone suppresses neuropathology and improves motor function in SCA1 mice. Hum Mol Genet 10:1511-1518.

Hunt CR, Dix DJ, Sharma GG, Pandita RK, Gupta A, Funk M, Pandita TK (2004) Genomic instability and enhanced radiosensitivity in Hsp70.1- and Hsp70.3-deficient mice. Mol Cell Biol 24:899-911.

Chapter 6

Conclusions and Future Directions

Future experiments to determine the normal function of PrP

In my thesis work I undertook the study of both the normal function of PrP as well as the study of prion diseases, which results from the misfolding of PrP. We made several attempts at finding a functional role for PrP in mammalian biology, as described in Chapter 2. In the first attempt we crossed PrP knockout mice to several transgenic models of neurodegenerative diseases. Surprisingly, deletion of PrP did not appreciably affect the phenotypes of mouse models of Parkinson's disease, Tauopathy, or Huntington's disease. It is noteworthy that a recent study has implicated PrP in the regulation of the beta-secretase complex, which generates the pathogenic fragment of the amyloid precursor protein associated with Alzheimer's disease (Parkin et al., 2007). Also, some human genetic studies have found associations of PRNP to Alzheimer's disease risk (Del Bo et al., 2006), but these results are controversial (Jeong et al., 2007). Thus, PrP may be involved in the pathogenesis of Alzheimer's disease but not in the disease models that I tested in my experiments. I also cannot rule out the possibility that PrP plays a subtle role in the diseases that I tested due to 1) failings of the mouse models—this is particularly important in the case of the Parkinson's model, which did not have a considerable phenotype and/or 2) the resolution of my phenotypic assays, which were crude. Alas, I did not have high resolution automated mouse behavior analysis technology (Steele et al., 2007a) up and running during the course of these studies.

Fortuitously, Cheng Cheng Zhang and Harvey Lodish enlisted our help to study the effects of PrP in hematopoietic stem cells. These studies led by Cheng Cheng Zhang, identified PrP as a hematopoietic stem cell marker and also showed that PrP null hematopoietic stem cells had a defect in self-renewal under the stressful condition of serial tranplanation (Zhang et al., 2006). Ongoing investigations that I have led in a continued collaboration with Harvey Lodish,

Cheng Cheng Zhang, and Megan Kaba demonstrated that aged PrP knockout mice have a depletion of hematopoietic stem cells, suggesting that the self-renewal phenotype that we observed during serial transplantation also manifests during the aging process. In terms of molecular characterization of the pathways connecting PrP to hematopoietic stem cell self-renewal, we could perform transcriptional profiling on highly enriched hematopoietic stem cells from aged PrP null mice or from serially transplanted bone marrow. However, these experiments are technically demanding and may not pinpoint a pathway, as transcriptional profiling may not reveal substantial changes especially considering that the effects that we have observed in PrP null hematopoietic stem cell are modest.

The work on PrP in hematopoiesis prompted to test if PrP had a role in neurogenesis, the making of neurons, in collaboration with Jason Emsley, Hande Ozdinler, and Jeffrey Macklis. We observed that in an *in vitro* assay of neural precursor differentiation that PrP null neurons are slower to develop into mature neurons, remaining in an undifferentiated state for longer than controls. Conversely, PrP overexpression is a rapid driver of differentiation into the mature neuronal fate (Steele et al., 2006). When we examined adult neurogenesis, we observed a small but significant decrease in cellular proliferation in the dentate gyrus of PrP null mice and a subtle but significant increase in cellular proliferation in the subventricular zone (Steele et al., 2006). When we challenged the adult neurogenesis system with environmental enrichment, which dramatically increases neurogenesis (Kempermann et al., 1997), we did not observe any substantial effect of PrP deletion or overexpression under these conditions, suggesting that environmental enrichment may have dwarfed the effects of PrP under these conditions.

Although we described some phenotypes in the PrP knockout mouse, we do not possess an understanding of how these effects are mediated at a molecular level. Since the effects that we

observed on hematopoiesis and neurogenesis were subtle, examination of any alterations in signaling pathways may have been difficult to discern in PrP KOs compared to controls. Given the striking conservation of PrP among mammals and even in fish and turtles (Rivera-Milla et al., 2006), one would suspect that PrP is essential for development. However, PrP KO mice do no present an overt defect, and one must wonder why the PrP knockout does not have a more clear-cut phenotype. One plausible answer is compensation for PrP loss by an undetermined gene(s). It is unlikely that this gene shares substantial sequence homology with PrP as PrP's closest homolog is Dpl, which shares approximately 25% amino acid identity with the C-terminal domain of PrP. Furthermore it is unclear that Dpl could compensate for loss of PrP as the expression pattern of Dpl is markedly different from that of PrP. Dpl is not expressed in the brain and can only be found on select blood cells and in the testis (Qin et al., 2006). Recently, there is increasing interest in a possible third member of the prion gene family (shadow of the prion protein) (Premzl et al., 2003). This is a small protein that in some ways resembles the medial portion of PrP, which contains a very hydrophobic domain (Premzl et al., 2003). Recently David Westaway and colleagues showed that shadoo is expressed in the brain and is dramatically down-regulated at the protein level during prion disease (Watts et al., 2007). Thus, the interplay of PrP with shadoo may be fruitful in deciphering PrP function. Double deletion of PrP and shadoo may possibly reveal a dramatic central nervous system phenotype.

Future experiments using high throughput video based technology to study neurodegenerative disease models and beyond

In Chapter 3, I described an alternative approach to assesses the behaviors of two mouse models of neurodegenerative disease of different etiology, Huntington's disease and prion

disease. Homecage activity determined by laser beam breaks was previously used with some success to diagnose prion disease (Dell'Omo et al., 2002) as well as polyglutamine disease (Jackson et al., 2003). However, these studies are inherently low in resolution, whereas our studies provided highly informative data regarding the fine details of mouse behavior (Steele, 2007 #13). Future experiments should examine a wide array of transgenic and chemical models of neurodegenerative disease, perhaps to find common diagnostic features of disease that would be useful for screening drugs *in vivo* in a pharmaceutical setting. Another outcome of discerning behavioral aberrations in precise detail would be to unravel the brain regions that are degenerating in prion and other diseases of the brain.

Future experiments will be aimed at developing next generation technology to study the social behavior of mice in a high resolution, automated manner. In our previous studies, we examined singly housed mice, which can induce stress and may not reflect normal mouse behavior as mice are stressed by single housing (Chourbaji et al., 2005). The original approach favored analysis of singly housed mice because two mice in the same cage may occlude the other from video detection, thus hindering analysis of both mice. We will address this problem by using two cameras at two different angles and design software analyze the fused video contents automatically from the two cameras to identify each unique mice and their social interactions.

Future experiments to elucidate cell death pathways in prion disease

Our studies of prion disease did not suggest a role for Caspase-12 or Bax in promoting prion toxicity, since deletion of these genes did not ameliorate disease (Steele et al., 2007b). Moreover overexpression of Bcl-2 did not delay disease (Steele et al., 2007b). However, Bax and Bcl-2 are not required for apoptosis mediated by extrinsic apoptotic pathways, such as Fas ligand

and death receptor induced pathways (Yuan, 1997). Thus, our experiments only rule out one arm of the apoptotic pathway (Bax dependent intrinsic pathway) acting on its own to promote prion pathogenesis (Steele et al., 2007b). In fact, although the Bax homolog Bak is not abundant in the brain, it is formally possible that Bak is compensating for Bax in the Bax KO background. However, I deem this explanation unlikely, as other experiments using the same Bax KO to study neurodegeneration have shown positive effects on neuronal survival in their systems, so Bak cannot be cannot be compensating in their systems(Selimi et al., 2000; Chiesa et al., 2005; Gould et al., 2006; Heitz et al., 2007; Li et al., 2007). It may be the case that when an apoptotic or necrotic pathway is diminished, one or the other is up-regulated in compensation (Degterev et al., 2005). Alternative cell death pathways may still efficiently lead to cell death even though apoptosis is defective. I suggest that future experiments to test apoptotic pathways in prion diseases should be directed toward extrinsic pathways.

Future experiments aimed at delineating the role of heat shock factor 1 in protecting against prion toxicity

Although prion replication can be recapitulated in cultured cells, there is no widely used surrogate assay for the study of prion toxicity *in vitro*. Thus, one is required to study prion toxicity *in vivo*, which is time-consuming and costly. If time and costs were not limiting, I would propose inoculating a genome wide deletion set of mice (Auwerx et al., 2004) to find genetic modifiers of prion disease. I predict that many of these genes will generalize to other protein misfolding disorders, such as Alzheimer's or Parkinson's diseases. The laborious genetically defined crosses that would be necessary in studying transgenic models of neurodegenerative disease are circumvented since we can directly inoculate prions into the brain. This is not to say

that the proposed experiment is free from caveats, in that sometimes knockout strategies are flawed, or deletion of a gene leads to a compensatory up-regulation of a functional ortholog or affects the expression of a nearby gene. To circumvent compensation, one can construct double and triple knockouts (by intercrosses); however, this brings up another limitation of knockout studies—the inability to readily study the effects of genes that are required for normal development, fertility, and/or homeostasis. At present and in the future more targeted deletions using conditional knockout strategies will be utilized to combat these issues. In addition neuronal and glial cell type specific deletions will be useful in understanding the effects are indeed neuronal or due to glial cells, which are underappreciated for their contributions to neurodegeneration (Darlington, 2005).

Studying prion disease in multiple genetically modified mice as an approach has limited feasibility. Thus, I chose heat shock factor 1 (Hsf1) knockout mice because it was an obvious place to begin to unravel the stress responsive pathways that may be activated in prion disease. I observed that Hsf1 knockouts, which do not show spontaneous neurodegeneration, succumbed to prion disease much faster than control mice (~20% enhancement of disease). It remains an open question as to how many other genes, when deleted, would give a similar enhancement after intracranial inoculation (many genes when deleted accelerate or delay peripheral prion pathogenesis due to immune phenotypes). Interestingly, although we observed an enhancement of prion disease in terms of survival, the other major features of prion disease—spongiform changes, gliosis, accumulation of proteinase K-resistant PrP, onset behavioral symptoms—all occurred with similar kinetics. But the Hsf1 knockouts do not persist for long after their symptoms develop. Thus, Hsf1 must act at a later stage of prion disease, just after symptoms

have developed. This hypothesis is reasonable given all that we know about the protective properties of Hsf1 in stressful conditions (McMillan et al., 1998; Xiao et al., 1999).

Determining the genes that are transcriptionally activated or repressed by Hsf1 during the clinical phase of prion disease is a crucial direction for future experiments. We hypothesized that Hsp70, which has well documented protective properties under numerous stress conditions, including protein misfolding, was a key transcriptional target of Hsf1 in prion disease. However, when we inoculated Hsp70 double knockouts or overexpression transgenics we did not observe any enhancement or delay in disease, respectively (described in the Appendix of Chapter 5). For future experiments I propose transcriptional profiling studies of purified neuronal and glial populations just after the onset of clinical symptoms. This study would tell us which genes are being transcribed or repressed at this important juncture in prion pathogenesis. These profiling studies would guide further therapeutic or genetic interventions in prion disease and possibly generalize to other protein misfolding disorders.

References

Auwerx J, Avner P, Baldock R, Ballabio A, Balling R, Barbacid M, Berns A, Bradley A, Brown S, Carmeliet P, Chambon P, Cox R, Davidson D, Davies K, Duboule D, Forejt J, Granucci F, Hastie N, de Angelis MH, Jackson I, Kioussis D, Kollias G, Lathrop M, Lendahl U, Malumbres M, von Melchner H, Muller W, Partanen J, Ricciardi-Castagnoli P, Rigby P, Rosen B, Rosenthal N, Skarnes B, Stewart AF, Thornton J, Tocchini-Valentini G, Wagner E, Wahli W, Wurst W (2004) The European dimension for the mouse genome mutagenesis program. Nat Genet 36:925-927.

Chiesa R, Piccardo P, Dossena S, Nowoslawski L, Roth KA, Ghetti B, Harris DA (2005) Bax deletion prevents neuronal loss but not neurological symptoms in a transgenic model of inherited prion disease. Proc Natl Acad Sci U S A 102:238-243.

Chourbaji S, Zacher C, Sanchis-Segura C, Spanagel R, Gass P (2005) Social and structural housing conditions influence the development of a depressive-like phenotype in the learned helplessness paradigm in male mice. Behav Brain Res 164:100-106.

Darlington CL (2005) Astrocytes as targets for neuroprotective drugs. Curr Opin Investig Drugs 6:700-703.

Degterev A, Huang Z, Boyce M, Li Y, Jagtap P, Mizushima N, Cuny GD, Mitchison TJ, Moskowitz MA, Yuan J (2005) Chemical inhibitor of nonapoptotic cell death with therapeutic potential for ischemic brain injury. Nat Chem Biol 1:112-119.

Del Bo R, Scarlato M, Ghezzi S, Martinelli-Boneschi F, Fenoglio C, Galimberti G, Galbiati S, Virgilio R, Galimberti D, Ferrarese C, Scarpini E, Bresolin N, Comi GP (2006) Is M129V of PRNP gene associated with Alzheimer's disease? A case-control study and a meta-analysis. Neurobiol Aging 27:770 e771-770 e775.

Dell'Omo G, Vannoni E, Vyssotski AL, Di Bari MA, Nonno R, Agrimi U, Lipp HP (2002) Early behavioural changes in mice infected with BSE and scrapie: automated home cage monitoring reveals prion strain differences. Eur J Neurosci 16:735-742.

Gould TW, Buss RR, Vinsant S, Prevette D, Sun W, Knudson CM, Milligan CE, Oppenheim RW (2006) Complete dissociation of motor neuron death from motor dysfunction by Bax deletion in a mouse model of ALS. J Neurosci 26:8774-8786.

Heitz S, Lutz Y, Rodeau JL, Zanjani H, Gautheron V, Bombarde G, Richard F, Fuchs JP, Vogel MW, Mariani J, Bailly Y (2007) BAX contributes to Doppel-induced apoptosis of prion-protein-deficient Purkinje cells. Dev Neurobiol 67:670-686.

Jackson WS, Tallaksen-Greene SJ, Albin RL, Detloff PJ (2003) Nucleocytoplasmic transport signals affect the age at onset of abnormalities in knock-in mice expressing polyglutamine within an ectopic protein context. Hum Mol Genet 12:1621-1629.

Jeong BH, Lee KH, Jeong YE, Hwang KA, Lee YJ, Carp RI, Ju YR, Kim YS (2007) Polymorphisms at codons 129 and 219 of the prion protein gene (PRNP) are not associated with sporadic Alzheimer's disease in the Korean population. Eur J Neurol 14:621-626.

Kempermann G, Kuhn HG, Gage FH (1997) More hippocampal neurons in adult mice living in an enriched environment. Nature 386:493-495.

Li A, Barmada SJ, Roth KA, Harris DA (2007) N-terminally deleted forms of the prion protein activate both Bax-dependent and Bax-independent neurotoxic pathways. J Neurosci 27:852-859.

McMillan DR, Xiao X, Shao L, Graves K, Benjamin IJ (1998) Targeted disruption of heat shock transcription factor 1 abolishes thermotolerance and protection against heat-inducible apoptosis. J Biol Chem 273:7523-7528.

Nakagawa T, Shimizu S, Watanabe T, Yamaguchi O, Otsu K, Yamagata H, Inohara H, Kubo T, Tsujimoto Y (2005) Cyclophilin D-dependent mitochondrial permeability transition regulates some necrotic but not apoptotic cell death. Nature 434:652-658.

Parkin ET, Watt NT, Hussain I, Eckman EA, Eckman CB, Manson JC, Baybutt HN, Turner AJ, Hooper NM (2007) Cellular prion protein regulates beta-secretase cleavage of the Alzheimer's amyloid precursor protein. Proc Natl Acad Sci U S A 104:11062-11067.

Premzl M, Sangiorgio L, Strumbo B, Marshall Graves JA, Simonic T, Gready JE (2003) Shadoo, a new protein highly conserved from fish to mammals and with similarity to prion protein. Gene 314:89-102.

Qin K, O'Donnell M, Zhao RY (2006) Doppel: more rival than double to prion. Neuroscience 141:1-8.

Rivera-Milla E, Oidtmann B, Panagiotidis CH, Baier M, Sklaviadis T, Hoffmann R, Zhou Y, Solis GP, Stuermer CA, Malaga-Trillo E (2006) Disparate evolution of prion protein domains and the distinct origin of Doppel- and prion-related loci revealed by fish-to-mammal comparisons. Faseb J 20:317-319.

Selimi F, Vogel MW, Mariani J (2000) Bax inactivation in lurcher mutants rescues cerebellar granule cells but not purkinje cells or inferior olivary neurons. J Neurosci 20:5339-5345.

Steele AD, Jackson WS, King OD, Lindquist S (2007a) The power of automated high-resolution behavior analysis revealed by its application to mouse models of Huntington's and prion diseases. Proc Natl Acad Sci U S A 104:1983-1988.

Steele AD, Emsley JG, Ozdinler PH, Lindquist S, Macklis JD (2006) Prion protein (PrPc) positively regulates neural precursor proliferation during developmental and adult mammalian neurogenesis. Proc Natl Acad Sci U S A 103:3416-3421.

Steele AD, King OD, Jackson WS, Hetz CA, Borkowski AW, Thielen P, Wollmann R, Lindquist S (2007b) Diminishing apoptosis by deletion of Bax or overexpression of Bcl-2 does not protect against infectious prion toxicity in vivo. J Neurosci 27:13022-13027.

Watts JC, Drisaldi B, Ng V, Yang J, Strome B, Horne P, Sy MS, Yoong L, Young R, Mastrangelo P, Bergeron C, Fraser PE, Carlson GA, Mount HT, Schmitt-Ulms G, Westaway D (2007) The CNS glycoprotein Shadoo has PrP(C)-like protective properties and displays reduced levels in prion infections. Embo J 26:4038-4050.

Xiao X, Zuo X, Davis AA, McMillan DR, Curry BB, Richardson JA, Benjamin IJ (1999) HSF1 is required for extra-embryonic development, postnatal growth and protection during inflammatory responses in mice. Embo J 18:5943-5952.

Yuan J (1997) Transducing signals of life and death. Curr Opin Cell Biol 9:247-251.

Zhang CC, Steele AD, Lindquist S, Lodish HF (2006) Prion protein is expressed on long-term repopulating hematopoietic stem cells and is important for their self-renewal. Proc Natl Acad Sci U S A 103:2184-2189.